Conceptual layout design for a Two-Shaft Pebble Bed Micro Model Configuration

L.D. Venter

Dissertation submitted in partial fulfilment of the degree

Master of Engineering

in the

School of Mechanical and Materials Engineering,

Faculty of Engineering

at the

North-West University, Potchefstroom Campus

Supervisor: Dr. BW Botha

Potchefstroom

2006

ABSTRACT

Title	:	Conceptual layout design for a two-shaft Pebble Bed Micro Model Configuration.
Author	:	L.D. Venter
Supervisor	:	Dr. B.W. Botha
School	:	Mechanical and Materials Engineering
Degree	:	Master of Engineering

The pre- and inter-cooled recuperative closed Brayton cycle can be configured to be either a single or a multi-shaft arrangement. In comparison to the single shaft, multi-shaft arrangements have not been used widely in the closed cycle environment. Therefore, during the development of a three-shaft Pebble Bed Modular Reactor (PBMR), a Pebble Bed Micro Model (PBMM) was constructed to illustrate the envisaged PBMR control methodologies. The PBMM now offers the opportunity to investigate other shaft arrangements. The main objective of this study is to perform a conceptual layout design for a two-shaft PBMM configuration. The major steps performed in the conceptual layout design of the two-shaft PBMM are preliminary studies, thermodynamic design point studies and turbo machine selection.

During the thermodynamic design point studies the influence of turbocharger selection on the cycle performance were investigated. Two optimum values for Overall Pressure Ratio (OPR) were found, one for maximum cycle efficiency and one for maximum cycle power output. This, together with the requirement for the OPR to be equally shared between the Low-Pressure Compressor (LPC) and the High-Pressure Compressor (HPC), was used to identify suitable turbocharger pairs. In order to evaluate the compressor operating points of the turbochargers, the unique matching characteristics for the pre- and inter-cooled recuperative closed Brayton cycle were derived. Final turbocharger selection was performed in Flownex. The turbocharger pair that enjoyed the highest cycle efficiency at thermodynamic conditions similar to that of the three-shaft PBMM configuration was suggested as the preferred turbocharger configuration.

Unexpectedly the turbochargers selected for the two-shaft configuration were found to be identical to that of the three-shaft PBMM configuration. This led to a comparison of matching characteristics of the two-shaft configuration to that of the three-shaft configuration. The close proximity of both configurations to the choking region of the LPT ensured the close proximity of their operating points on the HPT. The fact that the HPC operating point is only a function of the HPT operating point caused close proximity of the HPC operating points. The requirement for flow compatibility that must exist between the HPC and LPC limited the operating point of the LPC for both configurations to the same flow compatibility line, which ensured the close proximity of the LPC operating points.

OPSOMMING

Titel	:	Conceptual layout design for a two-shaft Pebble Bed Micro Model Configuration.
Outeur	:	L.D. Venter
Promotor	:	Dr. B.W. Botha
Skool	:	Meganiese en Materiaal-ingenieurswese
Graad	:	Magister in Ingenieurswese

Die voor- en tussen-verkoelde rekuperatiewe geslote Brayton siklus kan as `n enkel as of meer-assige siklus gekonfigureer word. Meer-assige siklusse is onbekend in die geslote siklus omgewing. Om dié rede is daar tydens die onwikkeling van 'n drie-as Pebble Bed Modular Reactor (PBMR) besluit om die Pebble Bed Micro Model (PBMM) op te rig. Die doel van die PBMM is om die beheermetodes van die drie-as PBMR te illustreer. Die PBMM bied egter nou die geleentheid om ander askonfigurasies te ondersoek. Daarom is die uitkoms van hierdie studie die konseptuele uitleg-ontwerp vir `n twee-as PBMM konfigurasie. Die konseptuele uitleg-ontwerp is uitgevoer deur middel van `n voorlopige studie, termodinamiese ontwerppuntanalise en turbomasjienseleksie.

Tydens die termodinamiese ontwerppuntanalise is die invloed ondersoek wat turbomasjienseleksie op die siklusvertoning het. Hierdie analise het getoon dat daar twee optimale siklusdrukvehoudings bestaan, een vir maksimum sikluseffektiwiteit en een vir maksimum siklusdrywingsuitset. Dit, tesame met die vereiste dat die siklusdrukverhouding gelyk verdeel moet word tusen die lae-druk-kompressor en die hoë-druk-kompressor, is gebruik om geskikte turbo-aanjaereenhede te identifiseer. Om die kompressorbedryfspunte te evalueer is die unieke verdelingsgedrag van turbomasjiene van die twee-as voor- en inter-verkoelde rekuperatiewe geslote Brayton siklus afgely. Finale seleksie is gedoen met behulp van Flownex. Die turbo-aanjaerverdeling wat die hoogste effektiwiteit by soortgelyke termodinamiese toestande as die drie-as PBMM konfiguratsie getoon het, is aanbeveel as die geskikte turbo-aanjaerkonfigurasie.

Daar is onverwags bevind dat die twee-as PBMM-konfigurasie die selfde turbo-aanjaers as die drie-as PBMM-konfigurasie kan geruik. Dit het gelei na `n ondersoek waarin die

verdelingsgedrag van die twee-as konfigurasie met dié van die drie-as konfigurasie vergelyk is. Die nabyheid van albei konfigurasies se lae-druk-turbine bedryfspunte aan hul smoorpunte het verseker dat hulle hoë-druk-turbine bedryfspunte naby aan mekaar het. Die feit dat die bedryfspunt op die hoë-druk-kompressor slegs `n funksie is van die bedryfspunt op die hoë-druk-kompressor, het verseker dat hul hoë-druk-kompressorbedryfspunte ook naby aan mekaar is. Die vereiste vir vlociversoenbaarheid tussen die lae-druk-kompressor en hoë-druk-kompressor het veroorsaak dat albei konfigurasies beperk was tot dieselfde vloei versoenbaarheidslyn, en dit het die nabyheid van die bedryfspunte op die lae-druk-kompressor verseker.

ACKNOWLEDGEMENTS

I thank God for the opportunity He provided and for the strength to persevere during testing times

Thank you to Dr. Barend Botha for his guidance and encouragement on a professional and personal level.

I thank my parents who have always put my interests before their own. Without their believe in me, evident through years of financial support, I would have accomplished nothing.

Thanks to Charl, Cobus, Deon and Riaan for their friendship.

TABLE OF CONTENTS

LIST OF FIGURES

LIST OF TABLES

ABBREVIATIONS

GT-MHR	-	Gas Turbine – Modular Helium Reactor
HPC	-	High-Pressure Compressor
HPT	-	High-Pressure Turbine
HTGR	-	High Temperature Gas-cooled Reactor
IC	-	Inter-Cooler
LPC	-	Low-Pressure Compressor
LPT	-	Low-Pressure Turbine
MCR	-	Maximum Continuous Rating
NDM	-	Non-Dimensional mass flow rate
NDS	-	Non-dimensional Speed
OPR	-	Overall Pressure Ratio
PBMM	-	Pebble Bed Micro Model
PBMR	-	Pebble Bed Modular Reactor
PC	-	Pre-cooler
PCU	-	Power Conversion Unit
PR	-	Pressure ratio
PT	-	Power Turbine
SBS	-	Start-up Blower System
TIT	-	Turbine Inlet Temperature
V&V	-	Verification and Validation

NOMENCLATURE

A	:	Area	[m^2]
c_p	:	Specific Heat (constant pressure)	[kJ/s-kg]
γ	:	Specific Heat Ratio	[-]
ΔP	:	Pressure difference	[kPa]
ΔT	:	Temperature difference	[°C]
D	:	Characteristic Geometrical Parameter	[m]
ε	:	Heat exchanger efficiency	[-]
f_{HX}	:	Heat exchanger friction loss factor	[-]
f_l	:	Pressure loss factor	[-]
f_{pipe}	:	Pipe friction loss factor	[-]
g	:	Acceleration due to gravity	[m/s^2]
h	:	Enthalpy	[kJ/kg]
η	:	Thermal efficiency	[-]
η_m	:	Mechanical efficiency	[-]
η_c	:	Compressor isentropic efficiency	[-]
η_t	:	Turbine isentropic efficiency	[-]
$\dot{m}$	:	Mass flow rate	[kg/s]
NDM	:	Non Dimensional Mass flow rate	$[kg/s\sqrt{K}\ bar^{-1}]$
NDS	:	Non Dimensional Speed	$[rpm/\sqrt{K}]$
OPR	:	Overall Pressure Ratio	[/]
P	:	Pressure	[kPa]
P_{0i}	:	Total Pressure at Node *i*	[kPa]
PR	:	Pressure Ratio	[/]
ρ	:	Density	[kg/m^2]
$\dot{Q}$	:	Heat or Power	[kW]
R	:	Gas Constant	[kJ/kg K]
s	:	Entropy	[kJ/kg K]
T	:	Temperature	[°C]
T_{0i}	:	Total Temperature at Node *i*	[°C]
V	:	Velocity	[m/s]

1 INTRODUCTION

The vastly increasing need for electricity with the concomitant depletion of natural resources is forcing utility companies to investigate alternative methods of generating electricity. The success of a helium cooled test reactor, developed in Germany during the sixties and seventies, proved the potential of helium as a superior coolant for gas-cooled reactors. It further illustrated the possibility of higher cycle efficiency due to high reactor outlet temperatures. However, the availability of helium and the lack of turbine technology during the seventies and early eighties caused researchers to concentrate on improving high temperature steam cycles. Since then, turbine technology and the availability of helium have improved. This resulted in renewed interest in combining the high temperature of helium cycles and the efficiency of gas turbines in a High Temperature Gas-cooled Reactor (HTGR) (Botha, 2002).

This has led various utility companies to the development of HTGR power plants. Subsequently, various concepts of the Power Conversion Unit (PCU) resulted, of which the four most common concepts are as follows (Botha, 2002):

- The direct helium gas turbine cycle.
- The indirect steam cycle.
- The combined helium gas turbine and steam cycle.
- The indirect combined air gas turbine and steam cycle power plant.

Currently, two designs of the HTGR power plant are under active development. These are the Pebble Bed Modular Reactor (PBMR) and the Gas Turbine – Modular Helium Reactor (GT-MHR). Both designs make use of a closed direct helium gas turbine cycle (IAEA, 2005).

The closed direct helium gas turbine cycle is based on the closed Brayton cycle. The Brayton cycle, without any phase change in the working fluid, is described by Sonntag *et al.* (1998:373) as the ideal cycle for a gas turbine. The cycle involves the compression, heating, expansion and cooling of the working fluid in a closed loop to produce useful shaft work.

Saravanamuttoo *et al.* (2001:3) note that it is important to realize that the processes of compression, heating, expansion and cooling do occur in a single component. They occur in components that are separate in the sense that they are designed, tested and developed individually. These components are not limited to the four processes already mentioned -- since more compressors and turbines can be added with inter-coolers between the compressors and reheat heaters between the turbines. A recuperator can be added to recover lost heat at the turbine outlet in order to minimize the heat that is necessary to achieve the maximum temperature. These components can be linked together in a variety of ways. The way in which these components are linked together not only affects the maximum overall thermal efficiency, but also the variation of efficiency with power output.

Botha (2002) explains that since industrial applications are intended to operate for extended periods, the drive is normally to improve cycle efficiency rather than power output. Therefore industrial applications commonly make use of the recuperated, pre- and inter-cooled Brayton cycle to reduce payback periods.

The pre- and inter-cooled recuperative Brayton cycle can, however, be configured in numerous ways. One of the features found to vary between various cycle configurations is the choice of shaft arrangement.

1.1 Shaft arrangements

Shaft arrangements can be categorised as single-shaft or multi-shaft. Two of the most notable concepts for HTGR power plants based on the closed loop Brayton cycle are the single- and three-shaft arrangements (Rousseau & Van Ravenswaay, 2003).

Provided that the single-shaft and three-shaft systems are configured to be recuperative, pre- and inter-cooled Brayton cycles, they will be thermodynamically identical. However, the transient and mechanical behaviour of the two cycles will differ substantially. For this reason this study investigated the advantages and disadvantages of single-shaft and three-shaft systems. The most comprehensive information was found to be given by Botha (2004). This is subsequently summarized.

Single Shaft

A single shaft arrangement, shown in Figure 1-1, consists of a turbine driving a generator and compressors through a common shaft.

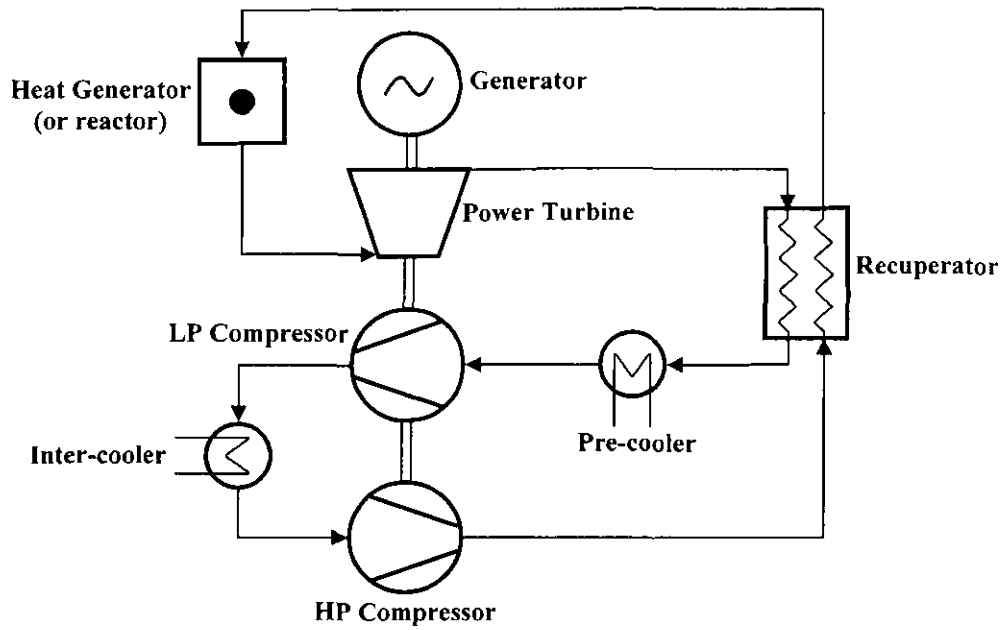

Figure 1-1 Single Shaft, pre- and inter-cooled, recuperative, closed Brayton Cycle

Advantages

- Simplest, most compact system available.
- Having the generator fitted to a compressor shaft, the generator can be used as a motor to drive the compressors during start-up, until the system has reached the state of self-sustainability.
- Reduced danger of over-speeding in the event of load rejection due to the inherent high inertia caused by the drag of the compressor.

Disadvantages:

- The shaft speed is limited by the generator to 3000 rpm. This relative low speed increases the relative outer diameters of the compressor to obtain the correct tip speed for the given compression ratio. This results in shorter blades in order to obtain the correct flow area. Shortened blades increase the relative tip leakage, reducing the efficiency and possibilities to increase it. This is aggravated when using helium. To improve this, frequency conversion of some sort can be implemented, but at the expense of a more complex system.

- The single shaft arrangement requires a longer shaft to accommodate the compressors, turbine and generator. The resulting reduction in shaft stiffness reduces the natural frequency of the system and therefore also its operating range.
- Although the generator can be used as a motor during start-up, a large amount of power is needed (Rousseau & Van Ravenswaay, 2003).

Three-Shaft

The three-shaft arrangement, Figure 1-2, divides the compression process into two steps. The two steps being mechanically separated ensures that each section can run at its own optimum speed leaving only the power turbine to be limited to the generator speed of 3000 rpm.

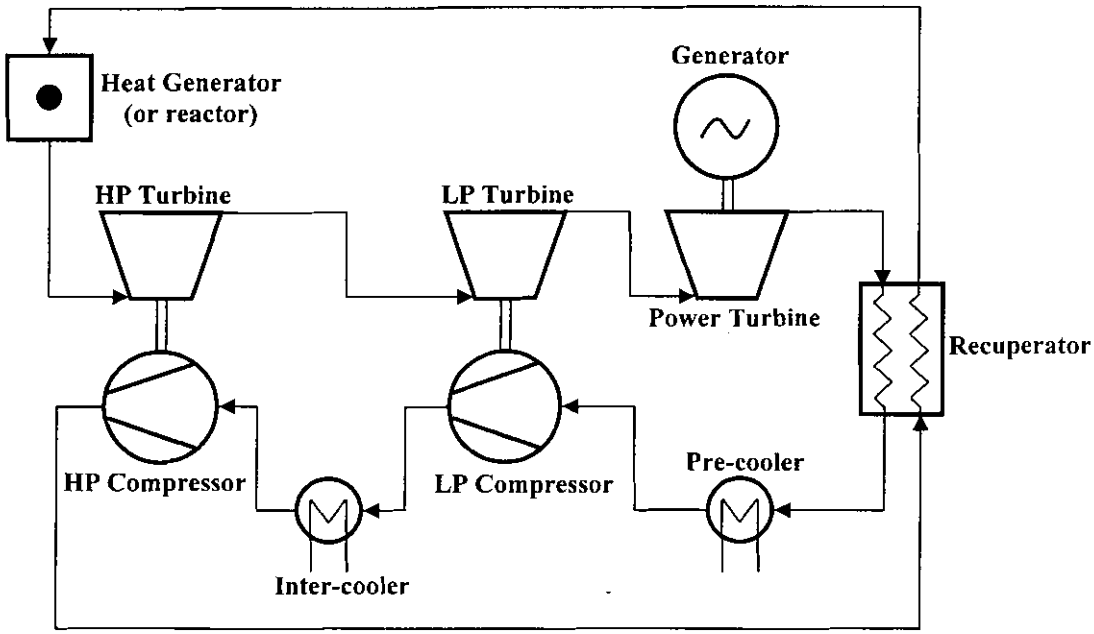

Figure 1-2 Three-Shaft, pre- and inter-cooled, recuperative, closed Brayton Cycle

Advantages:

- Only the free turbine is limited to the 3000 rpm required by the generator. The other turbo units are therefore left to operate at higher speeds, which decreases their outer diameters and therefore results in increased efficiency.
- Shorter shafts can be used, resulting in stiffer shafts, which results in turn in an increase of the natural frequency and the subsequent operating range.
- The power needed during start-up is about ten times less in comparison to that of the single-shaft arrangement (Rousseau & Van Ravenswaay, 2003).

Disadvantages:

- More complex and potentially more expensive.
- Not having a generator fitted on a compressor shaft calls for an external source to drive the compressor during start-up or the use of a Start-up Blower System (SBS).
- The lack of the braking effect of a compressor on the generator shaft makes the system more susceptible to over-speeding during the event of sudden load loss.

It is therefore clear that it is impossible to declare one of these configurations to be the best. It is, however, possible to identify the main factors influenced by the choice of shaft arrangements. These are:

- The start-up procedure.
- The power needed during start-up.
- Shaft speeds.
- Shaft lengths.
- Susceptibility to over-speeding in the event of sudden load loss.

1.1.1 The two-shaft arrangement

Alternatively to the single and three-shaft arrangements the pre- and inter-cooled recuperative Brayton cycle can be configured as a two-shaft arrangement. The two-shaft arrangement can take on two practical forms:

1. One shaft consisting of two compressors, the LPC and HPC, driven by the HPT and a second shaft consisting of a free turbine driving the generator.
2. One shaft consisting of one compressor, the HPC, driven by the HPT and a second shaft consisting of the HPC as well as a generator driven by the LPT as shown in Figure 1-3.

The second configuration, however, will be more suitable in order to combine the advantages of the single- and three-shaft configurations for the following reasons:

- The proposed two-shaft arrangement allows the use of the generator as a motor during start-up since the Low-Pressure Compressor (LPC) and generator share a common shaft.
- The High-Pressure Compressor (HPC) and High-Pressure Turbine (HPT) are free to operate at a high optimal speed.

- Having split the shaft, less components share a shaft allowing shorter shafts thus reducing the shaft lengths which increases the speed and speed operating range.
- The LPC fitted on the generator shaft makes the system less prone to over-speeding due to the added inertia and drag.

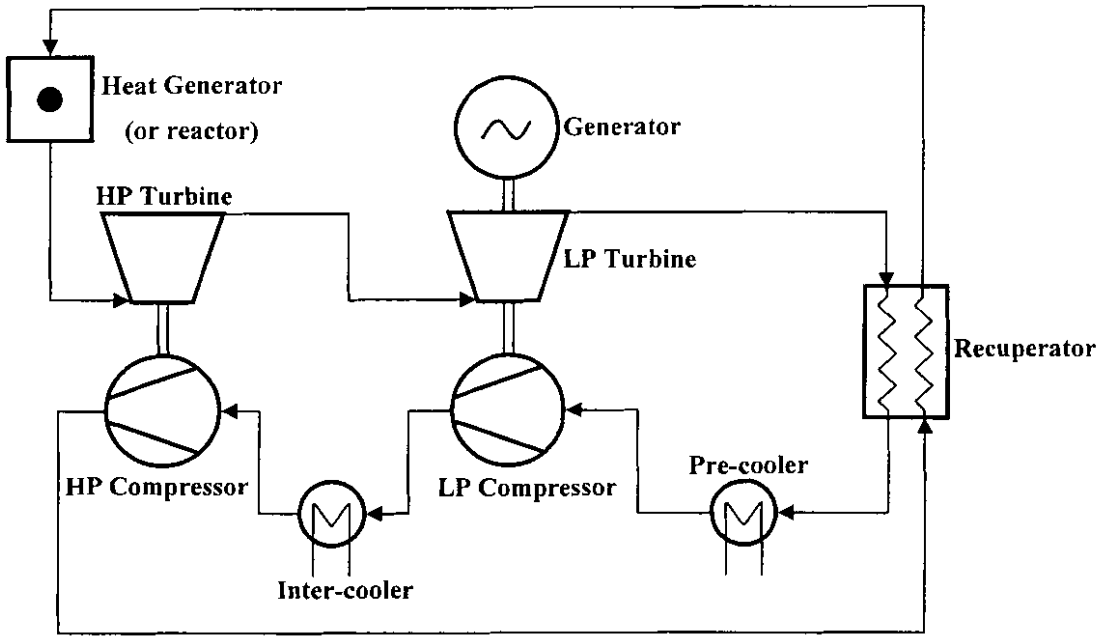

Figure 1-3 Two-Shaft, pre- and inter-cooled, recuperative, closed Brayton cycle

Having illustrated the potential of combining the advantages and disadvantages of the single and three-shaft arrangement this study focussed on the proposed two-shaft configuration shown in Figure 1-3.

1.2 Objective of the study

Multi-shaft arrangements, although used in open-cycles, have not been used widely in the closed cycle environment. It was therefore decided to construct a working model of the PCU with a view to the development of a three-shaft PBMR. The model known as the Pebble Bed Micro Model (PBMM) was designed to illustrate the envisaged PBMR control methodologies for start-up, load following, steady state full load and load rejection. The PBMM, as shown in Figure 1-4, was built by the Faculty of Engineering at the North West University (Van Niekerk *et al*, 2003).

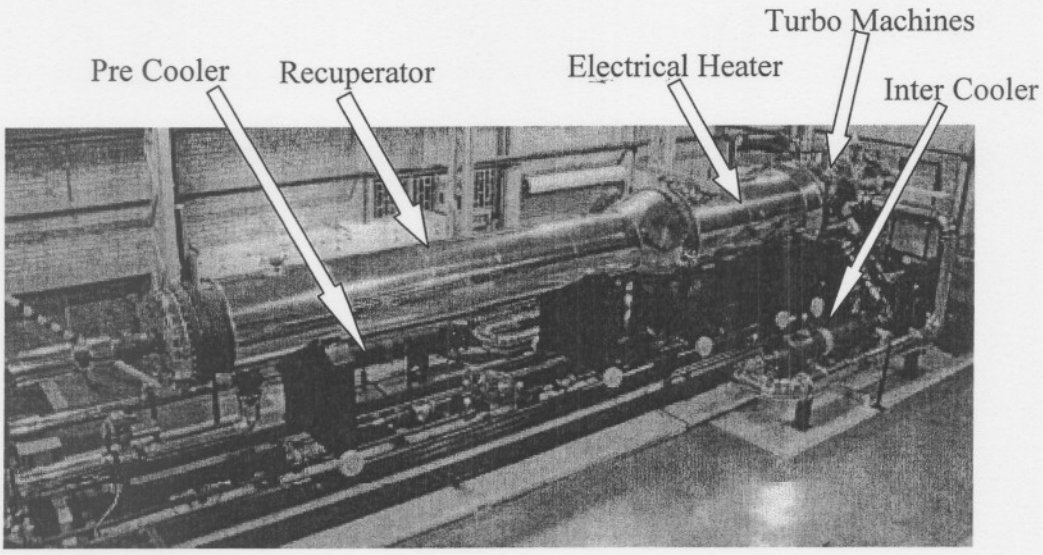

Figure 1-4 Photograph of the PBMM (Van Niekerk et al., 2003)

Since it has been operated successfully in an ongoing investigation into the behaviour of the three shaft arrangement, the PBMM now offers the opportunity to investigate other shaft arrangements. In order to investigate the potential of combining the advantages of the single and three-shaft arrangements the main objective of the study is to *design a conceptual layout of a two-shaft PBMM* (Figure 1-3). This will further the debate on shaft arrangements, broaden the over-all knowledge base on gas turbines and add to the functionality of the PBMM facility.

The aim of the study is therefore to investigate and propose a conceptual layout for a two-shaft PBMM configuration.

1.3 Research Methodology

In order to achieve the said objective, the study adopts the following method:

1. Literature survey: the literature survey focuses on the gas turbine design procedure and the design and development of the PBMM.
2. Preliminary study: in this section the thermodynamic limitations, the choice of turbomachinery and the load on the system is considered.
3. Thermodynamic design point calculations.
4. Turbocharger selection.
5. Comparison of the two- and three-shaft PBMM configurations.

2 LITERATURE STUDY

The main objective of the study stated in Chapter 1 is to do a conceptual layout design for a two-shaft PBMM configuration. For this reason Chapter 2 focuses on the typical gas turbine design procedure followed by an investigation into how the different aspects of this procedure was addressed during the design and development of the existing PBMM.

2.1 The gas turbine design procedure

Saravanamuttoo *et al.* (2003:38) describes the process of designing a gas turbine as a multi-disciplined process that combines thermodynamics, aerodynamics, mechanics, and control system design in a concurrent engineering process. Figure 2-1 shows a flow diagram of all the major steps in the design process.

The design process commences with a specification, which is the result of either market research or a customer requirement. The specification is not just a simple statement of required power and efficiency. Depending on the application, other important factors need to be considered, such as weight, cost, volume, life, and noise. These factors often act in opposition. For example, high efficiency usually comes at an increased capital cost.

Following the specification, the designer is confronted with the choice of cycle and what type of turbomachinery should be used. The layout of the engine must also be considered, for example, whether a single or multi-shaft design should be used.

The first major design step is to carry out thermodynamic design point studies. These are detailed calculations taking into account all important factors such as expected component efficiencies, fluid properties, and pressure losses and will be carried out over a range of Overall Pressure Ratio (OPR) and Turbine Inlet Temperature (TIT). After a suitable TIT and OPR have been determined, the mass flow required, to achieve a specific output, can be calculated.

With the mass flow, OPR and TIT determined by the thermodynamic design point calculations, attention can now be turned to the aerodynamic design of the turbomachinery. The annulus dimensions, rotational speeds and number of stages can now be determined.

With the completion of the thermodynamic and aerodynamic designs, having determined the key dimensions, the mechanical design can commence. During this stage in the design process important factors such as blade stress, vibration and bearings must be taken into consideration.

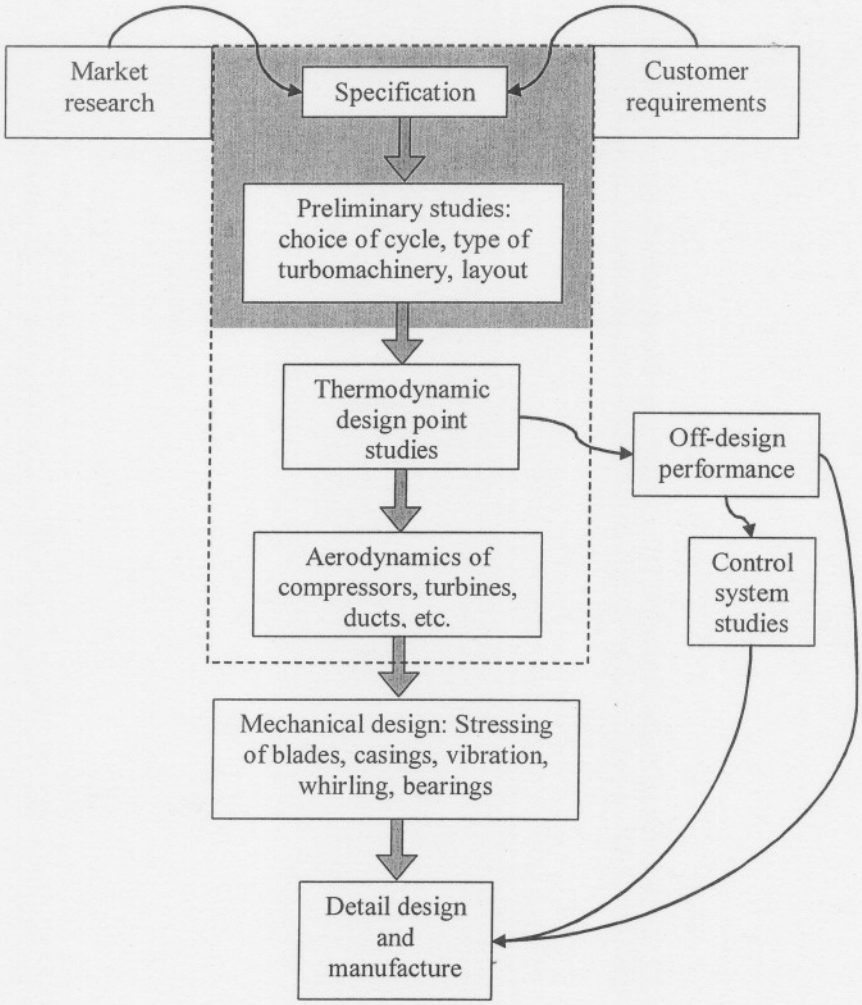

Figure 2-1 Gas Turbine Design Procedure (Saravanamuttoo *et al., 2001:39)*

At the same time all these studies are proceeding, off-design performance and control system design must be considered. Off-design operation includes varying ambient conditions and reduced power operation. Control system design is aimed at ensuring the safe and automatic operation of the gas turbine.

When performing the design of a gas turbine, essential criteria based on operational considerations must be taken into account. The most important of these criteria are (Boyce, 2002:12):

- High efficiency.
- High reliability.

- Ease of maintenance.
- Ease of installation.
- Control systems with high degree of reliability.
- Flexibility on service.

For the conceptual layout design of the two-shaft PBMM configuration, the steps enclosed by the dotted line (Figure 2-1) will be performed. As a starting-point to identify how these issues can be addressed, the design and development of the existing PBMM will now be discussed.

2.2 The design and development of the PBMM

The original PBMM was not necessarily designed from outset on the basis of the gas turbine design procedure given in Figure 2-1. The various steps were, however identified from literature and is subsequently summarised.

2.2.1 Specification

The aim of the PBMM was to illustrate the foreseen control methodologies and operation for the three-shaft PBMR. The facility was designed to allow experiments and measurements of major process variables, aiding in the Validation and Verification (V&V) of Flownex. It was designed to be similar in layout design to that of the three-shaft PBMR including all the major components in the same order. The components in the PBMM are not scaled-down versions of that intended for the PBMR, but only mimic the same qualitative behaviour with regard to power and heat input and output, frictional and other pressure losses as well as the thermal inertia during transients (Rousseau & Greyvenstein, 2002).

2.2.2 Preliminary studies

The main specification for the existing PBMM was therefore to be a three-shaft pre- and inter-cooled recuperative closed Brayton cycle.

Cycle Layout

The schematic layout of the three-shaft PBMM is shown in Figure 2-2. Starting at 1, nitrogen at relative low pressure and temperature is compressed by the Low-Pressure Compressor (LPC) to an intermediate pressure at 2, after which it is cooled in an Inter-Cooler (IC) from state 3 to 4. A High-Pressure Compressor (HPC) then compresses the nitrogen to the

maximum cycle pressure at 6. From 7 to 8 the nitrogen is preheated in the high pressure side of the recuperator. At 10 the nitrogen reaches its highest temperature after being heated by the electrical heat source. The necessary work needed by the HPC is produced by the High-Pressure Turbine (HPT) through expanding the nitrogen from 11 to 12. From 13 to 14 the expansion in the Low-Pressure Turbine (LPT) produces the work needed by the LPC. Expanding the nitrogen from 15 to 16 in the Power Turbine (PT) produces the useful shaft-work. From 17 to 18 the unused energy is utilized in the low-pressure side of the recuperator. In order to complete the cycle, the nitrogen is cooled back to the minimum temperature in the pre-cooler from 19 to 20.

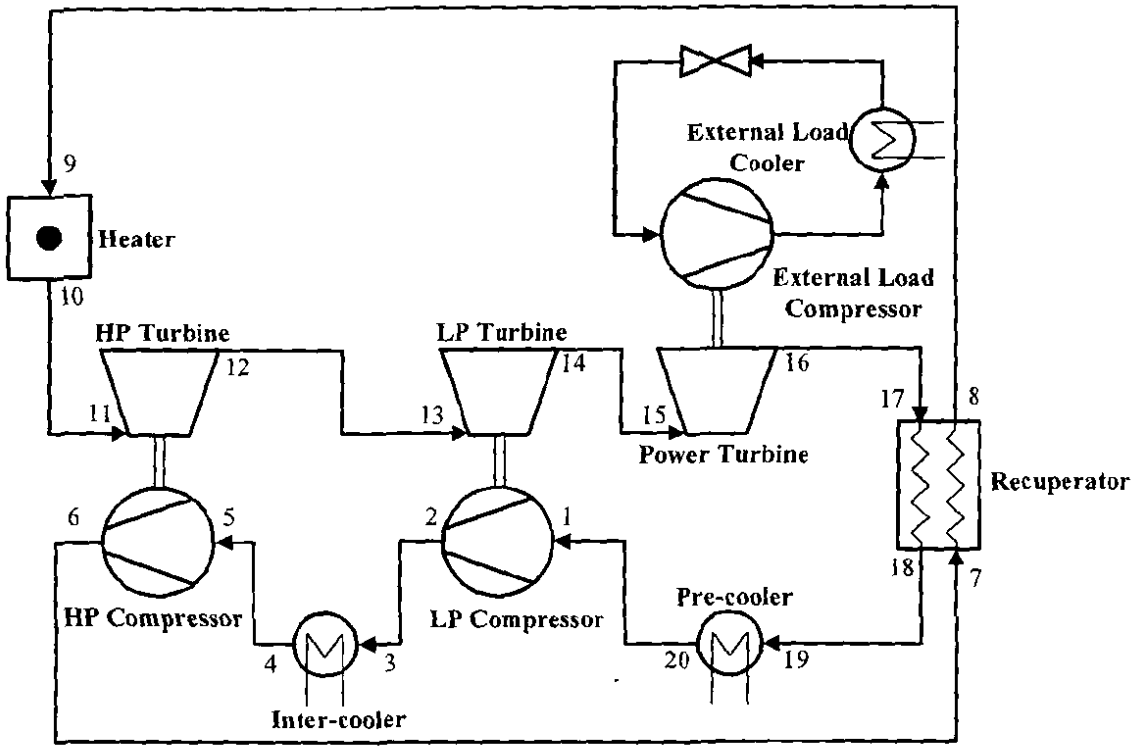

Figure 2-2 Schematic layout of the PBMM (Greyvenstein & Rousseau, 2002)

During this phase in the design of the PBMM the choice of working fluid, type of turbomachinery, choice of load on the system, choice of secondary cooling system and type of heat source were considered. Therefore, these issues are briefly discussed below.

Choice of turbomachinery

Off-the-shelf turbochargers are used for the turbomachinery in the PBMM. Although being of the centrifugal type rather than axial, their overall performance characteristics within the system is essentially the same with regard to pressure ratio and isentropic efficiency versus non-dimensional mass flow rate. These characteristics influence the overall cycle performance and are also the characteristics employed in the Flownex simulation models (Rousseau & Greyvenstein, 2002).

Choice of working fluid

The PBMR uses helium as working fluid. But since the PBMM was not intended to address specific issues such as the use of helium or to test the performance of the major components, the use of nitrogen was preferred. In addition to nitrogen being cheaper than helium, the use of nitrogen enabled the use of commercially available turbo chargers rather that expensive purpose designed axial turbomachines (Rousseau & Greyvenstein, 2002).

Choice of load

Since the power turbine is part of a turbocharger already consisting of a compressor, this compressor serves as load on the system. The compressor forms part of an external load loop. In addition to the compressor the external load loop consists of an external load cooler and control valve. With this external load loop it is possible to emulate the load behaviour (Rousseau & Greyvenstein, 2002).

Cooling system

The PBMM is not indented to study the behaviour of the secondary cooling system. Therefore, the secondary cooling system for the pre-and inter-coolers is cooling tower based rather than intermediate heat exchanger systems that finally rejects the heat in the ocean (Rousseau & Greyvenstein, 2002).

Heat source

The heat source is a pure electrical resistance heater instead of a pebble bed nuclear reactor. Although it could have been any other conventional heat source such as an external combustion gas heater, the control and measuring of the heat load is simplified by using an electrical heater (Rousseau & Greyvenstein, 2002).

2.2.3 Thermodynamic design point calculations

The aim of the thermodynamic design point analysis is to determine achievable and/or optimum thermodynamic conditions for the plant to operate at. This includes the pressure level, maximum temperature, optimum pressure ratio and power level for the plant to operate at.

Pressure levels

For a closed cycle the power output of the plant can be controlled by the pressure level within the cycle. This so called "inventory control" is achieved by injecting or extracting gas into or from the system. One of the distinguishing features of inventory control is that the temperatures, volume flow rates, velocities and pressure ratios remain unchanged. The absolute pressure together with the gas densities change resulting in the increase or decrease of the mass flow rate according to Equation (2-1)

$$\dot{m} = \rho A V \qquad (2\text{-}1)$$

where $\dot{m}$ the mass flow rate, ρ the density, A the cross-sectional area and V the gas velocity. According to Equation (2-2), all power levels (Q) will change as $\dot{m}$ changes even though ΔT remained unchanged (c_p is the specific heat capacity).

$$Q = \dot{m} c_p \Delta T \qquad (2\text{-}2)$$

In order to minimize leakage of air into the plant, the lowest pressure should always be above atmospheric pressure. The inventory control of the PBMR was specified to be able to take the power level down to 40% Maximum Continuous Rating (MCR). Since the relationship between pressure level and power level is nearly linear and the barometric pressure at location in Potchefstroom is 86kPa, the plant was designed to have the highest minimum pressure at least 215 kPa at 100% MCR. The PBMM was therefore designed to have a maximum minimum pressure of 250 kPa. Having a typical pressure ratio of three, this implies a maximum pressure of 750 kPa. The maximum design pressure for the PBMM however is 1000 kPa. This increased the flexibility of the plant to possible changes in the maximum design pressure (Rousseau & Greyvenstein, 2002).

Maximum temperature

The maximum temperature in the cycle is determined by one of two factors namely (i) the maximum temperature that can be achieved by the heat source or (ii) the maximum temperature tolerated by the highly stressed HPT blades. The heat source can achieve at least 900 °C, but since the normal operating temperature for a turbocharger turbine is 650 °C, the maximum temperature was dictated by the turbine (Rousseau & Greyvenstein, 2002). After detailed discussion with the manufacturer, however, it was agreed that the maximum temperature can be set to 700 °C. This was possible because the turbochargers will not use the upper extremes of their rotational speed operating ranges (Greyvenstein *et al.*, 2002).

Pressure ratios

Turbocharger compressors can easily produce the typical cycle pressure ratio of about 3. Therefore the pressure ratio was determined by the desire to obtain maximum cycle efficiency. For this reason, a simplified simulation model was set up that accounts for the complex interaction between the major components. The simulation model was set up in EES allowing for a quick and easy parametric study to determine the optimum pressure ratio (Rousseau & Greyvenstein, 2002).

The simulation model used to perform a first order cycle analysis required the assumption of certain parameters and limitations. Since these parameters were not available for the PBMM design, typical realistic values were assigned from experience (Greyvenstein & Rousseau, 2002). These values include the following:

- Pressure drops in pipes equal to 0.6% of the absolute pressure at the inlet to the pipe.
- For the recuperator and heat exchangers the pressure drop was assumed to be 0.5% of the absolute pressure at inlet.
- Compressor isentropic efficiency of 76 % which is determined by that achievable by a typical turbocharger compressor.
- Turbine isentropic efficiency of 69 %.
- Pre-and inter-cooler effectiveness of 95 %. Since low cost heat exchangers were employed this relatively high value was achieved by simply over-sizing the heat exchangers.
- The cost of the recuperator is strongly dependent on effectiveness. For initial analysis the recuperator effectiveness formed part of the parametric study. Recuperator effectiveness between 85% and 90 % were investigated.

- During the first order cycle analysis the heat source power level must be supplied. But since this is largely influenced by the mass flow which is dependent on the size of the turbomachines, the mass flow was taken as unity. A heat source power level per kg was determined.
- Since cycle efficiency is at its highest when the OPR is equally shared between the HPC and LPC, the HPC and LPC pressure ratios were set to be equal for the calculations.

Incorporating these values into the EES simulation model the optimum pressure ratios were found for maximum cycle efficiency and maximum specific power output, shown in Figure 2-3 and Figure 2-4 respectively.

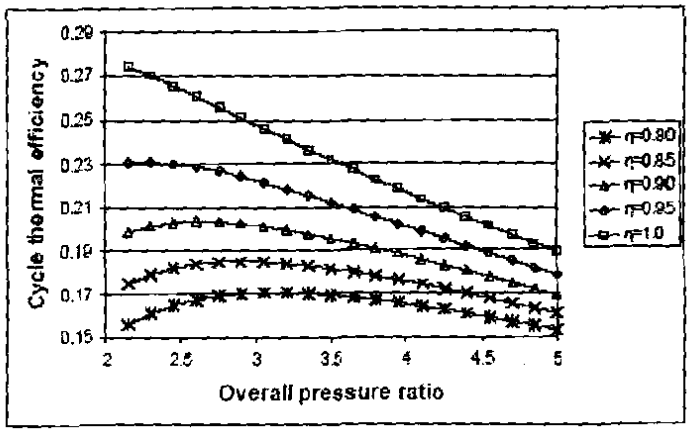

Figure 2-3 Thermal efficiency as a function of recuperator efficiency and overall pressure ratio

The recuperator efficiency is determined by the product of the area and the overall heat transfer coefficient and is therefore a design choice. The cost of the recuperator, however, increases with increasing efficiency. For this reason a recuperator efficiency of approximately 85% was chosen as a good compromise between performance and cost. In Figure 2-3 the optimum overall pressure ratio for maximum cycle efficiency at a recuperator efficiency of 85% is approximately 2.75. In Figure 2-4, however, it can be seen that the maximum specific work output occurs at an OPR of approximately 4.5. Optimum cycle efficiency is normally preferred over optimum power output, but since the cycle efficiency is not as sensitive to the OPR as power output, an OPR of 4 was chosen as a good compromise between the two. (Greyvenstein & Rousseau, 2002).

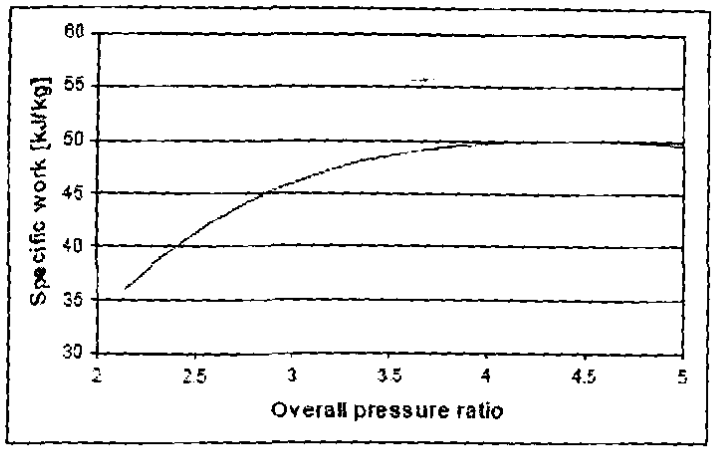

Figure 2-4 Specific work as a function of overall pressure ratio

2.2.4 Aerodynamic design

The aerodynamic design of gas turbines mainly consists of the design of the compressors and turbines to meet the thermodynamic design point discussed in the previous section. For the PBMM, however, the aim was to find suitable turbochargers to ensure a cycle operating point as close to that determined during the thermodynamic design point calculation. The selection of the turbochargers is documented in Greyvenstein *et al.* (2002) and is subsequently summarized.

The operating points of the turbo-machines are expressed in terms of corrected mass flow rate and pressure ratio. Table 2-1 shows the operating points of the individual machines determined by the first order cycle analysis.

Table 2-1 Operating point for the turbomachinery determined by cycle analysis

Turbo unit	Pressure ratio	Corrected mass flow [kg/s sqrt(K).bar]
LPC	2.0	17.3
HPC	2.0	8.7
HPT	1.6	8.1
LPT	1.7	12.4
PT	1.4	20.0

The PT, although having the lowest pressure ratio, has the largest corrected mass flow rate. Therefore, the turbocharger with the largest turbine, from a range of commercially available units, was selected as the power turbine. This turbine has a corrected mass flow of 10.8 at the required pressure ratio of 1.4, which fixes the mass flow rate at a value of 0.54 kg/s for a pressure level of 100 kPa.

Table 2-2 Recalculated corrected mass flow rates for a mass flow of 0.54 kg/s

Turbo unit	Pressure ratio	Corrected mass flow [kg/s sqrt(K).bar]
LPC	2.0	8.3
HPC	2.0	4.7
HPT	1.6	4.4
LPT	1.7	6.7
PT	1.4	10.8

Table 2-2 shows the recalculated operating points for the other turbomachines at the mass flow rate of 0.54 kg/s. Using these operating points, turbochargers were selected of which the turbines best match these operating points. The suitability of the compressors was verified with the aid of Flownex, which solved for speed of the different turbochargers (Greyvenstein & Rousseau, 2002).

2.2.5 Mechanical design

The choice of off-the-shelf turbochargers for the turbomachinery and the load in the PBMM simplified this phase of the design dramatically, provided that the turbochargers won't be subjected to conditions far different from that for which they were designed. In Greyvenstein *et al.* (2002), the maximum allowable axial thrust is briefly discussed. Through correspondence with the manufacturer it was determined that to keep the axial thrust bearing loading within limits the pressure difference between compressor exit and turbine inlet should be kept within 84.6 kPa.

2.2.6 Off-design performance and control

Control system design is aimed at ensuring the safe and automatic operation of the engine. In Van Niekerk *et al.* (2003) the major control methods of the PBMM is discussed and is summarized below.

Start-up

The start-up for the three-shaft PBMM is done by means of a Start-up Blower System (SBS). By closing the System In-line Valve (SIV) the SBS is used to circulate the working fluid at essentially a constant flow rate. Adding heat to the working fluid in the heater causes the TIT to increase resulting in an ever increasing turbine work output. This results in the compressors contributing to the circulation of the working fluid causing the pressure increase over the SIV to drop. The cycle will continue to spiral towards self sustained circulation until it is achieved

when the pressure increase over the SIV becomes less than zero. When this occurs the SBS is disengaged and the cycle is said to have bootstrapped.

Inventory control

The power output of the PT in a closed cycle is controlled by changing the mass inventory in the cycle. The LPC suction pressure is taken as an indication of the mass inventory. Injecting or extracting nitrogen into the system, however, causes unwanted transients. The immediate effect of injecting nitrogen into the cycle causes a temporary drop in power output, while extraction is associated with a temporary increase in power output. These unwanted transients are avoided to a large extent by the use of compressor by-pass valves.

Prior to ramping up the power output compressor these by-pass valves are slightly opened. As the nitrogen is injected these valves are gradually closed to decrease the load on the compressors and the dip in power output.

The power output is gradually changed by opening the compressor by-pass valves during nitrogen extraction. This prevents the sudden increase in power output because of the increased power turbine pressure ratio.

Load rejection

The rapid rejection of load is necessary when a sudden loss in load occurs in order to prevent the generator from over-speeding. This is done by means of opening the Gas Cycle By-pass Valve (GCBV). The GCBV connects the point of highest pressure to the point of lowest pressure. When the GCBV is opened, the OPR is reduced and therefore also the power output.

2.2.7 Flownex simulation

Apart from demonstrating the foreseen control methodologies, the aim of the PBMM was to aid in the Verification and Validation of Flownex. Flownex is a thermal-fluid network analysis code that enables users to perform detail analysis of complex systems such as gas turbines (Flownex, 2005).

Van Ravenswaay *et al.* (2004) compared experimental data with the Flownex simulation of the PBMM. The integrated-effects tests on the PBMM illustrated the ability of Flownex to

correctly balance the performance characteristics of all the components to find the operating point. Figure 2-5 shows the comparison between Flownex and PBMM data on a T-s diagram.

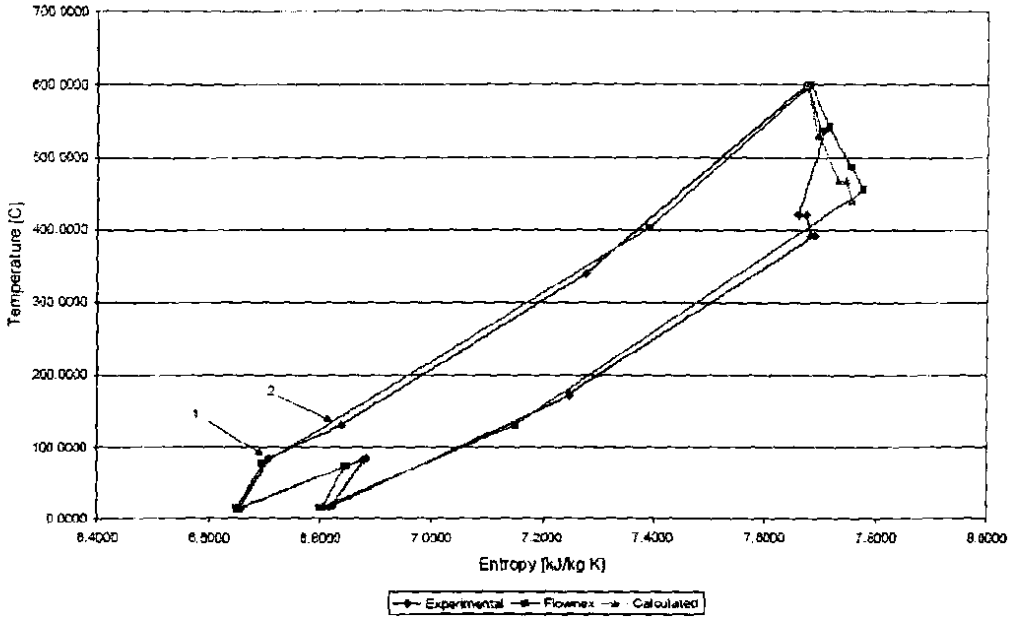

Figure 2-5 Comparison of Measured and Simulated values for the PBMM (Van Ravenswaay *et al.*, 2004).

The agreement between the experimental values and the simulation values for the compressors is quite good while the agreement for the turbines is not. In the Flownex simulation the expansion process through the turbines was assumed to be adiabatic. In the actual process the cool nitrogen flowing over the turbines causes the expansion process not to occur without heat losses. This is clear from Figure 2-5; the heat lost over the turbines is added at Point 1 and heats the nitrogen to Point 2 before it enters the recuperator.

2.3 Conclusion

In Paragraph 2.1 the typical gas turbine design procedure was discussed. For the conceptual design this design procedure was cut down to defining a specification, preliminary studies, thermodynamic design point calculations and turbo machine selection. Paragraph 2.2 discussed how these steps were performed during the conceptual layout design of the three-shaft PBMM.

The major steps followed during design and development of the three-shaft PBMM consists of a specification, preliminary studies, thermodynamic design point studies and selection of turbomachinery.

In order to perform the conceptual layout design of the two-shaft PBMM configuration this study will therefore perform the following:

1. Preliminary studies.
2. Thermodynamic design point studies.
3. Turbomachinery selection.

This chapter also illustrated the suitability of Flownex to accurately simulate the existing three-shaft PBMM. Flownex will therefore be used to verify the concept of re-configuring the existing PBMM to a two-shaft arrangement. This will be done by means of comparing a Flownex model of the two-shaft PBMM to that of the three-shaft PBMM.

In the next chapter the preliminary study will be conducted. It will focus:

- Defining the main limitations.
- Investigating and selecting the type of turbomachinery.
- Investigating and selecting the load on the system.

3 SPECIFICATION AND PRELIMINARY STUDIES

The previous chapter discussed the conceptual layout design of the three-shaft PBMM configuration. In this chapter, the specification of the two-shaft PBMM is defined followed by the preliminary study.

3.1 Specification

In order to reconfigure the PBMM to a two-shaft, pre- and inter-cooled, recuperative, closed Brayton cycle, it is important to retain most of the major components of the existing three-shaft PBMM. The major components in the PBMM are shown in Figure 3-1; they are the pre-cooler, inter-cooler, electrical heater, recuperator and turbomachinery. To achieve this, the main specification of the two-shaft PBMM configuration is to be thermodynamically similar to the three-shaft PBMM configuration.

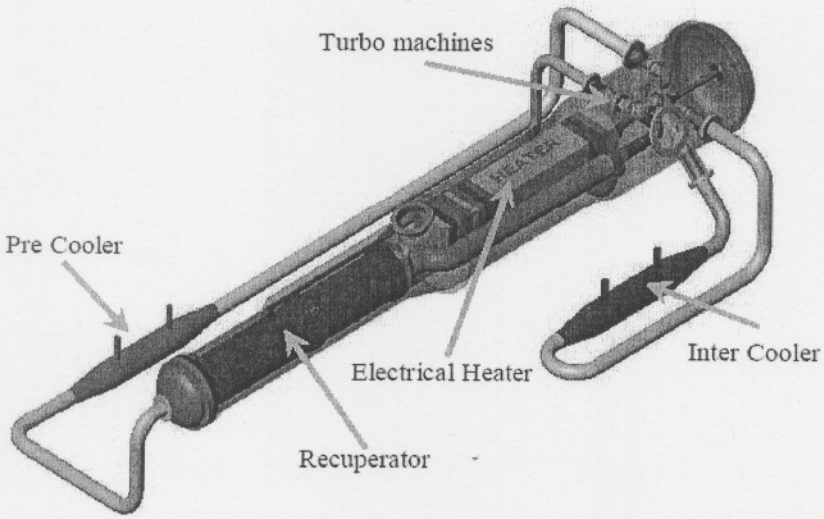

Figure 3-1 Solid model of the PBMM (Van Ravenswaay *et al.*, 2003)

In Table 3-1 the Flownex steady-state results for the three-shaft PBMM configuration are shown at two pressure levels. These results represent the thermodynamic operating conditions that must be targeted in the conceptual layout design of the two-shaft PBMM configuration.

Table 3-1 Steady-state results (Greyvenstein & Rousseau, 2002)

Component	LP compressor inlet pressure = 100 kPa						LP compressor inlet pressure = 250 kPa					
	P_{in} [kPa]	P_{out} [kPa]	T_{in} [°C]	T_{out} [°C]	Rating [kW]	Speed [rpm]	P_{in} [kPa]	P_{out} [kPa]	T_{in} [°C]	T_{out} [°C]	Rating [kW]	Speed [rpm]
LP Compressor	100.0	200.8	22.9	109.6	51.0	72078	250.0	496.9	26.0	112.1	124.3	71811
LP Turbine	248.5	150.5	628.5	549.0	51.0	72078	611.7	372.1	628.8	549.8	124.3	71811
HP Compressor	198.4	381.9	22.9	102.3	46.7	70009	491.3	938.0	26.1	105.1	114.1	69842
HP Turbine	378.0	249.1	700.0	628.5	46.7	70009	929.2	613.2	700.0	628.8	114.1	69842
Power Compressor	105.0	150.7	21.1	65.9	32.1	39073	262.0	372.1	22.9	66.6	76.8	38707
Power Turbine	149.7	105.0	549.0	498.2	32.1	39073	370.2	262.0	549.8	500.4	76.8	38707
Precooler	101.1	100.5	165.3	22.9	83.9	-	252.4	251.2	155.1	26.0	186.6	-
Intercooler	199.1	198.7	109.6	22.9	50.9	-	492.8	491.9	112.1	26.1	124.1	-
Recuperator hot side	103.0	102.3	498.2	165.3	202.6	-	257.1	255.2	500.4	155.1	515.6	-
Recuperator cold side	381.1	379.4	102.3	438.8	202.6	-	935.9	932.5	105.1	453.3	515.6	-
Load rejection HX	106.5	105.1	65.9	21.1	32.1	-	265.1	262.3	66.6	22.9	76.8	-

3.2 Preliminary studies

One of the main specifications is to retain most of the major components part of the existing three-shaft PBMM, as discussed in the previous section. Therefore the preliminary study will mainly focus on the choice of turbomachinery and the choice of load.

3.2.1 Choice of turbomachinery

As discussed in Paragraph 2.2.2 the turbomachinery used in the PBMM is off-the-shelf turbochargers. This shortened the development time and reduced the cost of the existing PBMM. For this reason the turbomachinery for the two-shaft PBMM will also be off-the-shelf turbochargers. Figure 3-2 shows a typical turbocharger with a centrifugal compressor and a radial flow turbine adopting the inboard mounted bearing arrangement.

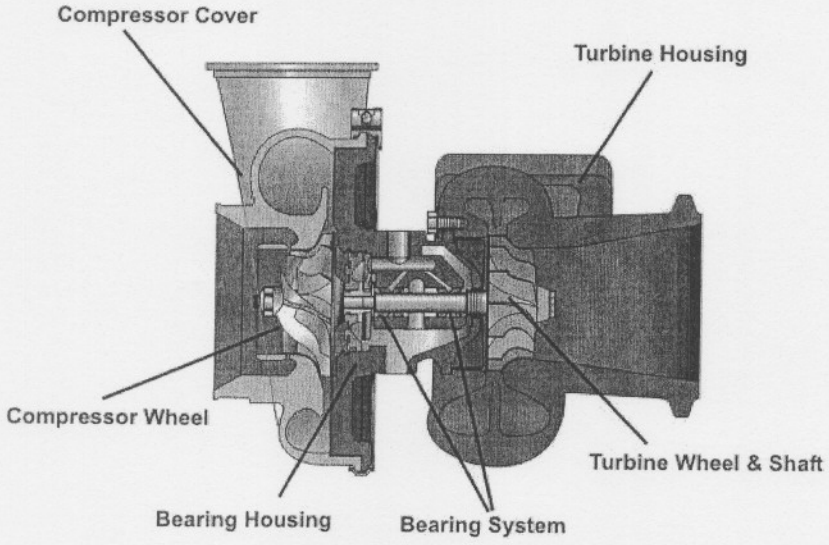

Figure 3-2 Typical turbocharger (TruckPro, 2005)

Although turbochargers operate successfully in the three-shaft PBMM, one problem encountered, was excessive wear on the HP thrust bearing. The thrust bearing capacity requirement is determined by disk pressures acting on the compressor and turbine, which are directly related to turbine and compressor design. One of the contributing factors is that the back face of the radial turbine in the turbocharger is heavily scalloped for reduced polar moment, while the compressor has a full back face for optimum aerodynamic efficiency (Baines, 2005:125).

Traditionally, turbochargers make use of fully floating journal bearings and tapered land thrust bearings. Ball bearings, however offer an attractive alternative (See Figure 3-3). Ball bearings have small frictional power losses, can be heavily overloaded and tolerate oil starvation for short periods. Traditionally low-cost roller bearings did not meet the durability requirements at the very high speed applications that are normal (Watson, 1982:43), but with the ever developing bearing technology, roller bearings are gradually being introduced in smaller and higher speed turbochargers (Baines, 2005:118).

Garrett (2005) discusses the advantages of roller bearings and it is subsequently summarized. Compared to sleeve bearings, ball bearings require less lubrication, are more tolerant to marginal lube conditions and are rotordynamically more stable. The angular contact bearing, further more eliminates the need for the thrust bearing, commonly a weak link in the turbo bearing system.

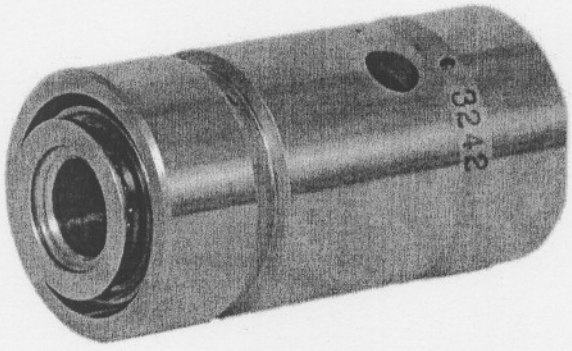

Figure 3-3 Typical turbocharger ball bearing (Garrett, 2005)

Based on the information above, the turbomachinery in the PBMM will be turbochargers, preferably with ball bearings.

3.2.2 Choice of load

Since the power turbine in the three-shaft PBMM is part of a turbocharger, already having a compressor, this compressor conveniently serves as load on the system. One of the major advantages of the two-shaft arrangement, however, is the use of the generator during start-up. Therefore the two-shaft PBMM must have a generator fitted to the LP shaft.

Conventionally a low speed (3000 rpm) wound rotor generator is used. At low power levels, however, optimum turbine speed increases above 3000rpm for optimum efficiency (Compact Power Systems, 2005). This means in order to accommodate the high speed of the turbocharger, the generator set must include a speed reduction gearbox. Alternatively a high speed generator can be used.

The incorporation of a high speed generator (mainly permanent magnet generators) has the following advantages (TAKASE, 2004):

- Higher efficiency with an operating efficiency of 98 %.
- Smaller footprint.
- Higher reliability and lower maintenance.
- Direct drive provides simplified assembly and integration.

Figure 3-4 shows the power and speed range capability of high speed permanent magnet generators (S2M, 2005).

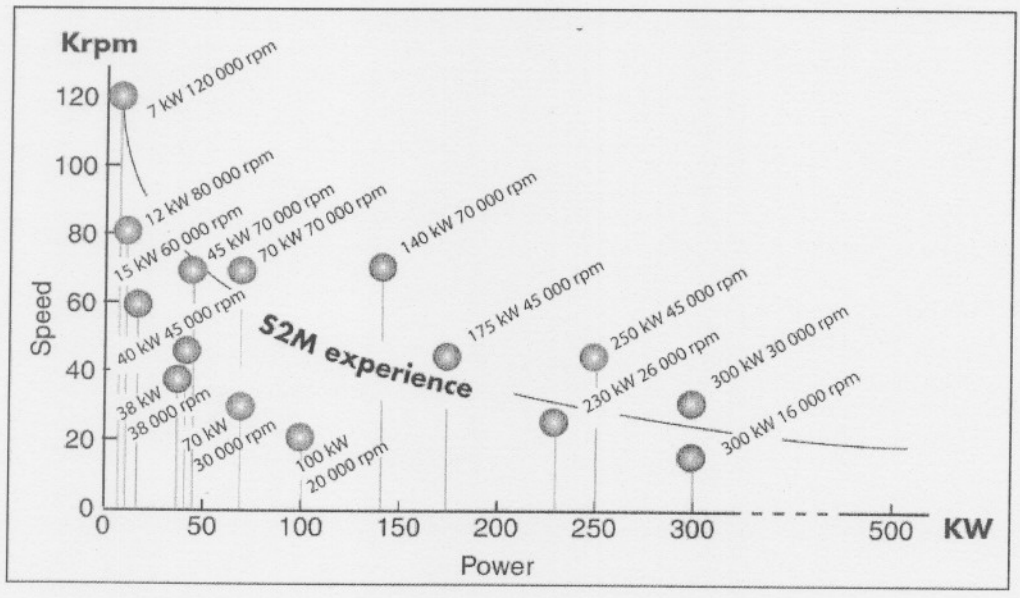

Figure 3-4 S2M power and speed range capability (S2M, 2005)

Although expensive, the high-speed permanent magnet generator is suggested for the load on the two-shaft PBMM configuration for the following reasons:

- The considerable reduction in size.
- High speed capability allows the use of turbocharger components for the LP rotor.

3.3 Conclusion

The major objective for the two-shaft PBMM configuration is to retain most of the major components of the existing three-shaft PBMM. To achieve this, the main specification of the two-shaft PBMM configuration is to be thermodynamically similar to the three-shaft PBMM configuration. In Table 3-1 the thermodynamic operating conditions of the three-shaft PBMM is tabulated. These operating conditions will therefore be targeted in the conceptual layout design of the two-shaft PBMM configuration.

The preliminary study focused on the choice of turbomachinery and the choice of load. It is suggested that the turbomachinery in the two-shaft PBMM configuration must be turbochargers with ball bearings. Ball bearings offer the potential of better stability and illuminate the vulnerability of traditional thrust bearings.

For the load on the two-shaft PBMM configuration a high speed generator was suggested for the following reasons:

- The considerable reduction in size.
- High speed capability allows the use of turbocharger components for the LP rotor.

4 THERMODYNAMIC DESIGN POINT CALCULATIONS

Chapter 2 identified thermodynamic design point studies as the first major design step in the conceptual design of a gas turbine. This chapter presents the integrated simulation performed to determine the optimum thermodynamic parameters.

4.1 The Pre-and Inter-cooled recuperative closed Brayton Cycle

Although the gas turbine cycle can take on a number of thermodynamic configurations, this study is concerned with the pre- and inter-cooled, recuperative, closed Brayton cycle. The T-s diagram in Figure 4-1 shows the thermodynamic processes involved in the pre- and inter-cooled, recuperative, closed Brayton cycle.

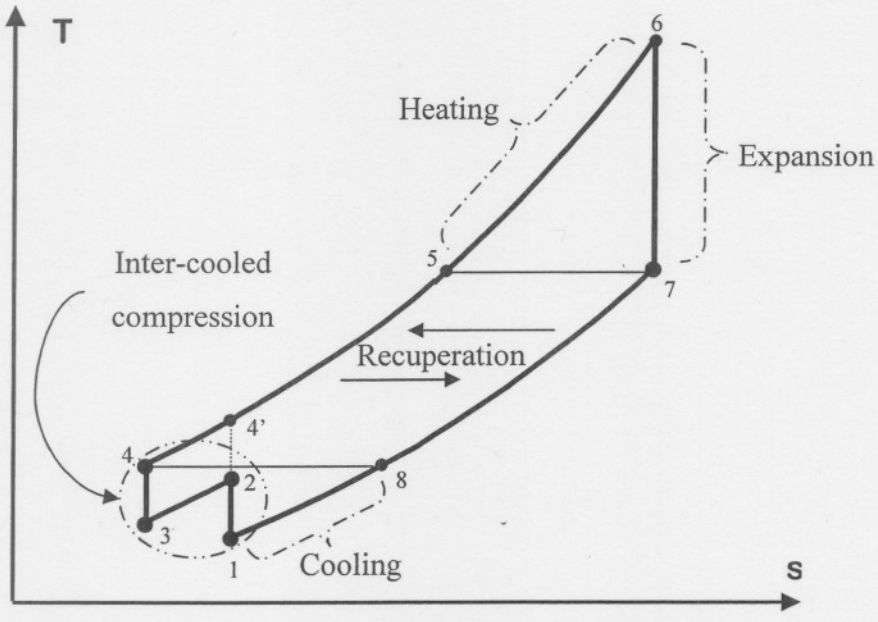

Figure 4-1 Idealized diagram for a pre- and inter-cooled, recuperative, closed Brayton cycle

Cycles with recuperation

The thermodynamic performance of a gas turbine is measured by the net power output and the thermal efficiency. In a simple gas turbine, consisting of the basic processes (compression, heating, expansion, and cooling), represented on Figure 4-1 as the process 1-4'-6-7-1, these two performance parameters are defined as:

The net power output:

$$Q_{net} = Q_{turbine} - Q_{compressor} = c_p(T_6 - T_7) - c_p(T_{4'} - T_1) \qquad (4\text{-}1)$$

The cycle efficiency:

$$\eta = \frac{net\ power\ output}{heat\ addition} = \frac{c_p(T_6 - T_7) - c_p(T_{4'} - T_1)}{c_p(T_6 - T_{4'})} \quad (4\text{-}2)$$

Cycle efficiency, however, can be increased by adding a recuperator. When incorporating a recuperator. the turbine outlet temperature is exposed to the compressor outlet temperature. This results in an increase of the heat source inlet temperature, and subsequently reduces the heat needed to be added. Equation (4-2) can now be rewritten as:

$$\eta = \frac{c_p(T_6 - T_7) - c_p(T_{4'} - T_1)}{c_p(T_6 - T_5)} \quad (4\text{-}3)$$

Since $T_5 > T_{4'}$, $c_p(T_6 - T_5) < c_p(T_6 - T_{4'})$, it can be seen that η is increased by the incorporation of a recuperator.

Cycles with inter-cooled compression

The work absorbed by a compressor is directly proportional to the absolute temperature at compressor inlet. In an adiabatic compressor a large pressure ratio will cause a large increase in temperature. The work required to accomplish an incremental pressure ratio at the latter part of the compression will be much larger than that for the same incremental pressure ratio in the low-pressure part. It is therefore an attractive option to split the compression process into several parts and cooling the compressed working fluid between the stages or groups of stages. The power required for compression, even with inefficient compressors, is less than that for isentropic compression (Wilson & Korakianitis, 1998:106).

Inter-cooled compression is represented by the process 1-2-3-4 on Figure 4-1. Without inter-cooling, compression takes place from 1-4'. The subsequent reduction in compression outlet temperature ($T_4 > T_4$) will increase the heat needed to achieve the required TIT. Therefore, an inter-cooler can only by utilized to its full extent if a recuperator is also incorporated.

Closed Cycles vs. Open cycles

The same thermodynamics apply to closed cycles than for open cycles. In open cycles air is compressed from atmosphere, mixed with fuel in a combustion process, expanded through a turbine, and discharged back to atmosphere. In a close cycle the working fluid is usually a gas with favourable characteristics suited to the application. If there is a requirement for low blade speeds and a low number of stages, a gas with high molecular weight is chosen. For nuclear

applications, however, gases like hydrogen or helium can be used to run at low Mach numbers and to utilize the favourable thermal and nuclear properties of these gases. This usually comes at the price of a large number of stages (Wilson & Korakianitis, 1998:157).

Heating in a closed cycle must take place without the degrading of the gas properties, which can be accomplished by external combustion or a nuclear reactor. Heat must be transferred to the fluid usually through heat-exchanger surfaces. Since these surfaces cannot be cooled in the same way the turbine blades are cooled, it normally leads to a lower TIT. Closed cycles make use of a pre-cooler to cool the working fluid back to compressor inlet temperature. This temperature will, therefore, be a little higher than ambient (Wilson & Korakianitis, 1998:157).

4.2 Simulation Model

In order to perform the thermodynamic design point analysis the cycle needs to be simulated in an integrated manner. A simulation model has the following generic structure (Rousseau, 2004):

- Conservation laws.
- Component characteristics: Heat transfer rates, pressure drops, efficiencies, etc.
- Fluid properties: Thermodynamic property tables, gas laws, etc.
- Boundary values: Temperatures, pressures, mass flows, etc

4.2.1 Conservation laws

All the components in the cycle are governed by the three conservation laws. These are the conservation of mass, momentum and energy.

Conservation of mass:

$$V\frac{\partial \rho}{\partial t} + \dot{m}_e - \dot{m}_i = 0 \qquad (4\text{-}4)$$

Conservation of momentum

Incompressible:

$$\rho L\frac{\partial V}{\partial t} + (p_{oe} - p_{0i}) + \rho g(z_e - z_i) + \Delta p_{oL} = 0 \qquad (4\text{-}5)$$

Compressible:

$$\rho L\frac{\partial V}{\partial t} + \frac{p}{p_0}(p_{oe} - p_{0i}) + \frac{1}{2}\rho V^2\frac{1}{T_0}(T_{0e} - T_{0i}) + \rho g(z_e - z_i) + \Delta p_{oL} = 0 \qquad (4\text{-}6)$$

Conservation of energy:

$$\dot{Q}+\dot{W}=V\frac{\partial}{\partial t}(\rho h_0-p)+\dot{m}_e h_{0e}-\dot{m}_i h_{0i}+\dot{m}_e g z_e-\dot{m}_i g z_i \qquad (4\text{-}7)$$

Since the thermodynamic design point analysis is the first step in the conceptual design process the following assumptions are made:

- Only steady-state conditions are investigated.
- The fluid is assumed to be incompressible.

The above assumptions result in the simplification of the conservation equations to the following:

- Mass conservation:

$$\dot{m}_e-\dot{m}_i=0 \qquad (4\text{-}8)$$

- Momentum conservation:

$$(p_{0e}-p_{0i})+\Delta p_{0L}=0 \qquad (4\text{-}9)$$

- Energy conservation:

$$\dot{Q}+\dot{W}=\dot{m}_e h_{0e}-\dot{m}_i h_{0i} \qquad (4\text{-}10)$$

Equations (4-8) through (4-10) are valid for any thermal-fluid component whether it is a pipe, heat exchanger or turbo machine. However, in order for these equations to be solved for a specific component it is necessary to calculate values for Δp_{0L}, $\dot{Q}$ and $\dot{W}$. These three parameters represent the specific characteristics of a particular component design. The level of complexity and accuracy with which the component characteristics are calculated will determine the level of complexity of the simulation model (Rousseau, 2004).

4.2.2 Component characteristics

During the first order cycle analysis, simplified component models are used to compute these characteristics. These component characteristics are summarized in Table 4-1.

Table 4-1 Component characteristics

Component	Δp_{0L}	$\dot{Q}+\dot{W}$
Pipe	$f_{pipe}\ p_{0i}$	0
Heat exchanger	$f_{HX}\ p_{0i}$	$\varepsilon\dot{Q}_{max}$ $\dot{Q}_{max}=C_{min}\Delta T_{max}$
Compressor	$p_{0i}(1-PR_c)$ $PR_c=\frac{p_{oe}}{p_{0i}}$	$\dot{m}c_pT_{0i}\frac{1}{\eta_c}\left(PR^{\left(\frac{\gamma-1}{\gamma}\right)}-1\right)$
Turbine	$p_{0i}(1-PR_t)$ $PR_t=\frac{p_{oi}}{p_{0e}}$	$\dot{m}c_pT_{0i}\eta_t\left(PR^{\left(\frac{\gamma-1}{\gamma}\right)}-1\right)$

4.2.3 Fluid properties

The working fluid in a gas turbine is a gas that is well removed from its liquefaction temperature in the cycle conditions chosen. A good approximation under these conditions is treating the working fluid as a perfect or semi-perfect gas, defined as a substance that obeys the equation of state, (4-11) (Wilson & Korakianitis, 1998:96):

$$pv = RT \qquad (4\text{-}11)$$

where p is the pressure, v is the specific volume, R is the gas constant and T the absolute temperature. During the thermodynamic design point calculations the aim is to gain better insight into the variations that might be expected from changes in cycle conditions. It is therefore convenient to assume perfect-gas behaviour since the calculations is simplified to a great extend.

4.2.4 Boundary values

Apart from component characteristics the performance of a gas turbine is determined by boundary values. Boundary values include minimum and maximum temperature, base pressure and mass flow.

4.3 Simulation of the two-shaft PBMM

4.3.1 Cycle layout

The schematic layout of the two-shaft PBMM is shown in Figure 4-2. Starting at 1, nitrogen at relative low pressure and temperature is compressed by the LPC to an intermediate pressure at 2, after which it is cooled in the IC from state 3 to 4. The HPC then compresses the nitrogen to the maximum cycle pressure at 6. From 7 to 8 the nitrogen is preheated in the high pressure side of the recuperator. At 10 the nitrogen reaches its highest temperature after being heated by the electrical heat source. The necessary work needed by the HPC is produced by the HPT, through expanding the nitrogen from 11 to 12. From 13 to 14 the expansion in the LPT produces the work needed by the LPC in addition to the useful shaft-work. From 15 to 16 the unused energy is utilized in the low-pressure side of the recuperator. In order to complete the cycle the nitrogen is cooled back to the minimum temperature in the PC from 17 to 18.

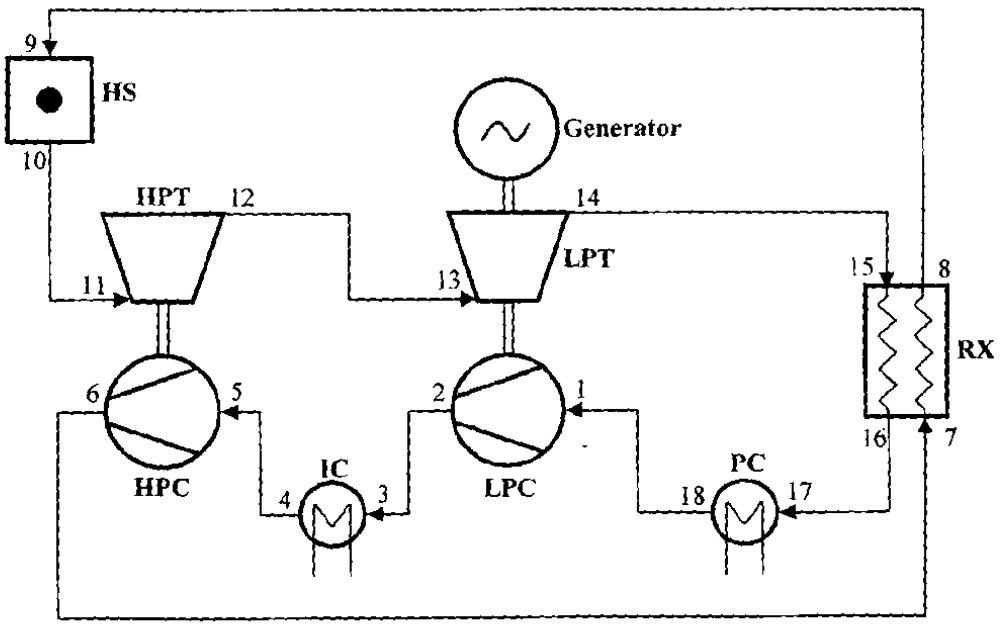

Figure 4-2 Cycle layout of the two-shaft PBMM

4.3.2 Assumptions and limitations

A number of parameters must be supplied as input to the model besides the minimum pressure and maximum temperature. This includes the magnitude of the pressure drops in pipes and heat exchangers, effectiveness of heat exchangers as well as efficiencies of compressors and turbines.

These values include the following assumptions (Greyvenstein & Rousseau, 2002):

- Pressure drops in pipes are equal to 0.6% of the absolute pressure at the inlet to the pipe.
- Pressure drops in the recuperator and the heat exchangers are 0.5% of the absolute pressure at the inlet.
- The isentropic efficiencies of the compressors are 76%, which is realistic for a turbocharger compressor.
- The isentropic efficiencies of the turbine are 72%.
- The effectiveness if the pre- and inter-cooler are 95%.
- Effectiveness of the recuperator is taken as 88%.

Base pressure and mass flow

The barometric pressure on location in Potchefstroom is approximately 86 kPa. In order to prevent leakage of air into the system the minimum base pressure was set to 100 kPa. Since closed cycles use inventory control, the base pressure can be controlled. Similar to the three-shaft PBMM the two-shaft PBMM will be designed to achieve part-load conditions of about 40% MCR. Since power output is linear to the base pressure this means a maximum base pressure of 250 kPa.

The mass flow rate is dependent on the base pressure. The relation between base pressure and mass flow rate is influenced by the size of the turbomachinery. As the turbomachinery has not been selected at this stage, the mass flow rate is taken as unity.

Maximum temperature

The maximum temperature in the PBMM is limited by the maximum temperature allowed for the HPT blades. Since the turbochargers will not be operated near the upper extremes of their rotational speeds, a maximum temperature of 700°C is acceptable.

Minimum temperature

The minimum temperature is dictated by the supply temperature of the cooling water and is taken as 20°C.

Pressure ratio

One of the aims of the thermodynamic design point calculations is to optimise the OPR to achieve optimal cycle performance. Since the cycle incorporates a recuperator two OPRs will exist, one for maximum efficiency and one for maximum power output.

Saravanamuttoo *et al.* (2003:52) explains cycles with inter-cooled compression. If the compression is split into a LPC and a HPC, the cycle efficiency is at a maximum when the OPR is divided equally between the compressors, provided that the working fluid is inter-cooled to the same temperature prior to compression. Table 4-2 gives a summary of the assumptions discussed above.

Table 4-2 First order cycle analysis assumptions.

Cycle Parameter	Assumption
p_{min}	100 - 250 kPa
$\dot{m}$	1 kg/s
T_{max}	700 °C
α_{pipe}	0.006
α_{hx}	0.005
η_c	0.76
η_t	0.69
PR_{HPC}	PR_{LPC}
η_m	0.98
ε_{rx}	0.88
ε_{hx}	0.95

4.3.3 Optimum OPR

Optimum OPR for maximum cycle power output

To one extreme, a small OPR (close to unity) will result in little work needed by the compressors but, subsequently also in little work produced by the turbines. Net power, therefore, will be insignificantly small. To the other extreme, having a large OPR will result in a high temperature rise during compression. Little or no heat can therefore be added to reach the maximum TIT limit. This results in the immediate expansion to the base pressure. Consequently, turbine work will be less than compressor work, producing no useful output. In

between these two unwanted extremes there is an OPR at which net work produced is at a maximum. Adding a recuperator to improve the efficiency of the cycle, assuming no additional pressure losses through the recuperator, will have no effect on this optimum OPR for maximum power output (Wilson & Korakianitis, 1998:97).

The simulation model set up in EES was therefore used to conduct a parametric study. Figure 4-3 shows the variation of power output with changes in OPR. At an OPR of 4.414 the power output is at a maximum of 52.26 kW/kg s.

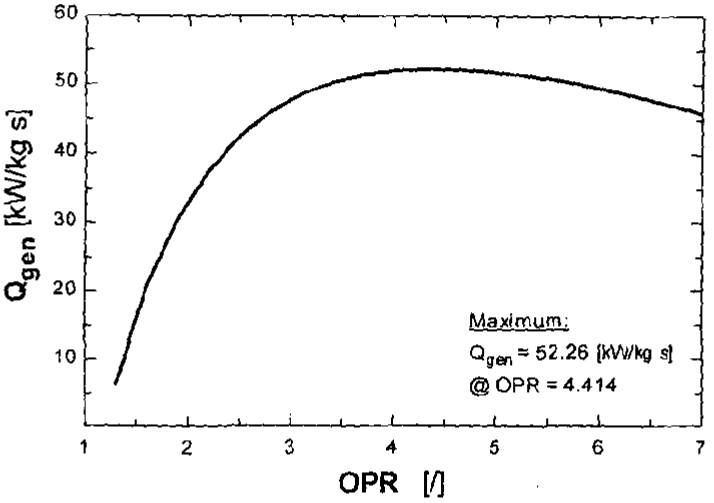

Figure 4-3 Specific power output as a function of OPR

Optimum OPR for maximum cycle efficiency

The choice of OPR for maximum efficiency is greatly affected by the addition of a recuperator. If the cycle does not incorporate a recuperator, maximum efficiency will be at approximately the same OPR as that for maximum power output. However, including a recuperator will result in an optimum OPR, for maximum efficiency, lower than that for maximum power output (Wilson & Korakianitis, 1998:101).

In order to demonstrate this statement, assume recuperator effectiveness of unity (meaning compressor discharge will be brought up to the turbine outlet temperature) and zero pressure losses through the recuperator. Increasing the OPR above the OPR for maximum power output, results in a decrease of turbine outlet temperature. Subsequently the heat source inlet temperature also falls, and more heat must be added to keep the TIT at the desired level. When, on the other hand, the OPR is decreased below that for maximum power output, the turbine outlet temperature will rise and with it the heat source inlet temperature. This results

in a reduction of heat that needs to be supplied to achieve the desired TIT. Therefore, the optimum OPR for maximum cycle efficiency is lower than that for maximum power output when a recuperator is incorporated (Wilson & Korakianitis, 1998:102).

The variation of cycle efficiency as a function on OPR for the two-shaft PBMM is shown in Figure 4-4. At an OPR of 2.88 the cycle efficiency is at a maximum of 19.2 %.

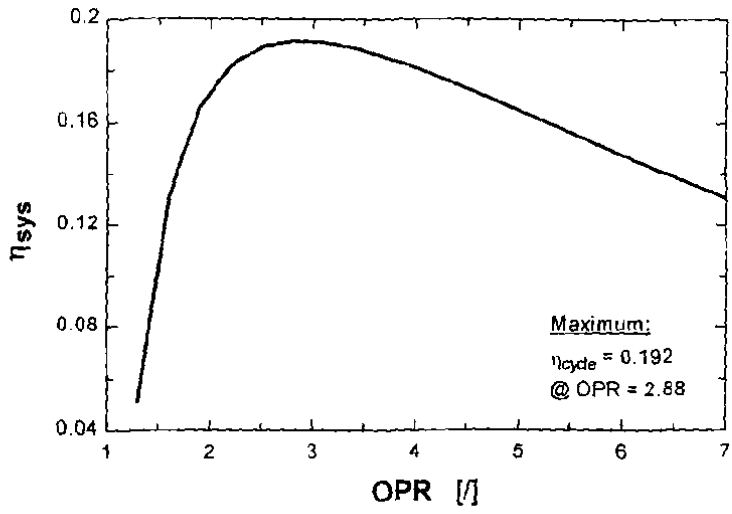

Figure 4-4 Cycle efficiency as a function of OPR

Choice of OPR

Botha (2002) explains that since industrial applications are intended to operate for extended periods, the drive is normally to improve cycle efficiency rather than power output. Usually this will be achieved by custom designed turbomachinery. In the case of the PBMM, however, off-the-shelf turbochargers are used resulting in that the exact OPR cannot be specified. Therefore, at this stage of the design process, the OPR can only be narrowed down to the range of OPRs that exist between maximum efficiency and maximum power output (Figure 4-5).

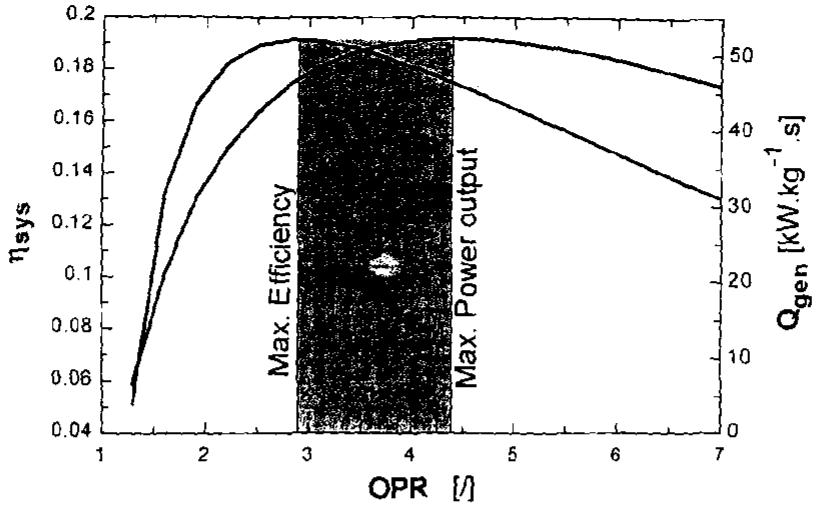

Figure 4-5 OPR range

The matching of turbochargers, allowing the operation of the cycle at an OPR between 2.88 and 4.414, with the highest cycle efficiency will be selected. Figure 4-6 shows a T-s diagram of the cycle at maximum efficiency.

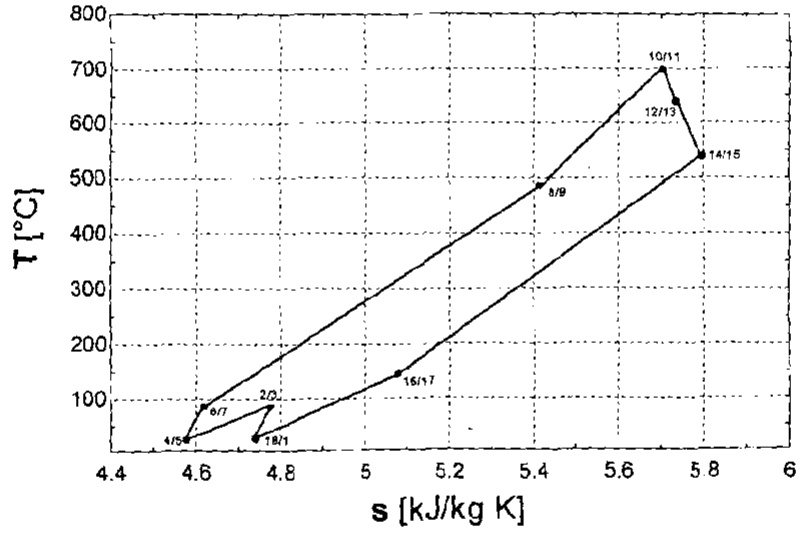

Figure 4-6 T-s diagram at maximum efficiency

4.4 Sensitivity analysis

Figure 4-3 and Figure 4-4 can be combined to form the graph in Figure 4-7. The graph shows the variation of cycle efficiency with specific power output as a function of OPR. The performance of the system is dependent on the values supplied in Table 4-2. Compressor efficiency, turbine efficiency, mass flow and pressure ratio sharing is dependent on the turbocharger selection while the base pressure and TIT is used to alter the cycle output during part-load operation. For this reason the sensitivity of the cycle to changes in these parameters are investigated.

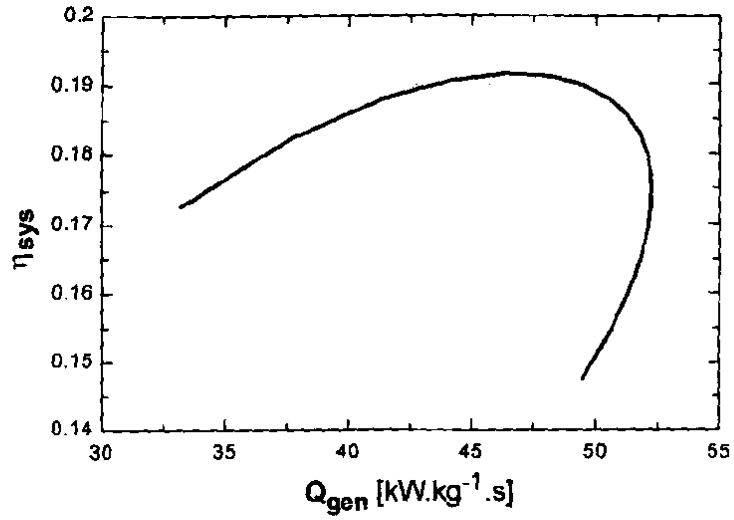

Figure 4-7 Cycle efficiency versus specific power output as a function of OPR

4.4.1 Turbomachinery efficiencies

In Table 4-2, efficiencies for the turbomachinery were assumed. Although they are realistic, they are not always correct and will only be known after the effects the turbomachinery have on each other had been taken into account. It is therefore necessary to investigate the sensitivity of the cycle performance to changes in turbomachinery efficiency.

Figure 4-8 shows the variation of efficiency with specific power output as a function of OPR at various compressor efficiencies. It is obvious from the graph that both efficiency and power output is reduced by a reduction in compressor efficiency.

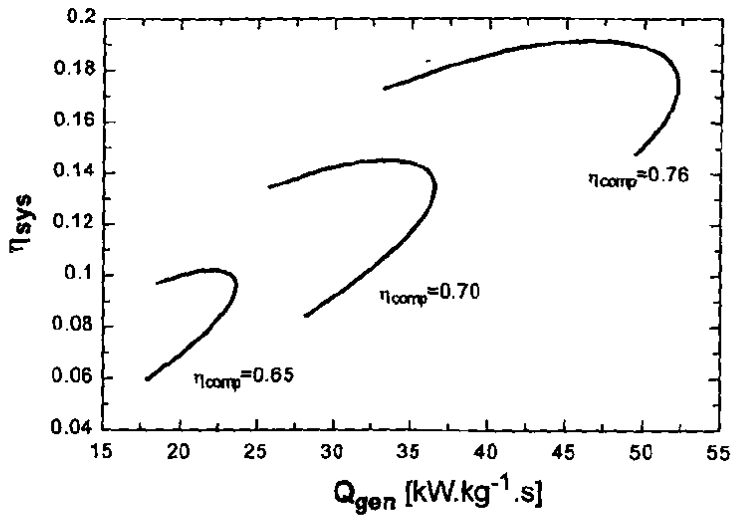

Figure 4-8 Cycle efficiency versus specific power output as a function of OPR and compressor efficiency

Figure 4-9 shows the variation of efficiency with specific power output as a function of OPR at various turbine efficiencies. It is obvious from the graph that both efficiency and power output is reduced by a reduction in turbine efficiency.

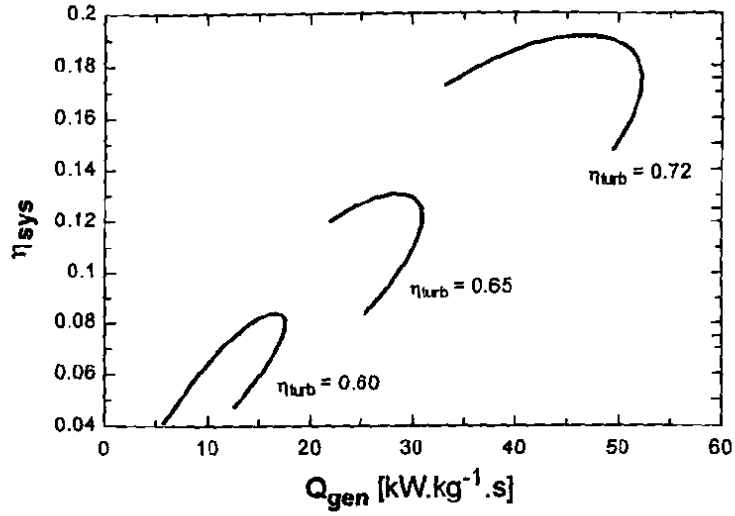

Figure 4-9 Cycle efficiency versus specific power output as a function of OPR and turbine efficiency

4.4.2 Pressure ratio sharing

Figure 4-10 and Figure 4-11 illustrates the importance of the OPR to be equally divided between the LPC and HPC. It is clear from the graphs that both power output and cycle efficiency rapidly decreases if the OPR is not equally shared between the two compressors.

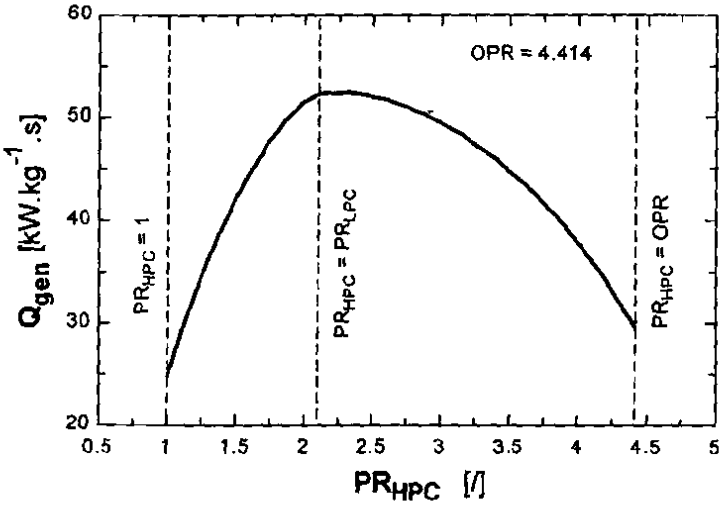

Figure 4-10 Specific power output as a function of PR_{HPC}

Figure 4-10 shows the sensitivity of specific power output to PR_{HPC} for a constant OPR. When the OPR is divided equally between the two compressors, meaning $PR_{HPC} = PR_{LPC}$, the specific power output is at it maximum.

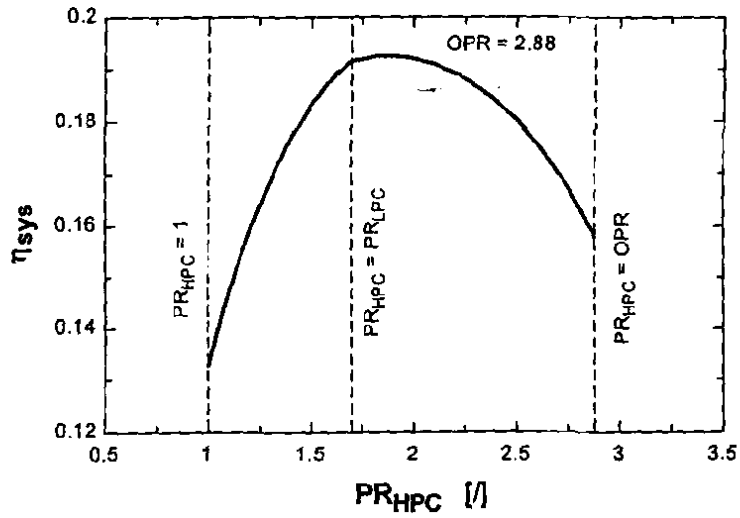

Figure 4-11 Cycle efficiency as a function of PR_{HPC}

Figure 4-11 shows the sensitivity of cycle efficiency to PR_{HPC} for a constant OPR. The cycle efficiency is at a maximum where PR_{HPC} is slightly higher than PR_{LPC}. Possibly because T_5 is slightly lower that T_1.

4.4.3 Maximum temperature and mass flow

The TIT is often used to change the power output of the cycle, however, looking at Figure 4-12 it is clear that the reduction in power output comes at the expense of cycle efficiency.

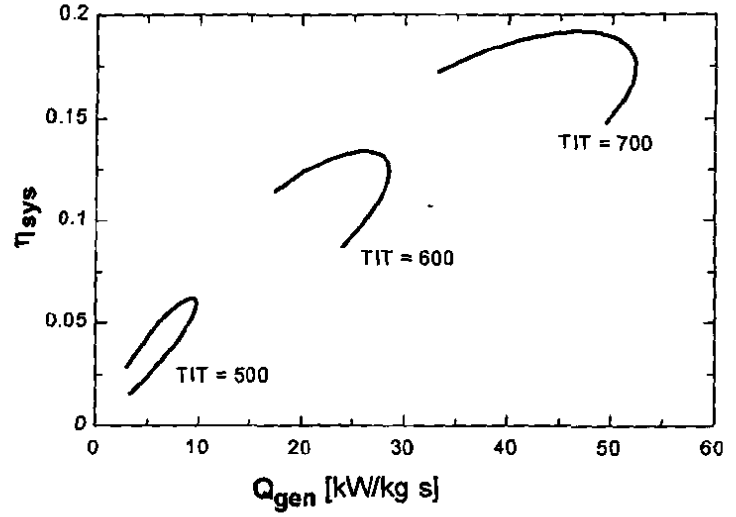

Figure 4-12 Cycle efficiency versus specific power output as a function of OPR and TIT

Having a closed cycle, however, permits the use of inventory control to alter the cycle power output. This type of control allows all temperatures, volume flow rates, velocities and pressure ratios in the cycle to remain approximately the same. By varying the pressure inside the cycle, the mass flow is changed to adjust power output of the cycle (See Paragraph 2.2.3).

Since mass flow is determined by the size of the turbomachinery, the initial assumption was to take mass flow as unity. Once the turbomachinery are selected, however, mass flow becomes a function of the pressure inside the cycle, according to Equation (2-1). Assuming that turbomachinery efficiency is maintained at these various mass flows, it can be seen (Figure 4-13) that cycle efficiency remained constant while the specific power output increased with an increasing mass flow rate.

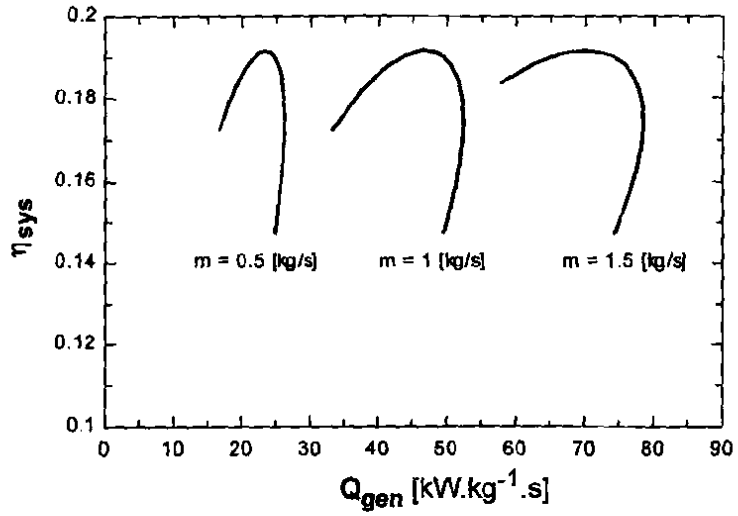

Figure 4-13 Cycle efficiency versus specific power output as a function of OPR and mass flow rate

Figure 4-14 shows that the shape of the T-s diagram stays virtually unchanged at different pressure levels. This means that pressure -and temperature ratios remain unaffected and therefore also the cycle efficiency.

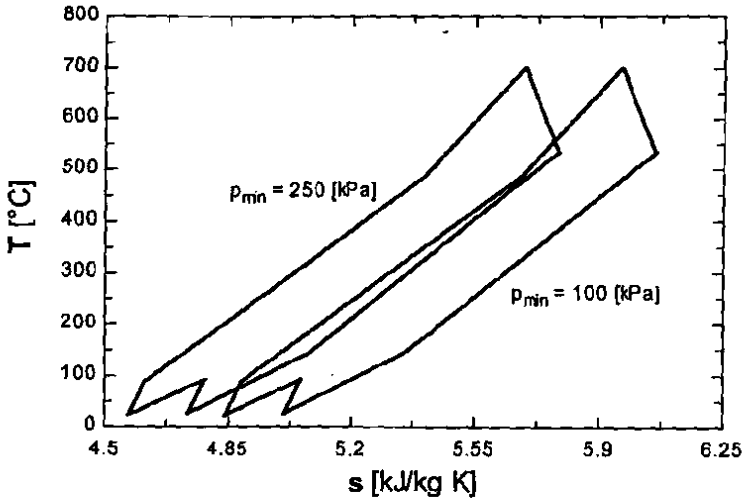

Figure 4-14 T-s diagram for minimum and maximum base pressure

4.5 Conclusion

In this chapter the thermodynamic design point study of the two-shaft PBMM was presented. Simplified equations for conservation of mass, momentum and energy were derived for all the components making up the two-shaft PBMM. These equations were implemented in an EES program. As input to this simulation model, a number of assumptions were made together with the identification of limitations of the PBMM. These assumptions and limitations were summarized in Table 4-2.

Through a parametric study the effect of cycle performance as a function of OPR was investigated. Two optimum values for OPR was found, one for maximum cycle efficiency at 2.88, and one for maximum cycle power output at 4.414. Normally turbomachinery will be custom designed to achieve maximum cycle efficiency. In the case of the PBMM, however, an off-the-shelf turbocharger will be selected. The OPR was therefore only narrowed down to the range of OPRs that exists between maximum efficiency and maximum power output, Figure 4-5.

The values supplied in Table 4-2, although realistic, are not correct since they are dependent on the final selection of the turbomachinery. Therefore a sensitivity analysis was conducted, which had the following results:

- Cycle efficiency and cycle power output is reduced by reduction in turbine and compressor efficiency.
- For optimum power output and cycle efficiency the OPR must be equally shared between the LPC and HPC.
- A reduction of the TIT results in a reduction of power output and cycle efficiency.
- As mass flow decreases so does cycle power output at constant cycle efficiency.

These results are used in Chapter 5 to identify a suitable turbocharger paring.

5 TURBOCHARGER SELECTION

In the previous chapter the thermodynamic design point study of the two-shaft PBMM was presented and the optimum thermodynamic conditions were determined. In this chapter the turbocharger selection is done to achieve these optimum conditions.

The chapter begins with a discussion on the characteristics of compressors and turbines as individual components. This is followed by an investigation on how these components interact with each other in a two-shaft pre- and inter-cooled recuperative closed Brayton cycle. Finally the chapter finishes off with the turbocharger selection.

5.1 Compressor characteristics

Compressor characteristics are specified by curves of delivery pressure and temperature plotted against mass flow for various fixed values of rotational speed. However, these characteristics are dependent on other variables such as the conditions of pressure and temperature at the entry of the compressor and the physical properties of the working fluid. The full variation of these properties would involve an excessive number of experiments and a practical presentation of these results would prove to be impossible. In Saravanamuttoo *et al.* (2001:173) this complication is eliminated by using the technique of dimensional analysis. Through dimensional analysis the variables may be combined to form a more manageable number of dimensional groups. The dimensional analysis of a compressor is backed by the following important points:

- When considering the dimension of temperature it is useful to associate it with the gas constant R. This results in a combined variable RT that is equal to p/ρ and has the dimensions $ML^{-1}T^{-2}/ML^{-3} = L^2T^{-2}$, which is the same as $(\text{velocity})^2$. Using the same gas during the testing and subsequent use of the compressor, R can finally be eliminated. However, if there is a change from one gas to another, R must be retained in the final expression.
- The behaviour of the compressor is undoubtedly influenced by the density of the gas. If the pressure p and the RT product is also sited, however, its inclusion is not required since $\rho = p/RT$.
- The viscosity μ of the gas can be included since in theory it will also influence the behaviour of the compressor. The addition of this variable would result in the

emergence of the Reynolds number. Due to the highly turbulent flow during normal operating conditions for compressors, experience indicates that the influence of this variable is negligibly small, and its effect may be excluded.

Keeping the above points in mind, the various quantities, which will influence the behaviour of the compressor and dependent on it, can be considered. The solution takes on the form of an equation in which a function of all the variables equates to zero.

$$f_1(D, N, \dot{m}, p_{01}, p_{02}, RT_{01}, RT_{02}) = 0 \quad (5\text{-}1)$$

Where D is a characteristic geometrical parameter of the compressor, usually taken as the impeller diameter and N is the rotational speed. The subscripts 1 and 2 denote the inlet and exit stations respectively.

Using dimensional analysis, the seven variables of Equation (5-1) can be reduced to four non-dimensional groups. The resulting dimensionless parameters are:

$$f_2\left(\frac{p_{02}}{p_{01}}, \frac{T_{02}}{T_{01}}, \frac{\dot{m}\sqrt{RT_{01}}}{D^2 p_{01}}, \frac{ND}{\sqrt{RT_{01}}}\right) = 0 \quad (5\text{-}2)$$

For a compressor the pressure ratio is defined as

$$PR_c = \frac{p_{02}}{p_{01}} \quad (5\text{-}3)$$

Using isentropic flow relations, it is possible to replace the temperature ratio parameter with isentropic efficiency. For a compressor isentropic efficiency is defined as

$$\eta_c = \frac{\left(PR_c^{(\gamma-1)/\gamma} - 1\right)}{\left(\frac{T_{02}}{T_{01}} - 1\right)} \quad (5\text{-}4)$$

Subsequently, for a compressor, Equation (5-2) reduces to

$$f_2(PR_c, \eta_c, NDM, NDS) = 0 \quad (5\text{-}5)$$

Where the Non-Dimensional Mass flow rate (NDM) is defined as

$$NDM = \frac{\dot{m}\sqrt{RT_{01}}}{D^2 p_{01}} \quad (5\text{-}6)$$

And the Non-dimensional Speed (NDS) is defined as

$$NDS = \frac{ND}{\sqrt{RT_{01}}} \qquad (5\text{-}7)$$

5.1.1 Compressor performance maps

Using the four variables in Equation (5-5), the performance for any compressor can be given as a set of two curves, namely pressure ratio as a function of NDM for various constant NDS curves (Figure 5-1), as well as isentropic efficiency, plotted in the same manner (Figure 5-2). These curves, although plotted in two dimensions, are really representing a surface formed in three-dimensional space (Flownex, 2005).

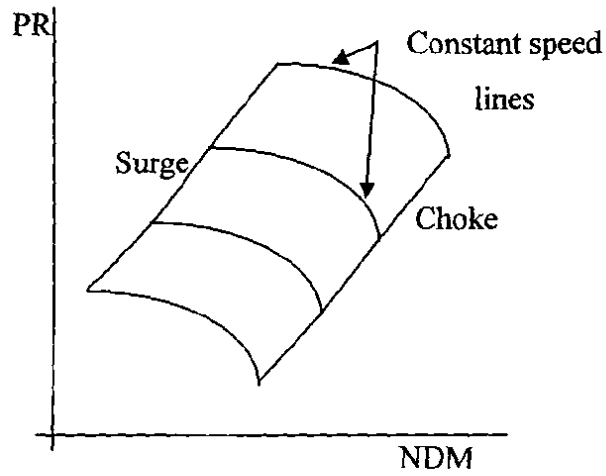

Figure 5-1 Typical compressor pressure ratio characteristic

The compressor map in Figure 5-1 shows three identifiable regions. The region to the left is known as the surge region while the region to the right is known as the choke region. Stable operation is represented by the region bounded by these two unwanted regions of instability.

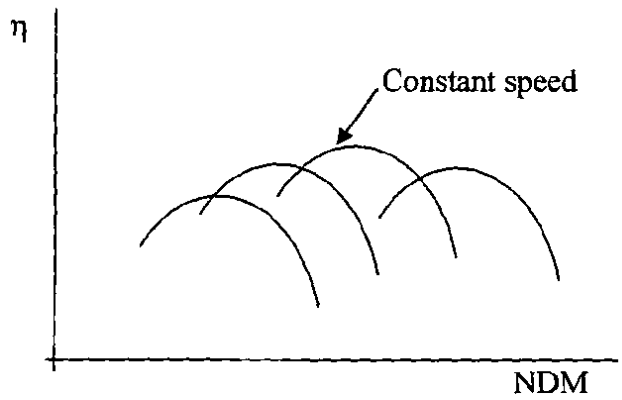

Figure 5-2 Typical compressor efficiency characteristic

5.2 Turbine characteristics

Turbine characteristics can be represented in the same manner as a compressor by the four non-dimensional groups in Equation (5-2). For a turbine the pressure ratio is defined as:

$$PR_t = \frac{p_{0i}}{p_{02}} \tag{5-8}$$

Using isentropic flow relations, it is possible to replace the temperature ratio in Equation (5-2) with isentropic efficiency. For a turbine isentropic efficiency is defined as:

$$\eta_t = \frac{\left(PR_t^{(\gamma-1)/\gamma} - 1\right)}{\left(\frac{T_{02}}{T_{01}} - 1\right)} \tag{5-9}$$

Subsequently, for a turbine Equation (5-2) reduces to

$$f_2\left(PR_t, \eta_t, NDM, NDS\right) = 0 \tag{5-10}$$

where NDM and NDS are defined by Equation (5-6) and (5-7) respectively.

5.2.1 Turbine performance maps

Using the four variables in Equation (5-10), the performance for any turbine can be given as a set of two curves, namely pressure ratio as a function of NDM for various NDS (Figure 5-3), as well as the isentropic efficiency plotted in the same manner (Figure 5-4).

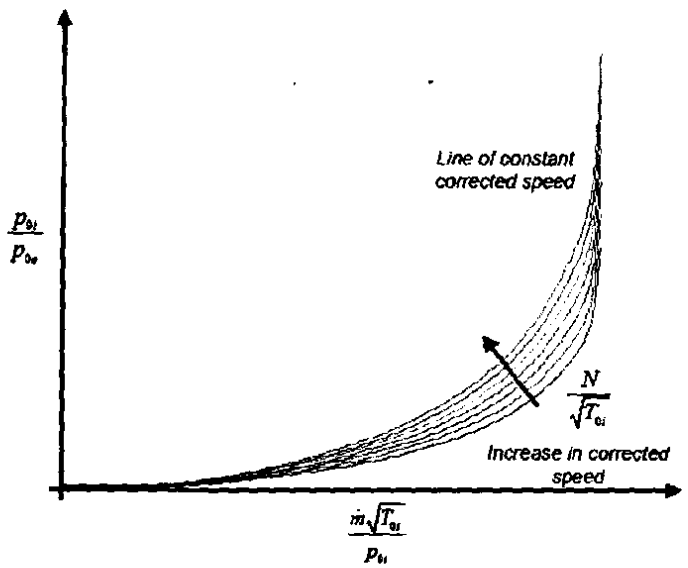

Figure 5-3 Typical turbine pressure ratio characteristic (Flownex, 2005)

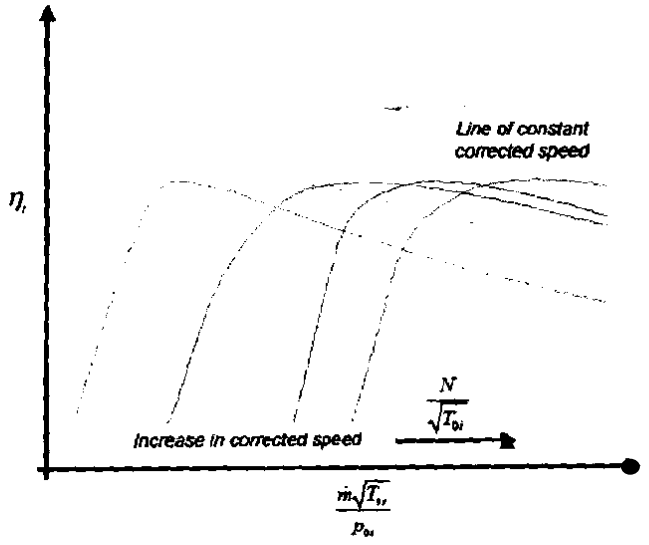

Figure 5-4 Typical turbine efficiency characteristic (Flownex, 2005)

In practice, however, it is found that turbines do not exhibit significant variation in NDM with variation in NDS. The turbine operating region is in most cases restricted by the component downstream of it (Saravanamuttoo *et al.*, 2001:378).

5.3 Prediction of performance

The design point for a system is defined as being the point of operation when the system is operating at the specific speed, optimum pressure ratio and mass flow for which the components where designed. Off-design performance is defined as the complete operating range of speed and power output that is achievable by the system (Saravanamuttoo *et al.*, 2001:374).

Performance characteristics for individual components are determined by experience or obtained by actual tests. When components are linked together, however, the component's range of possible operation is considerably reduced. Depending on the cycle layout various parameters can be changed to deliver a range of possible engine outputs. For various specific speeds the influence of changes in the controllable parameters are plotted on the compressor maps to form equilibrium running diagrams. The engine is in equilibrium when the engine is operating at a steady speed. The equilibrium running diagrams shows the proximity of the operating points to compressor surge and if the compressor is operating in a region of adequate efficiency. The aim is to keep the compressor operating point near the locus of maximum compressor efficiency for the complete operating range of the engine (Saravanamuttoo *et al.*, 2001:374). The unique relationship that exists between the

components for the two-shaft pre- and inter-cooled recuperative closed Brayton cycle is discussed in Paragraph 5.4

Depending of the cycle layout, the engine will reveal a variation of efficiency with reduction in power output. This phenomenon referred to as part load performance, is of major importance where the engine is required to operate at reduced power for extended periods (Saravanamuttoo *et al.*, 2001:375).

5.4 Turbo machine matching of a two-shaft pre- and inter-cooled recuperative closed Brayton cycle

In Saravanamuttoo *et al.* (2001) matching procedures for various cycle configurations are described. These cycles are all open cycles, however, the fundamentals of satisfying work and flow compatibility are just as appropriate when dealing with closed cycles. Therefore, as a result of the literature found in Saravanamuttoo *et al.* (2001), the unique relationship that exists between the components was derived for the two-shaft pre- and inter-cooled recuperative closed Brayton cycle. Figure 5-5 shows the turbomachinery layout of the two-shaft PBMM.

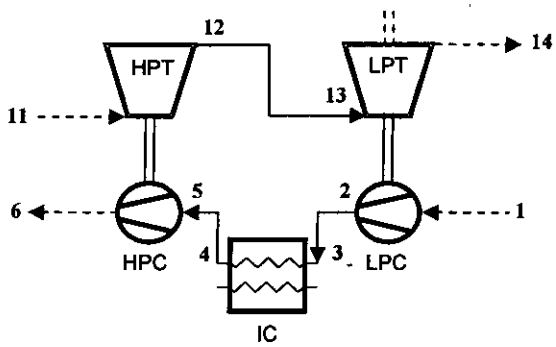

Figure 5-5 Two-shaft PBMM turbomachinery layout

5.4.1 Turbines in series

The matching of two-shaft engines can be considerably simplified if the behavior of turbines in series is considered. The value of $\dot{m}\sqrt{T_{012}}/p_{012}$ at HPT exit can be calculated from Equation (5-11).

$$\frac{\dot{m}\sqrt{T_{012}}}{p_{012}} = \frac{\dot{m}\sqrt{T_{011}}}{p_{011}} \times \frac{p_{011}}{p_{012}} \times \frac{\sqrt{T_{012}}}{\sqrt{T_{011}}} \qquad (5\text{-}11)$$

where

$$\frac{\sqrt{T_{012}}}{\sqrt{T_{011}}} = \sqrt{1 - \frac{\Delta T_{0HPT}}{T_{011}}} \qquad (5\text{-}12)$$

and

$$\frac{\Delta T_{0HPT}}{T_{011}} = \eta_{HPT}\left[1 - \left(\frac{1}{p_{011}/p_{012}}\right)^{(\gamma-1)/\gamma}\right] \qquad (5\text{-}13)$$

Applying Equations (5-11) through (5-13) to the points on the single curve of the HPT characteristic, a single curve representing the HPT outlet flow characteristics can de obtained. The result is shown by the dotted line in the Figure 5-6.

The effect of operating two turbines in series is shown in the Figure 5-6, where it can be seen that the requirement for flow compatibility between the two turbines places a major restriction on the operation of the HPT. In particular, as long as the LPT is choked, the HPT will operate at the fixed point marked (a). With the LPT unchoked, the HPT will be restricted to operate at a fixed pressure ratio for each LPT pressure ratio, e.g. (b) and (c).

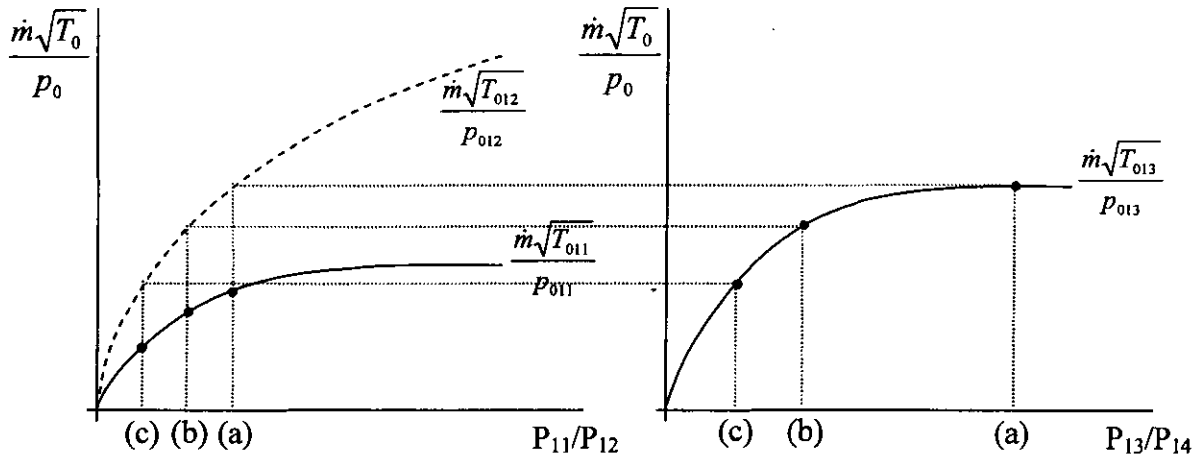

Figure 5-6 Behaviour of turbines in series

Thus the maximum pressure ratio across the HPT is determined by the choking of the LPT, and at all times the HPT pressure ratio is controlled by the swallowing capacity of the LPT. Therefore a fixed relation exists between pressure ratios of the HPT and the LPT.

5.4.2 HP rotor

The effect of the HPT on the HPC characteristics can be determined by considering the HP rotor alone, for flow and work compatibility.

Flow compatibility:

The relation that exists between the HPT and HPC for flow compatibility is given by Equation (5-14)

$$\frac{\dot{m}\sqrt{T_{011}}}{p_{011}} = \frac{\dot{m}\sqrt{T_{05}}}{p_{05}} \times \frac{p_{05}}{p_{06}} \times \frac{p_{06}}{p_{011}} \times \frac{\sqrt{T_{011}}}{\sqrt{T_{05}}} \qquad (5\text{-}14)$$

where

$$\frac{\dot{m}\sqrt{T_{011}}}{p_{011}} = NDM_{HPT}, \quad \frac{\dot{m}\sqrt{T_{05}}}{p_{05}} = NDM_{HPC}, \quad \frac{p_{05}}{p_{06}} = \frac{1}{PR_{HPT}} \text{ and } \frac{p_{06}}{p_{011}} = PR_{loss}.$$

Equation (5-14) can therefore be rewritten as:

$$PR_{HPC} = \left(\frac{1}{NDM_{HPT}} \times PR_{loss} \times \frac{\sqrt{T_{011}}}{\sqrt{T_{05}}} \right) \times NDM_{HPC} \qquad (5\text{-}15)$$

Where:

- PR_{loss} is the pressure ratio across the recuperator and the heat source assumed to be constant and close to unity.
- $\frac{\sqrt{T_{011}}}{\sqrt{T_{05}}}$ is unchanged since inventory control is used in a closed cycle

Therefore, unique lines exist on the HPC characteristic, for constant values of NDM_{HPT}. Figure 5-7 shows a typical HPC compressor map with superimposed HPT flow compatibility lines.

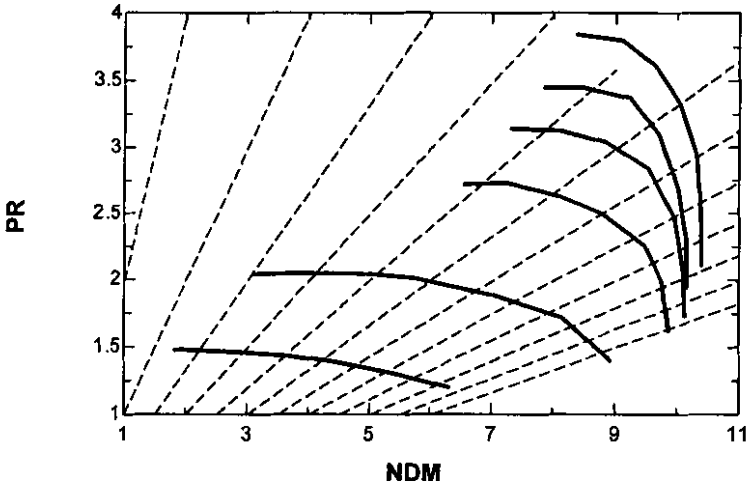

Figure 5-7 Flow compatibility of the HP rotor

Work compatibility:

The relation that exists between the HPT and HPC for work compatibility is given by Equation (5-16).

$$\frac{\Delta T_{0HPT}}{T_{011}} = \frac{\Delta T_{0HPC}}{T_{05}} \times \frac{T_{05}}{T_{011}} \times \frac{cp_h}{cp_c \eta_{mH}} \qquad (5\text{-}16)$$

where

$$\frac{\Delta T_{0HPT}}{T_{011}} = \eta_{HPT}\left[1-\left(\frac{1}{PR_{HPT}}\right)^{(\gamma-1)/\gamma}\right] \qquad (5\text{-}17)$$

and

$$\frac{\Delta T_{0HPC}}{T_{05}} = \frac{1}{\eta_{HPC}}\left[PR_{HPC}{}^{(\gamma-1)/\gamma} - 1\right] \qquad (5\text{-}18)$$

Therefore, assuming constant $\frac{T_{05}}{T_{011}}$, unique lines exist on the HPC characteristic, for constant values of PR_{HPT}. Figure 5-8 shows a typical compressor map with superimposed work compatibility lines.

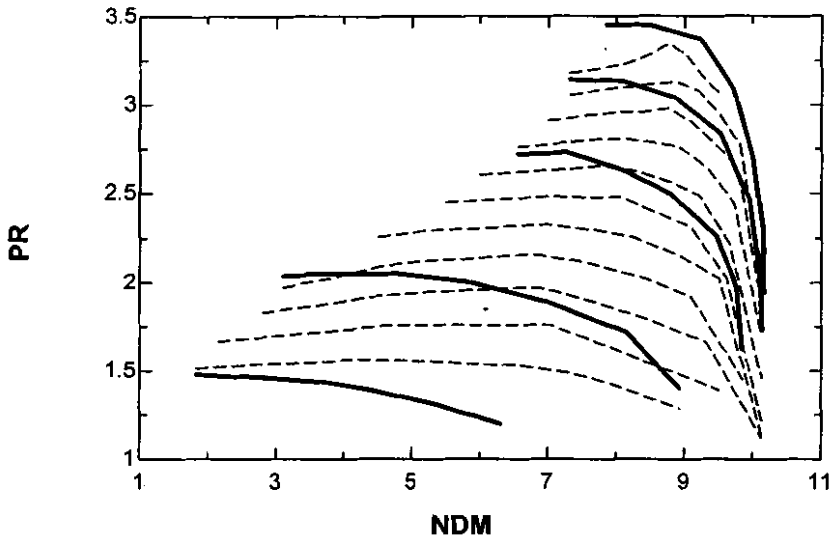

Figure 5-8 Work compatibility of the HP rotor

HPC flow compatibility is only a function of NDM_{HPT} (5-15) and work compatibility is only a function of PR_{HPT} (5-16). Therefore, the intersection of the flow and work compatibility lines acquired from a point on the HPT characteristic provides a unique matching point on the HPC characteristic. Such a matching point exists for every point on the HPT characteristic. Joining up the matching points a matching line can be acquired. Figure 5-9 shows a typical HPC characteristic map with a superimposed HPT matching line.

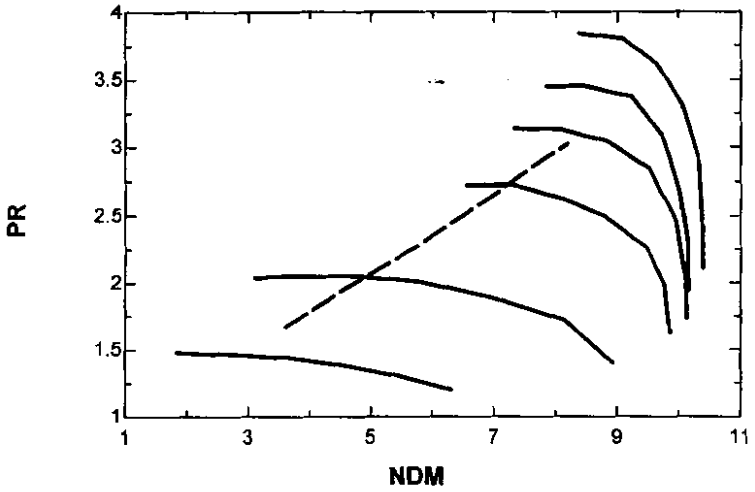

Figure 5-9 HP rotor matching line

5.4.3 LP rotor

Flow compatibility:

The relation that exists between the HPC and LPC for flow compatibility is given by Equation (5-19).

$$\frac{\dot{m}\sqrt{T_{05}}}{p_{05}} = \frac{\dot{m}\sqrt{T_{01}}}{p_{01}} \times \frac{p_{01}}{p_{02}} \times \frac{p_{02}}{p_{05}} \times \frac{\sqrt{T_{05}}}{\sqrt{T_{01}}} \qquad (5\text{-}19)$$

The above flow compatibility equation can be rewritten as:

$$PR_{LPC} = \left(\frac{1}{NDM_{HPC}} \times PR_{IC} \times \frac{\sqrt{T_{05}}}{\sqrt{T_{01}}} \right) \times NDM_{LPC} \qquad (5\text{-}20)$$

Where:

- PR_{IC} the pressure ratio across the inter-cooled is assumed to be constant close to unity.
- $\frac{\sqrt{T_{05}}}{\sqrt{T_{01}}}$ is assumed to be constant for a closed cycle (Close to unity).

Therefore, unique lines exist on the LPC characteristic, for constant values of NDM_{HPC}. Figure 5-10 shows a typical LPC compressor map with superimposed HPC flow compatibility lines.

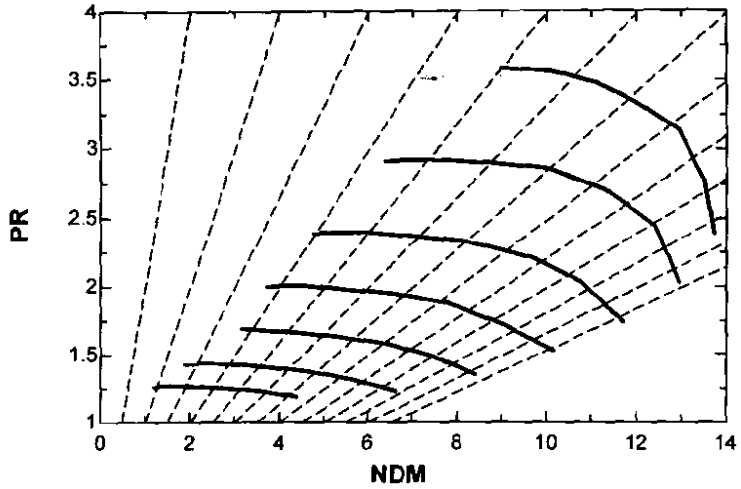

Figure 5-10 Flow compatibility between LPC and HPC

Work Compatibility

Work compatibility of the LP rotor must equate the work delivered by the LPT, the power dissipated by the generator and the power needed by the LPC. This work compatibility of the LP rotor, however, can be considerably simplified. This is done by assuming that the generator will dissipated the difference between the power developed by the LPT and that needed by the LPC.

In order to achieve a specific operating point on the LPT, the LPC must contribute a specific amount of pressure ratio to the Overall Pressure Ratio. The OPR is determined by:

$$OPR = f_l \times PR_{LPT} \times PR_{HPT} \qquad (5\text{-}21)$$

Where f_l is a factor accounting for pressure losses. .

The OPR can also be defined as:

$$OPR = PR_{LPC} \times PR_{HPC} \qquad (5\text{-}22)$$

The division of the OPR by the turbines is dictated by the behavior of two turbines in series described in Paragraph 5.4.1. The pressure ratio over the HPC is determined by the operating point of the HPT. Therefore, the pressure ratio needed by the LPC can be calculated from Equation (5-22).

LPC flow compatibility is only a function of NDM_{HPC}, Equation (5-20), and PR_{LPC} a function of the OPR and PR_{HPC}, Equation (5-22) . Therefore, the intersection of the flow

compatibility line and the calculated PR_{LPC}, determined by the operating point on the HPC, provides a matching point on the LPC characteristic. Consequently, for each operating point on the HPC characteristic there exists a corresponding matching point on the LPC characteristic. Figure 5-11 shows a typical matching line.

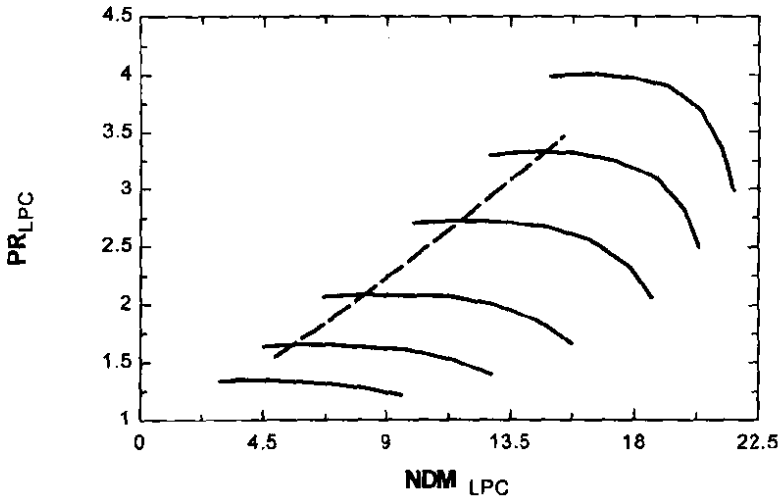

Figure 5-11 LPC matching line

5.5 Selection

On the bases of the matching characteristics of the two-shaft pre-and inter-cooled recuperative closed Brayton cycle discussed in Paragraph 5.4, suitable turbochargers can now be identified. The first step in this identification process is to determine suitable turbocharger turbines. This is followed by the evaluation of the HPC and LPC operating points with relation to high efficiency, surge and choke regions. Finally the identified turbocharger pairs are simulated in Flownex in order to compare important cycle characteristic values for the different configurations.

5.5.1 Turbine selection

Figure 5-12 shows the performance maps of five commercially available turbocharger turbines. The mass flow rate of these machines can be used as an indication of their size. Therefore, Turbine A (TA) is the biggest and Turbine E (TE) is the smallest.

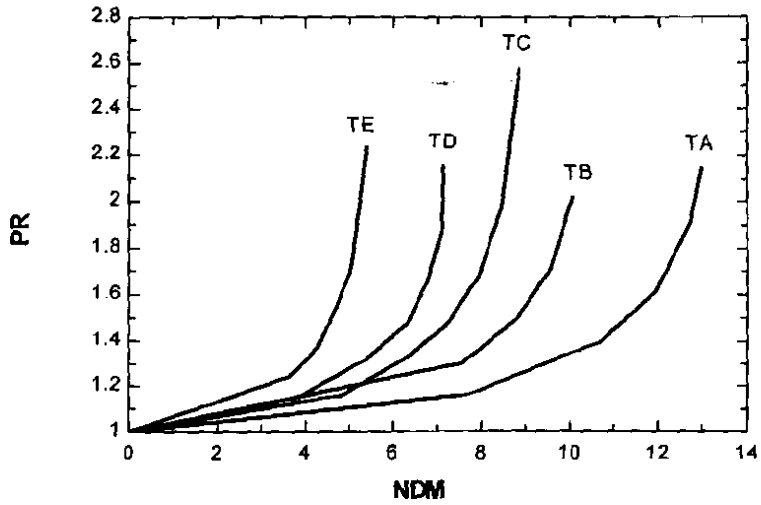

Figure 5-12 Performance maps of turbocharger turbines

Using the predictable behaviour of two turbines in series, discussed in Paragraph 5.4.1, the fixed relation that exists between the pressure ratios of the LPT and HPT can be plotted on a single graph, with the x-axes PR_{LPT} and the y-axes PR_{HPT}. This was done for all the turbines in Figure 5-12 and is shown in Figure 5-14 to Figure 5-18. In order to evaluate this combined behaviour of the turbines in series, however, it is necessary to define a suitable operating region on this graph to identify appropriate turbine parings.

Selection criteria

This region is defined with the help of the optimum thermodynamic operating conditions determined in Chapter 4. These are:

- Two optimum values for OPR exist, one for maximum cycle efficiency at 2.88, and one for maximum cycle power output at 4.414 (Paragraph 4.3.3).
- For optimum power output and cycle efficiency the OPR must be equally shared between the LPC and HPC (Paragraph 4.4.2).

The first requirement these thermodynamic operating conditions put on the selection of the two turbines, is that the combined pressure ratio of the two turbines must be between 2.88 and 4.414. With the OPR known and substituting it into Equation (5-21) two equilateral hyperbola curves are defined, one for OPR = 2.88 and one for OPR = 4.414 respectively (See Figure 5-13).

Implementing the second requirement into Equation (5-22) determines PR_{LPC} and PR_{HPC} as follows:

$$R_{LPC} = PR_{HPC} = \sqrt{OPR} \quad (5\text{-}23)$$

Substituting Equations (5-17) and (5-18) into the work compatibility equation for the HP rotor, Equation (5-16), the amount of pressure ratio dissipated by the HPT to allow the HPC to produce its share of the pressure ratio can be determined by Equation (5-24).

$$\eta_{HPT}\left[1-\left(\frac{1}{PR_{HPT}}\right)^{(\gamma-1)/\gamma}\right] = \frac{1}{\eta_{HPC}}\left[PR_{HPC}^{(\gamma-1)/\gamma}-1\right]\times\frac{T_{05}}{T_{011}}\times\frac{cp_h}{cp_c\eta_{mH}} \quad (5\text{-}24)$$

Where:

- $\eta_{HPT} = 0.69$ (Assumption Table 4-2)
- $\eta_{HPC} = 0.76$ (Assumption Table 4-2)
- $PR_{HPC} = \sqrt{OPR}$ according to Equation (5-23)
- $\frac{T_{05}}{T_{011}}$ is constant for a closed cycle.
- $cp_h \approx 1.045$
- $cp_c \approx 1.162$
- $\eta_{mH} = 0.99$ (Assumption Table 4-2)
- $\gamma = 1.4$ for nitrogen

Substituting the calculated PR_{HPT} into Equation (5-21) the relationship that must exist between the pressure ratios of the LPT and HPT for the compressors to equally share the OPR is determined. This is represented by the straight lines on Figure 5-13. Where the one with the slope m=0.65 is for an OPR=2.88 and the one with the slope of m=0.58 is for an OPR=4.414.

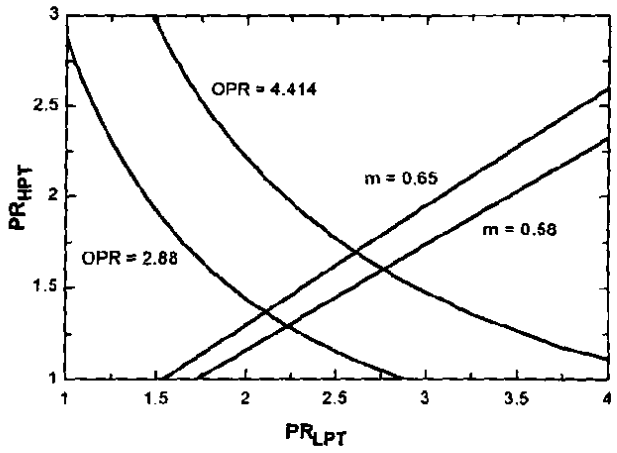

Figure 5-13 Turbine selection criteria

Turbine identification

In Figure 5-14 to Figure 5-18 each turbine, shown in Figure 5-12, alternately takes a turn to be the LPT. Superimposing the selection criteria on each of these graphs makes it possible to identify suitable turbine pairs.

From Figure 5-14, with turbine A as the LPT, it is clear that having turbine E and D as the HPT does not meet the criteria. Turbines A, B and C, however, do meet the criteria since the curves intersect the suitable operating region. Therefore the following configurations can be identified:

- Configuration 1: LP unit turbocharger A – HP unit turbocharger C
- Configuration 2: LP unit turbocharger A – HP unit turbocharger B
- Configuration 3: LP unit turbocharger A – HP unit turbocharger A.

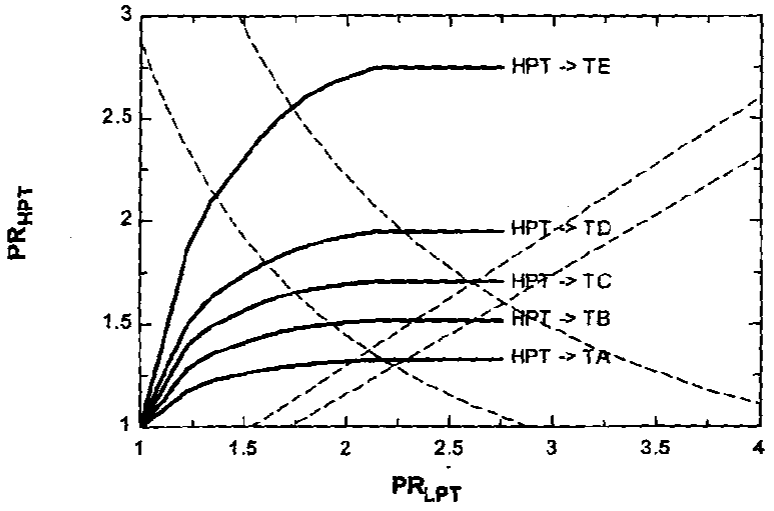

Figure 5-14 PR_{HPT} vs. PR_{LPT} with LPT model A

From Figure 5-15, with turbine B as the LPT, it is clear that having turbine E and A as the HPT does not meet the criteria. Turbines D, C and B, however, do meet the criteria since the curves intersect the suitable operating region. Therefore the following configurations can be identified:

- Configuration 4: LP unit turbocharger B – HP unit turbocharger D
- Configuration 5: LP unit turbocharger B – HP unit turbocharger C
- Configuration 6: LP unit turbocharger B – HP unit turbocharger B

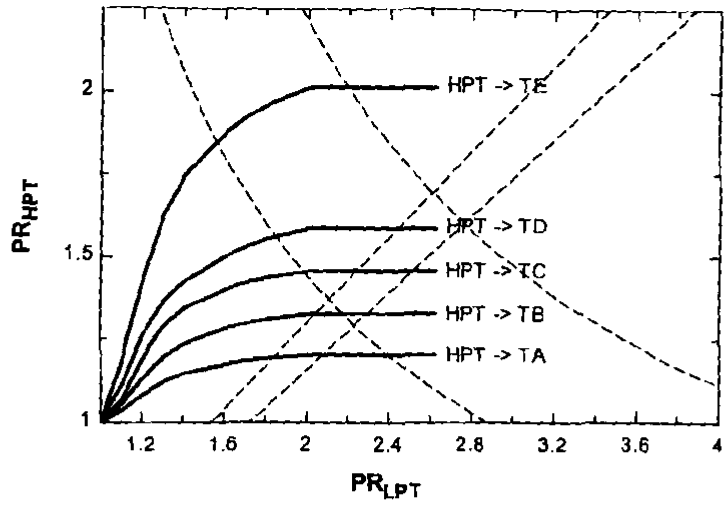

Figure 5-15 PR_{HPT} vs. PR_{LPT} with LPT model *B*

From Figure 5-16, with turbine C as the LPT, it is clear that having turbine E, B and A as the HPT does not meet the criteria. Turbines D and C, however, do meet the criteria since the curves intersect the suitable operating region. Therefore the following configurations can be identified:

- Configuration 7: LP unit turbocharger C – HP unit turbocharger D
- Configuration 8: LP unit turbocharger C – HP unit turbocharger C

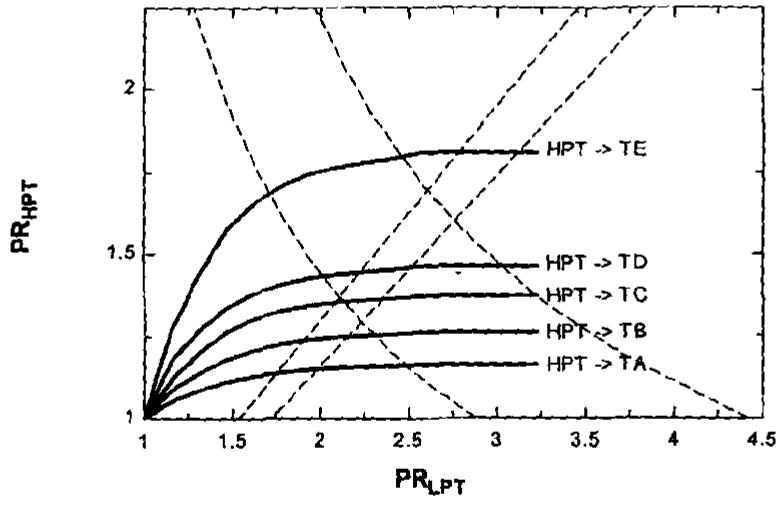

Figure 5-16 PR_{HPT} vs. PR_{LPT} with LPT model C

From Figure 5-17, with turbine D as the LPT, it is clear that having turbines A, B and C as the HPT do not meet the criteria. Turbines D and E, however, do meet the criteria since the curves intersect the suitable operating region. Therefore the following configurations can be identified:

- Configuration 9: LP unit turbocharger D – HP unit turbocharger E
- Configuration 10: LP unit turbocharger D – HP unit turbocharger D

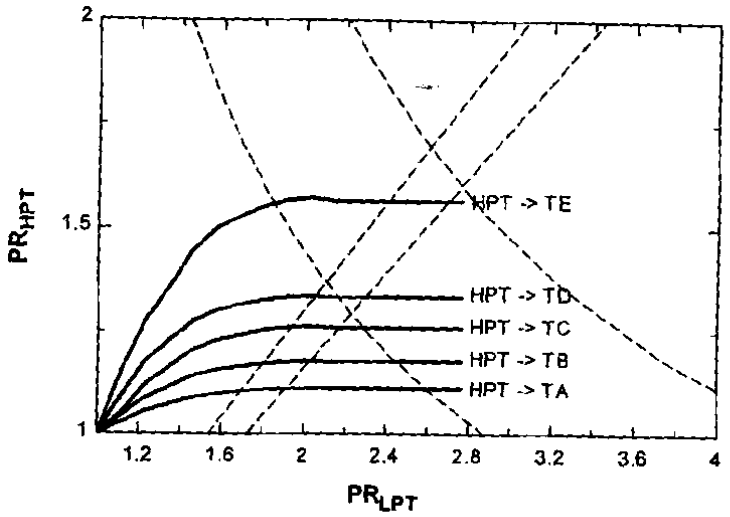

Figure 5-17 PR_{HPT} vs. PR_{LPT} with LPT model D

From Figure 5-18, with turbine E as the LPT, it is clear that having turbines A, B, C and D as the HPT do not meet the criteria. Turbine E, however, does meet the criteria since the curve intersects the suitable operating region. Turbine E, however, being the smallest of the turbines, this configuration will not be further investigated.

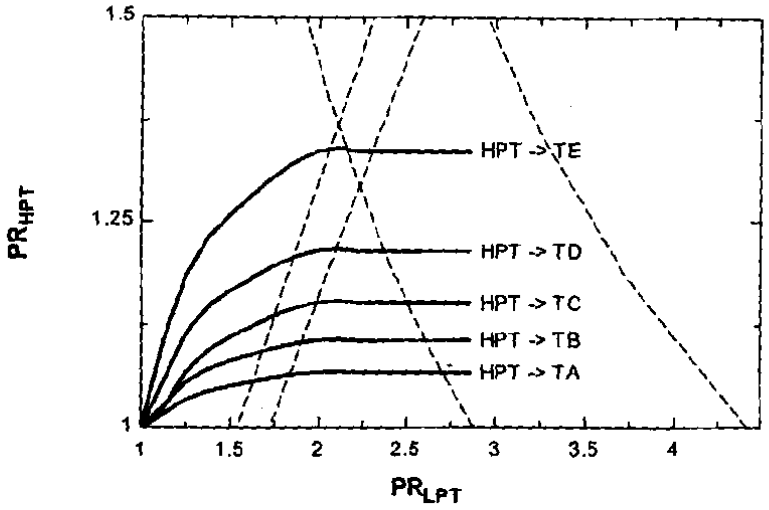

Figure 5-18 PR_{HPT} vs. PR_{LPT} with LPT model E

The identified configurations are summarized in Table 5-1. With suitable turbocharger turbines now identified, the next step is to evaluate the compressors of these turbochargers as HPC and LPC compressors in the two-shaft PBMM.

Table 5-1 Turbocharger parings

Configuration	Turbocharger	
	LP	HP
1	A	C
2	A	B
3	A	A
4	B	D
5	B	C
6	B	B
7	C	D
8	C	C
9	D	E
10	D	D

5.5.2 Evaluation of compressor operating points

The previous section determined suitable turbocharger turbines. Figure 5-19 shows the performance maps of the five commercially available turbocharger compressors. The mass flow rate of these machines can be used as an indication of their size. Therefore, Compressor A (CA) is the biggest and Compressor E (CE) is the smallest.

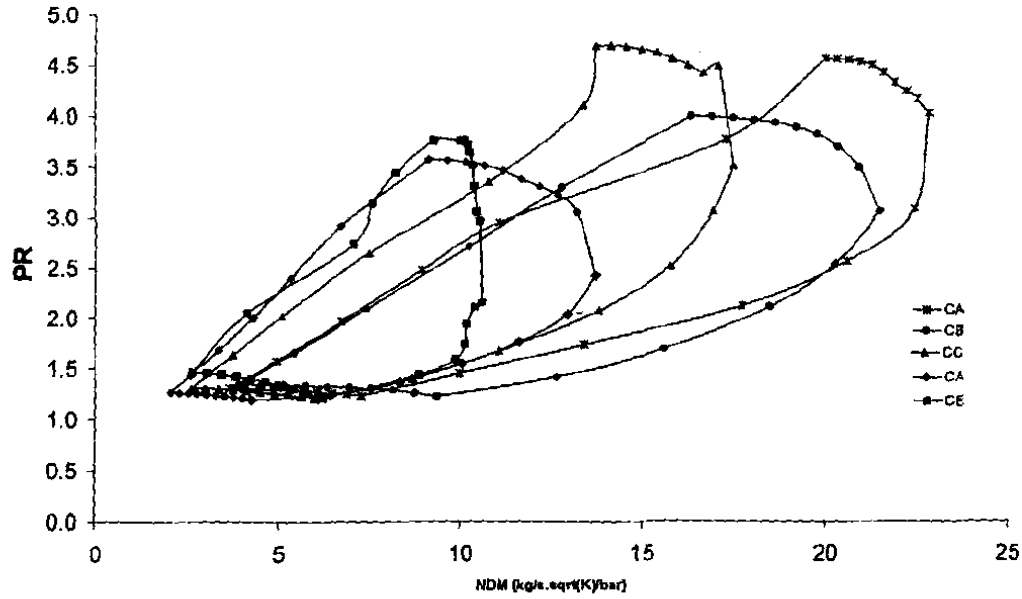

Figure 5-19 Performance maps of turbocharger compressors

5.5.3 HPC operating point evaluation

The requirement for flow and work compatibility that must exist between the HPT and the HPC, discussed in Paragraph 5.4.2, was used to determine the operating lines of all the configurations tabulated in Table 5-1. The results are shown in Figure 5-20 to Figure 5-24.

Figure 5-20 shows the evaluation of compressor A as the HPC in Configuration 1. The operating line is within the high efficiency region and well removed from the surge and choking regions.

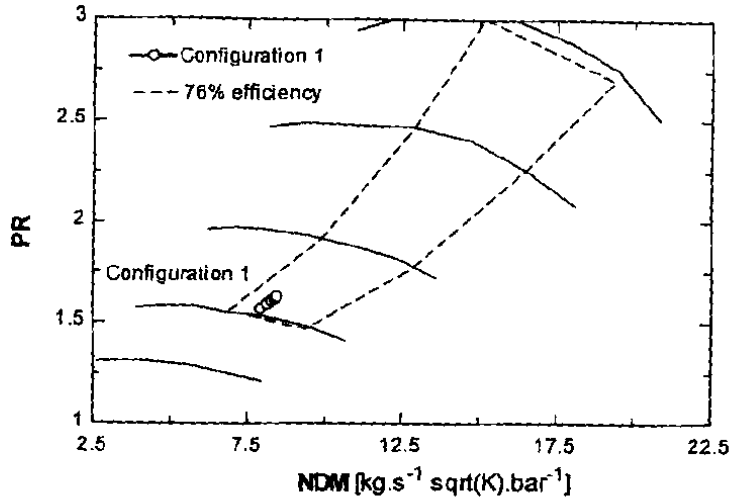

Figure 5-20 Evaluation of compressor A as HPC

Figure 5-21 shows the evaluation of compressor B as the HPC in Configurations 2 and 3. The operating lines are in close proximity to the high-efficiency region and well removed from the surge and choking regions.

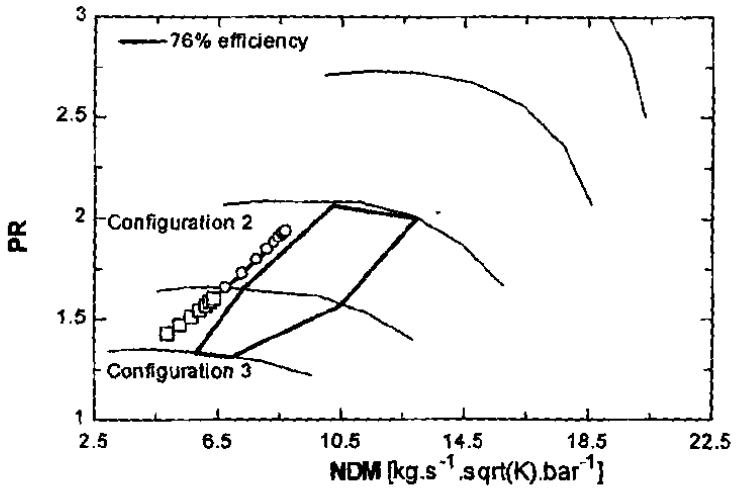

Figure 5-21 Evaluation of compressor B as HPC

Figure 5-22 shows the evaluation of compressor C as the HPC in Configurations 4 and 6. The operating lines are not in close proximity to the high efficiency region. It is, however, well removed from the surge and choking regions.

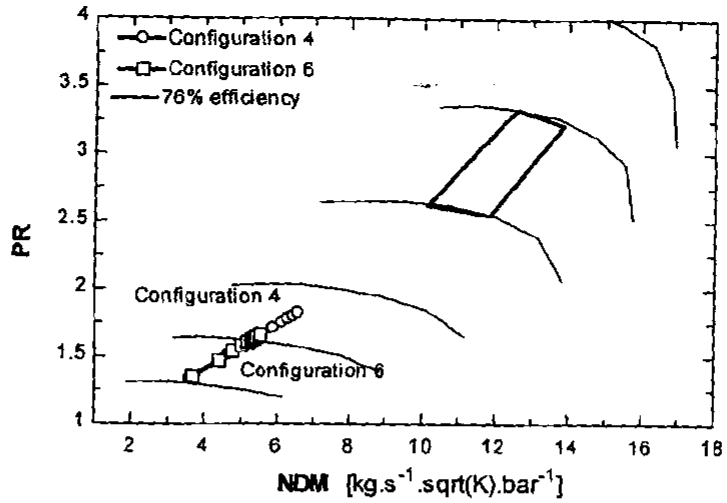

Figure 5-22 Evaluation of compressor C as HPC

Figure 5-23 shows the evaluation of compressor D as the HPC in Configurations 5, 7 and 8. The operating lines are in close proximity to the high efficiency region and well removed from the surge and choking regions.

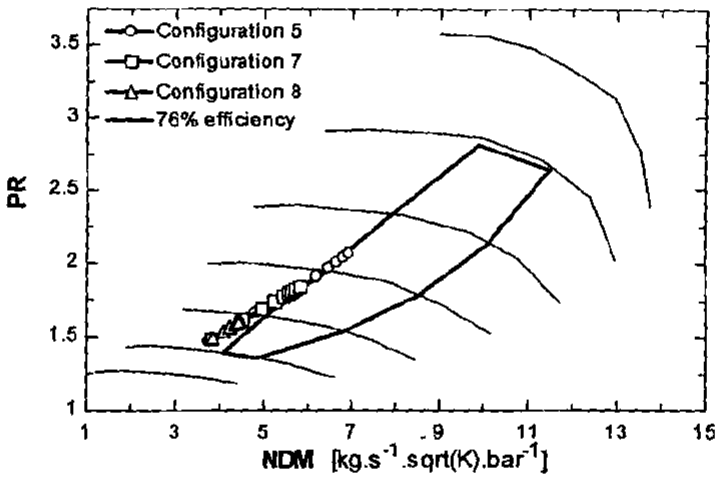

Figure 5-23 Evaluation of compressor D as HPC

Figure 5-24 shows the evaluation of compressor E as the HPC in Configurations 9 and 10. The operating lines are in close proximity to the high efficiency region and well removed from the surge and choking regions.

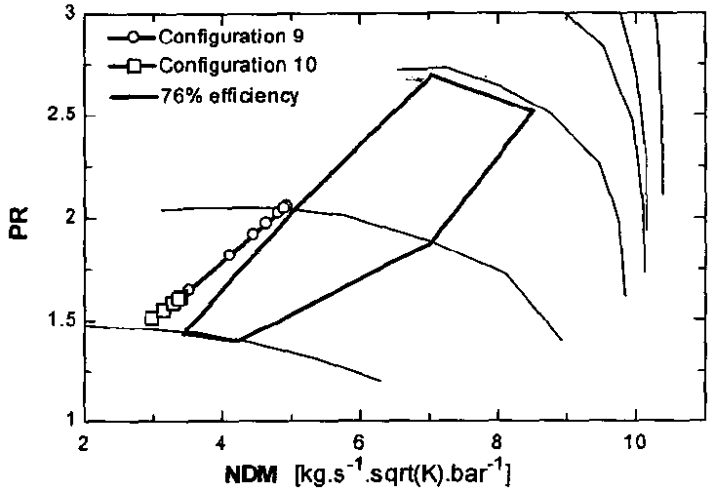

Figure 5-24 Evaluation of compressor E as HPC

5.5.4 LPC operating point evaluation

In Paragraph 5.4.3 the matching requirements for the LPC were discussed. This was used to determine the operating lines of all the Configurations tabulated in Table 5-1. The results are shown in Figure 5-20 to Figure 5-24.

Figure 5-25 shows the evaluation of Compressor A as the LPC in Configurations 1 and 2. The operating line is in close proximity to the high efficiency region and well removed from the surge region. The close proximity to the choking region, however, is unwanted.

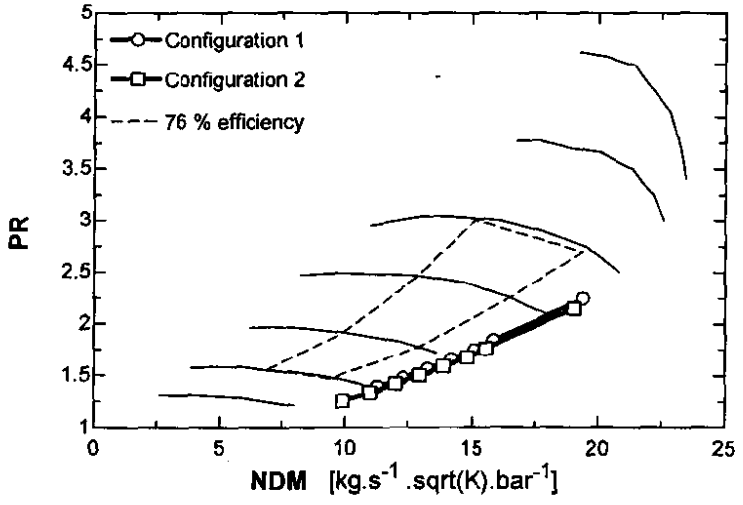

Figure 5-25 Evaluation of compressor A as LPC

Figure 5-26 shows the evaluation of Compressor B as the LPC in Configurations 3, 4 and 5. The operating lines are in close proximity to the high efficiency region and well removed from the surge and choking regions.

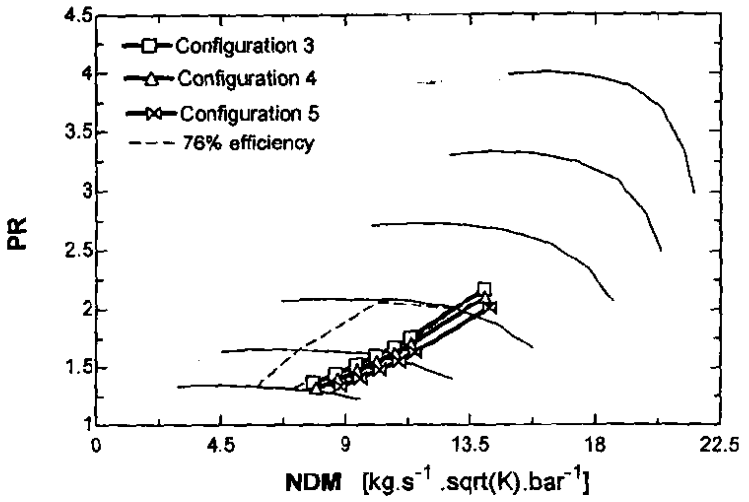

Figure 5-26 Evaluation of compressor B as LPC

Figure 5-27 shows the evaluation of Compressor C as the LPC in Configurations 6 and 7. The operating lines are not in close proximity to the high efficiency region. It is, however, well removed from the surge and choking regions.

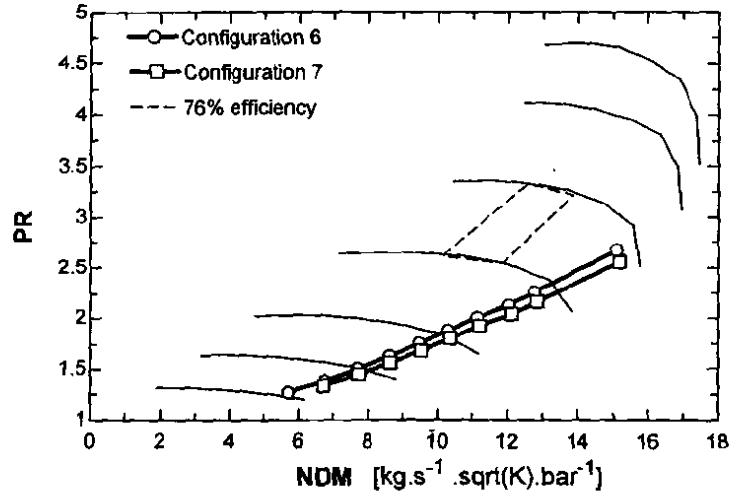

Figure 5-27 Evaluation of compressor C as LPC

Figure 5-28 shows the evaluation of Compressor D as the LPC in Configurations 8 and 9. The operating lines are in close proximity to the high efficiency region and well removed from the surge and choking regions.

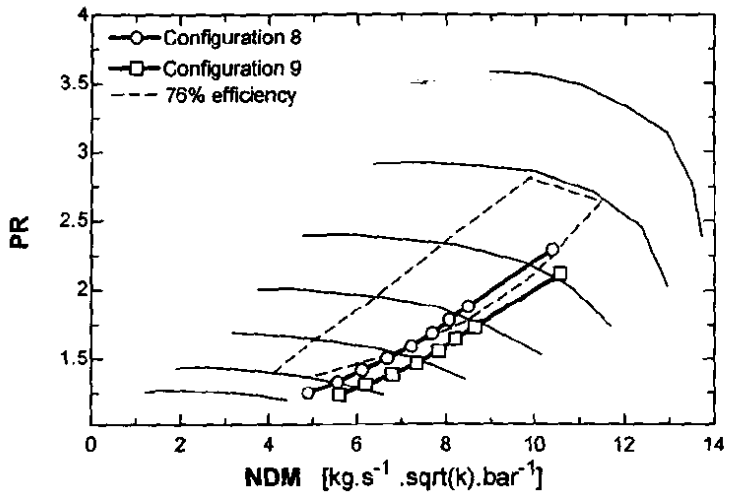

Figure 5-28 Evaluation of compressor D as LPC

Figure 5-29 shows the evaluation of Compressor E as the LPC in Configurations 10. The operating line is in close proximity to the high efficiency region and well removed from the surge and choking regions.

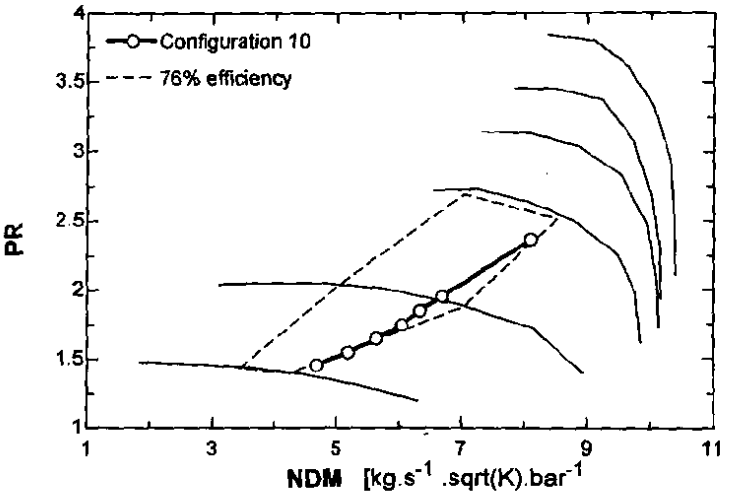

Figure 5-29 Evaluation of compressor E as LPC

In Table 5-2 the results of the compressor evaluation is summarized. Most of the configurations had good results making the selection of the turbochargers only on the basis of this evaluation, impractical. Therefore, all the configurations were simulated in Flownex. This allowed the comparison of the different configurations.

Table 5-2 Results of compressor evaluation

	HP			LP		
Configuration	Efficiency	Surge	Choke	Efficiency	Surge	Choke
1	✓	✓	✓	✓	✓	X
2	✓	✓	✓	✓	✓	X
3	✓	✓	✓	✓	✓	✓
4	X	✓	✓	✓	✓	✓
5	✓	✓	✓	✓	✓	✓
6	X	✓	✓	X	✓	✓
7	✓	✓	✓	X	✓	✓
8	✓	✓	✓	✓	✓	✓
9	✓	✓	✓	✓	✓	✓
10	✓	✓	✓	✓	✓	✓

5.5.5 Configuration comparison and final selection

The two-shaft configuration having a generator fitted on a compressor shaft makes the speed of the LP rotor a design choice. Figure 5-30 shows the variation of power output with variation of shaft speed, while Figure 5-31 shows the variation of cycle efficiency with variation of shaft speed. For all the configurations, the rotational speed at which maximum power was achieved is higher than the speed at which maximum efficiency was achieved. This behaviour is consistent with the thermodynamic behaviour observed in Paragraph 4.3.3. In this paragraph optimum OPRs were determined for maximum power output and maximum cycle efficiency. With the pressure ratio of the LPC being a function of its rotational speed, an increase of its rotational speed will increase the pressure ratio. An increase in the pressure ratio of the LPC will in turn increase the OPR.

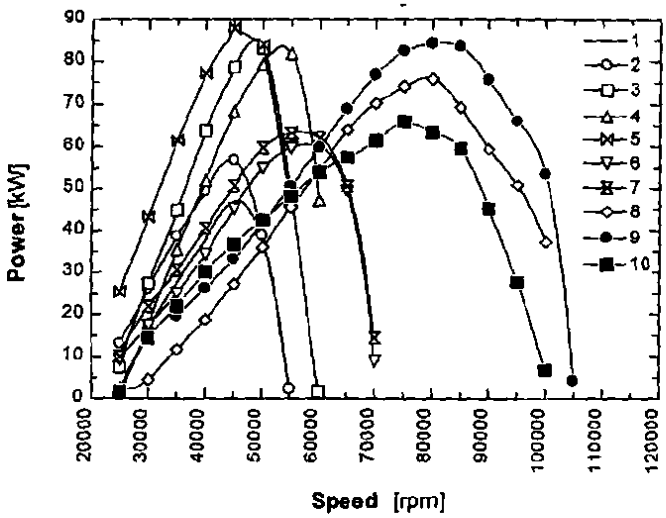

Figure 5-30 Power vs. LP rotor speed

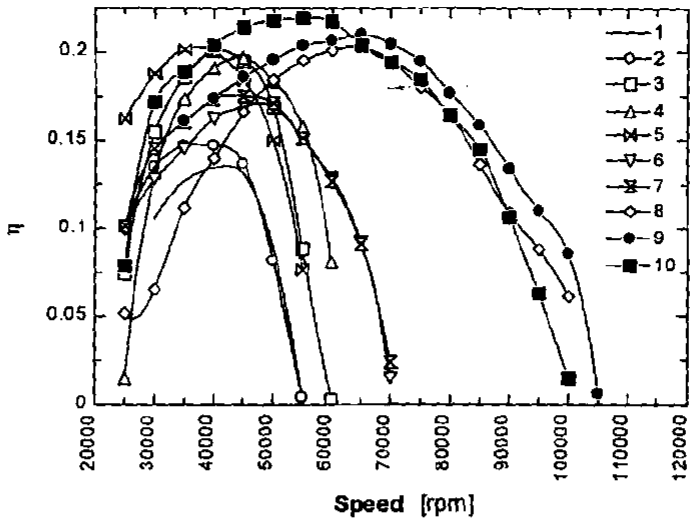

Figure 5-31 Efficiency vs. LP rotor speed

Since the base pressure, minimum and maximum temperatures are part of the specification; the only other major thermodynamic operating parameter with some degree of freedom is the maximum pressure. The three-shaft configuration has a maximum pressure of approximately 910 kPa when operating at a base pressure of 250 kPa and maximum temperature of 700°C. Achieving thermodynamic similarity between the three and two-shaft configurations will add to the functionality of the reconfiguration since it will now be possible to compare these two configurations more accurately. Therefore, the efficiency of the all configurations at a maximum pressure of 910 kPa was compared in Figure 5-32.

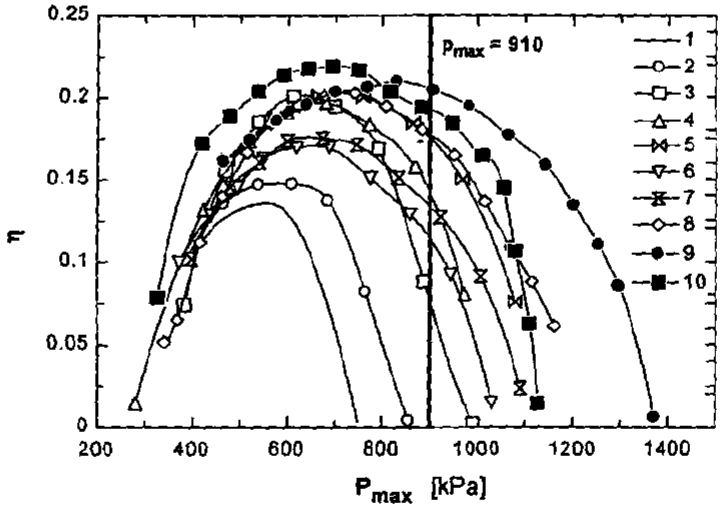

Figure 5-32 Configuration comparison at P_{max}=910 kPa

As Figure 5-32 shows, Configuration 9 has the highest efficiency at the 910 kPa maximum pressure target. It was therefore decided that Configuration 9 is the most suitable and is subsequently suggested as the preferred turbomachinery configuration.

5.6 Conclusion

This chapter presented the turbocharger selection. It started of by discussing the characteristics of compressors and turbines as individual components. This was followed by an investigation into the way these components interact with each other in the two-shaft pre- and inter-cooled recuperative closed Brayton cycle.

Using the unique matching characteristics of the two-shaft pre- and inter-cooled Brayton cycle and the optimum thermodynamic operating conditions determined in Chapter 4, suitable turbocharger configurations were identified. These configurations are tabulated in Table 5-1. Through inspection the operating lines of the LPC and HPC were evaluated. Most configurations operated in close proximity to the high efficiency regions and had sufficient surge and choke margins (Table 5-2).

The final selection was based on results obtain through simulating the different configurations in Flownex. Configuration 9 had the highest efficiency at the required maximum pressure of 910 kPa and is therefore the suggested turbocharger configuration.

6 COMPARISON OF THE TWO- AND THREE-SHAFT PBMM CONFIGURATIONS

In the previous chapter the turbocharger selection was performed. With the turbochargers now selected, the exact operating point of the two-shaft PBMM can be specified. In this chapter the results obtained through simulating the two-shaft PBMM in Flownex is presented.

6.1 Thermodynamic comparison

In Chapter 5 the turbocharger selection was performed. Having specified the turbocharger configuration the operating points of all the major components in the two-shaft PBMM can be determined. As a measure of the achievability to reconfigure the PBMM to a two-shaft configuration, the two-and three-shaft PBMM configurations were compared on a T-s diagram. In Figure 6-1, the T-s diagram of the three-shaft PBMM is compared to the high efficiency operating point of the two-shaft PBMM configuration.

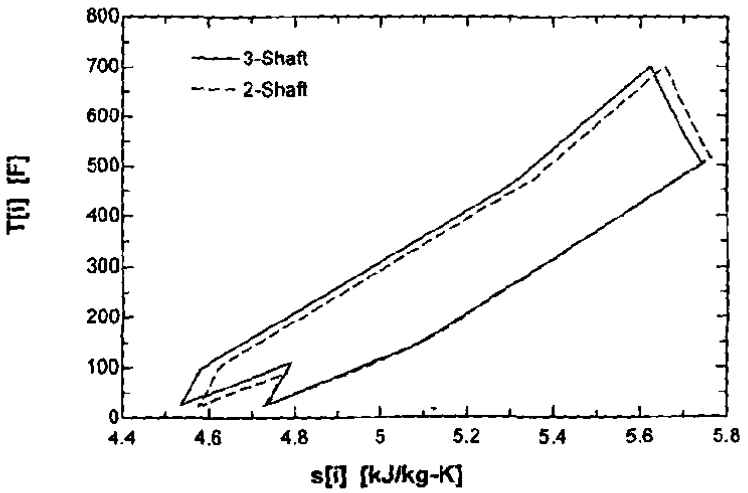

Figure 6-1 T-s diagram comparison at maximum efficiency

The comparison, shown in Figure 6-1, shows a slight variation between the two configurations. This variation, however, can be minimized by adjusting the LP rotor speed. The adjustment of the LP rotor speed enables the two-shaft PBMM configuration to more closely resemble the thermodynamic operating point of the three-shaft PBMM configuration. This thermodynamic similarity, shown in Figure 6-2, comes at the penalty of a slight reduction in the two-shaft PBMM cycle efficiency.

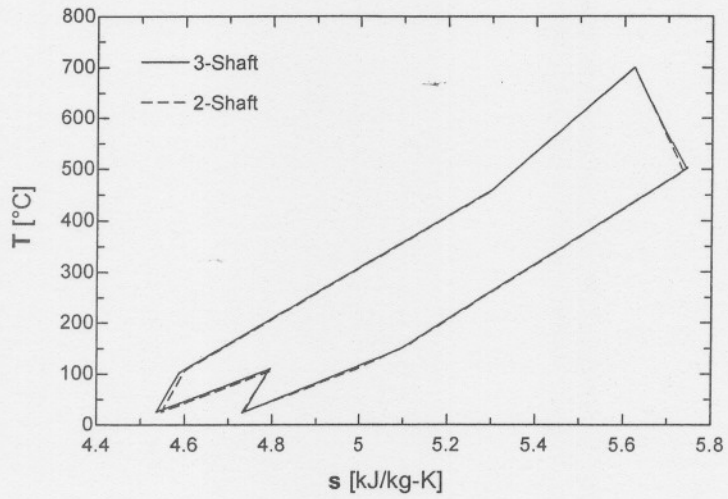

Figure 6-2 T-s diagram showing thermodynamic similarity

In Figure 6-3 and Figure 6-4 the temperature and pressure conditions at the inlet and outlets for the various components in the two-shaft and three-shaft PBMM configurations is shown. Apart from points 15 and 16, which is the inlet and outlet of the PT in the three-shaft configuration, the comparison between the two- and three-shaft PBMM configurations is very good.

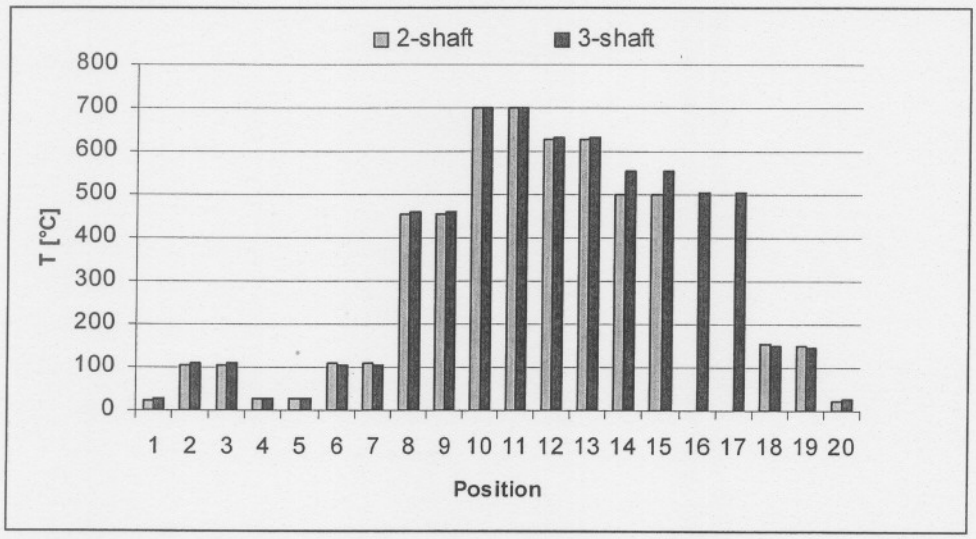

Figure 6-3 Component inlet and outlet Temperature comparison

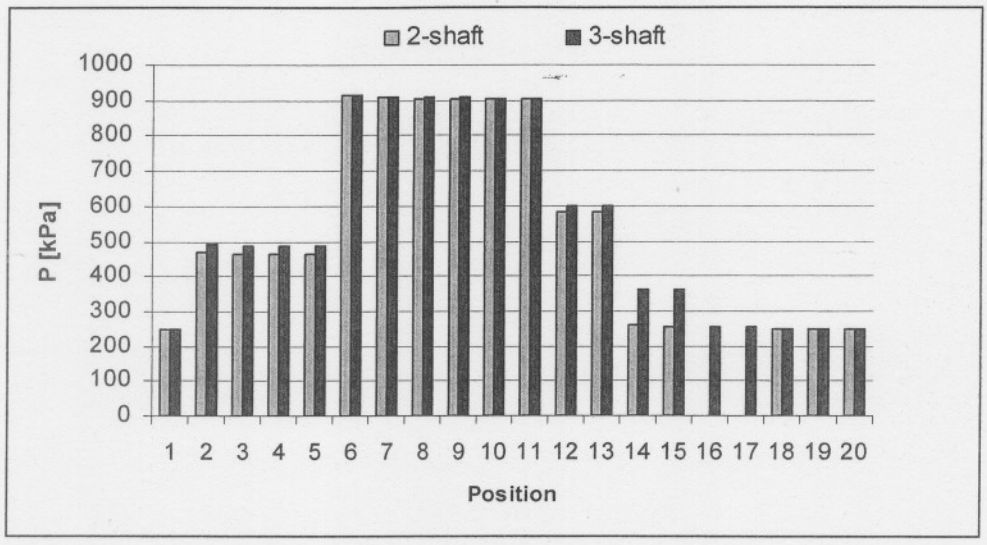

Figure 6-4 Component inlet and outlet pressure comparison

Figure 6-5 shows comparison of the power and heat levels of the different components. The only major difference is the power produced in the LPT. This difference, however, is because of the existence of the PT in the three-shaft configuration.

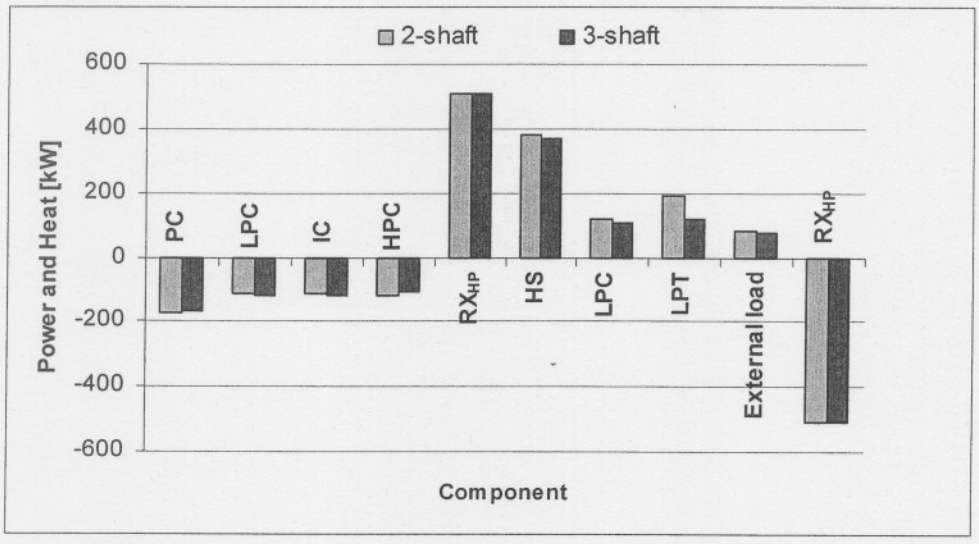

Figure 6-5 Component power level comparison

Figure 6-2 to Figure 6-5 illustrates the excellent thermodynamic comparison between the two- and three-shaft PBMM configurations. Therefore, the three-shaft PBMM configuration can be reconfigured to a two-shaft PBMM without changes in most of the major components. The only obvious difference in components between the two- and three-shaft PBMM configurations is the difference in turbomachinery layout. The newly selected turbochargers (Chapter 5), however, is exactly the same used for the HP- and LP-rotors in the three-shaft

PBMM. Therefore the next section compares matching in the two-shaft PBMM to that of the three-shaft PBMM configuration.

6.2 Turbomachine Matching comparison

The thermodynamic similarity illustrated in the previous section was achieved partly because both the configurations had the same boundary values and the same thermodynamic layout, but importantly also because of the similarity in the way the turbomachines match. Therefore, in this section the matching characteristic of the two-shaft PBMM configuration is compared to that of the three-shaft PBMM configuration.

6.2.1 Turbine in series

In Paragraph 5.4.1 the behaviour of turbines in series were discussed. Using this unique relationship that exists between turbines in series, the turbine operating points of the two- and three-shaft PBMM configurations are compared in Figure 6-6.

For the three-shaft PBMM configuration the LPT operating point is determined by the swallowing capacity of the PT. The LPT operating point in turn determines the operating point of the HPT. The selection of the turbochargers in the three-shaft PBMM configuration is such that the LPT operates near its choking point.

For the two-shaft PBMM configuration the LPT must produce the useful shaft work in addition to the work needed by the LPC. This can only be achieved if the LPT nears and enters its choke region. This implies that the HPT will also operate near or at its maximum PR determined by the choking point of the LPT.

The asymptotic behaviour of the LPT ensures that the difference in pressure ratios, for the two- and three-shaft PBMM configurations, does not result in a significant difference in their NDMs. This in turn results in the close proximety of their HPT operating points.

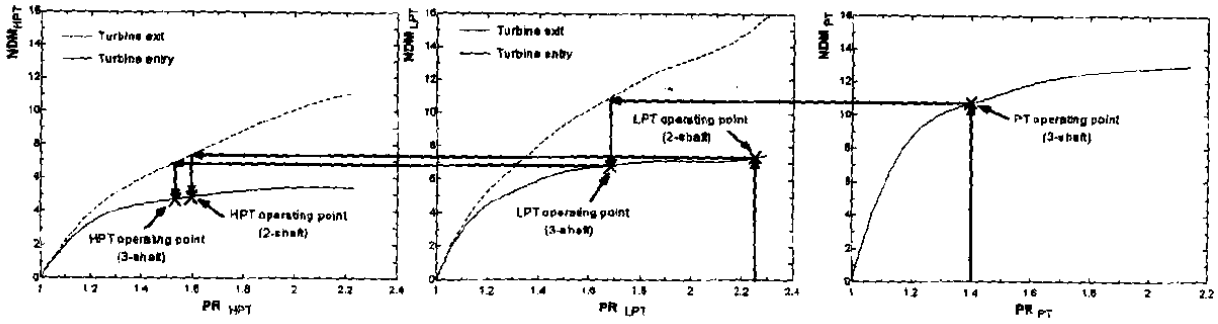

Figure 6-6 Turbines in the three-shaft PBMM

6.2.2 HPC operating point

The previous section illustrated the close proximity of the HPT operating points for the two- and three-shaft PBMM configurations. In Paragraph 5.4.2 the relationship between the HPT and HPC is discussed. It was found that the HPC operating point is only a function of the HPT operating point. Therefore the close proximity of the HPT operating points ensures a close proximity of the HPC operating points for the two- and three-shaft PBMM configurations. This is illustrated by Figure 6-7, where the only noticeable difference is observed between the flow compatibility lines.

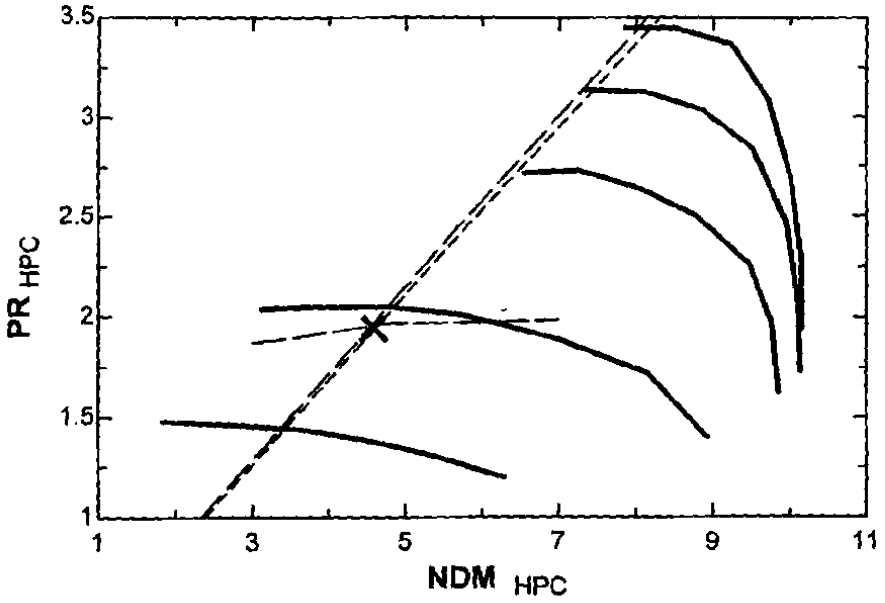

Figure 6-7 Comparison of HPC operating points

6.2.3 LPC operating point

The previous section illustrated that the HPCs in the two-shaft and three-shaft PBMM configurations has approximately the same operating point. This point can be represented on the LPC characteristic as a flow compatibility line (Figure 6-8), since flow compatibility must exist between the LPC and the HPC (Paragraph 5.4.3).

For work compatibility, however, there are some differences. In the three-shaft configuration work compatibility of the LP rotor must equate the power delivered by the LPT and that dissipated by the LPC. This line is calculated as follows:

$$\frac{\Delta T_{0LPT}}{T_{013}} = \frac{\Delta T_{0LPC}}{T_{01}} \times \frac{T_{01}}{T_{013}} \times \frac{cp_h}{cp_c \eta_{mH}} \qquad (6\text{-}1)$$

where

$$\frac{\Delta T_{0LPT}}{T_{013}} = \eta_{LPT}\left[1 - \left(\frac{1}{PR_{LPT}}\right)^{(\gamma-1)/\gamma}\right] \qquad (6\text{-}2)$$

and

$$\frac{\Delta T_{0LPC}}{T_{01}} = \frac{1}{\eta_{LPC}}\left[PR_{LPC}{}^{(\gamma-1)/\gamma} - 1\right] \qquad (6\text{-}3)$$

Therefore, assuming constant $\frac{T_{01}}{T_{013}}$, unique lines exist on the LPC characteristic, for constant values of PR_{LPT}. This work compatibility line for the three-shaft PBMM configuration is shown in Figure 6-8. The intersection of this work compatibility line with the flow compatibility line reveals the operating point of the LPC in the three-shaft PBMM configuration.

For the two-shaft PBMM configuration, work compatibility of the LP rotor must equate the work delivered by the LPT, the power dissipated by the generator and the power needed by the LPC. The PR_{LPC} is determined by Equation (5-22), discussed in Paragraph 5.4.3. The intersection of this work compatibility line with the flow compatibility line reveals the operating point of the LPC in the two-shaft PBMM configuration (Figure 6-8).

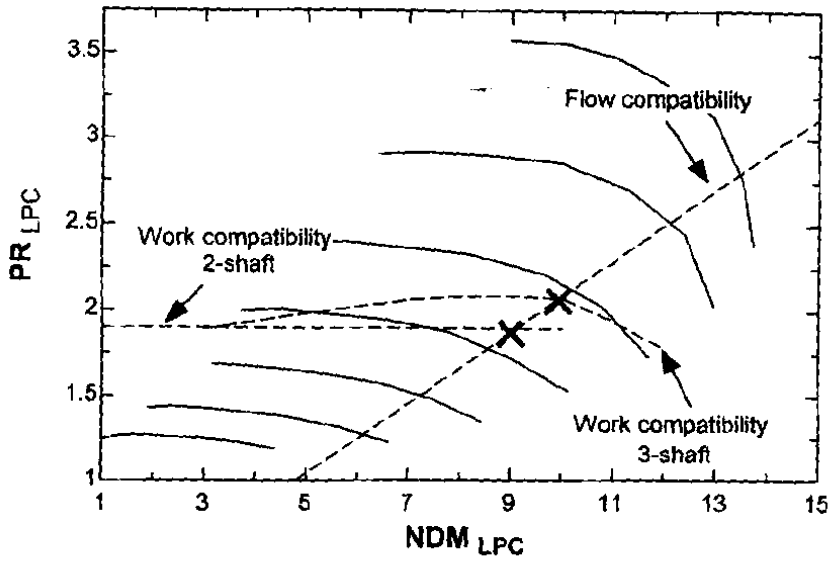

Figure 6-8 Comparison of LPC operating points

The two-shaft configuration having a generator fitted on a compressor shaft makes the speed of the LP rotor a design choice, as previously discussed in Paragraph 5.5.5. The operating point of the LPC, however, is limited to the flow compatibility line. Therefore any variation of shaft speed can only cause the operating point of the LPC to move along the flow compatibility line. The operating points on the LPC for the two- and three-shaft PBMM configurations are limited to the same flow compatibility line and will therefore ensure their close proximity.

This has therefore illustrated why it is possible for the two- and three-shaft PBMM configurations to make use of the same turbochargers.

6.3 Conclusion

Chapter 6 compared the two-shaft PBMM configuration to the three-shaft PBMM configuration. It illustrated the excellent thermodynamic comparison between the two- and three-shaft PBMM configurations. This thermodynamic similarity ensures that the two-shaft PBMM configuration can use most of the major components currently part of the existing PBMM. The only major difference in components between the two- and three-shaft PBMM configurations is the obvious difference in turbomachinery layout. Therefore, the matching characteristics of the two configurations were compared.

To summarize, the close proximity of both configurations to the choking region of the LPT ensured the close proximity of their operating points on the HPT. With the HPC operating

point only being a function of the HPT operating point, this caused close proximity of the HPC operating points. The requirement for flow compatibility that must exist between the HPC and LPC, limited the operating point of the LPC for both configurations to the same flow compatibility line, which ensured the close proximity of the LPC operating points. This means that the two-shaft PBMM configuration can make use of the same turbochargers as the three shaft configuration.

7 CONCLUSIONS AND RECOMMENDATIONS

This chapter provides a dissertation summary which presents the most important findings as obtained from each chapter. Conclusions are made based on these findings. Subsequently the chapter provides recommendations for further research.

7.1 Chapter Summary

In Chapter 1 the history leading up to the renewed interest into combining the high temperature of helium cycles and the efficiency of gas turbines in a HTGR was briefly discussed. HTGRs under active development make use of the recuperated, pre- and inter-cooled closed Brayton cycle. The recuperated, pre- and inter-cooled closed Brayton cycle, however, can be configured either as a single-shaft or multi- shaft setup. Investigating the advantages and disadvantages of the single- and three-shaft configurations led to identification of the main factors influenced by the choice of shaft arrangement. Using these factors, the potential of combining some of the advantages of the single and three-shaft arrangements in a two-shaft arrangement was illustrated. The main objective of this study was therefore stated as follows: in order to investigate the behaviour of a two-shaft pre- and inter-cooled recuperative Brayton cycle a conceptual layout design for a two-shaft PBMM configuration had to be expounded.

Chapter 2 identified the process of designing a gas turbine as a multi-disciplined process that combines thermodynamics, aerodynamics, mechanics and control system design in a concurrent engineering process. In order to identify methods for the purpose of addressing the different aspects of the gas turbine design procedure, the design and development of the existing three-shaft PBMM configuration was investigated. As result of this the following steps were identified:

- Specification and preliminary studies.
- Thermodynamic design point studies.
- Turbomachinery selection.

The first of these steps -- specification and preliminary studies -- was performed as demonstrated in Chapter 3. In order for the reconfiguring of the PBMM to a two-shaft PBMM configuration, most of the major components of the existing facility had to be retained. In order to achieve this, the main specification of the two-shaft PBMM configuration was to be

thermodynamically similar to the three-shaft PBMM configuration. The preliminary study found that turbochargers with ball bearings provide a good alternative to turbochargers with conventional bearings and as a result it was suggested that the turbomachines in the two-shaft PBMM configuration make use of these. A high speed permanent magnet generator was identified as suitable for the PBMM environment since it was small in size and its high operating speed would allow the use of turbocharger components for the LP rotor.

Chapter 4 presented the first major design step which was to determine the optimum thermodynamic conditions. Through a simulation model in EES a parametric study revealed two optimum OPRs: one for maximum cycle efficiency at 2.88 and one for maximum power output at 4.414. A sensitivity analysis was performed to investigate the influence that turbocharger selection would have on the cycle performance. The sensitivity analysis revealed the following:

- Reduction in turbine and compressor efficiency results in the reduction of cycle efficiency and cycle power output.
- The OPR must be equally shared between the LPC and HPC for optimum power output and cycle efficiency.
- A reduction of the TIT results in a reduction of power output and cycle efficiency.
- As mass flow decreases so does cycle power output at constant cycle efficiency.

Chapter 5 presented the manner in which the turbocharger selection was performed. Firstly, the characteristics of compressors and turbines as individual components were discussed. This was followed by an investigation of how these components interacted with each other in a two-shaft pre- and inter-cooled recuperative closed Brayton cycle. Using the unique matching characteristics of the two-shaft pre- and inter-cooled closed Brayton cycle and the optimum thermodynamic operating conditions determined in Chapter 4, suitable turbocharger configurations were identified. The final selection was made by comparing the Flownex results of all the configurations. The one with the highest efficiency at the required thermodynamic operating conditions, Configuration 9, was suggested as the preferred turbocharger configuration.

Chapter 6 compared the two-shaft PBMM configuration to the three-shaft PBMM configuration. By comparing the Flownex results of the two configurations, the excellent thermodynamic similarity that existed between the two- and three-shaft PBMM

configurations was illustrated. This thermodynamic similarity was achieved partly because both the configurations had the same boundary values and the same thermodynamic layout, but importantly also because of the similarity in the way in which the turbomachines matched. Therefore thermodynamic similarity was achieved because the two-shaft PBMM uses the same turbochargers as the three-shaft PBMM configuration.

7.2 Conclusion

- In order to reconfigure the PBMM to a two-shaft configuration successfully, the main specification for the two-shaft PBMM configuration was to be thermodynamically similar to the existing three-shaft PBMM.

- Thermodynamic similarity was achieved, partly because both the configurations had the same boundary values and the same thermodynamic layout, but importantly also because of the similarity in the way in which the turbomachines matched.

- The close proximity of the operating points in the case of both configurations to the choking region of the LPT ensured the close proximity of their operating points on the HPT. Since the HPC operating is only a function of the HPT operating point this caused close proximity of the HPC operating points. The requirement for flow compatibility that had to exist between the HPC on LPC limited the operating point of the LPC for both configurations to the same flow compatibility line which ensured the close proximity of the LPC operating points. Therefore in order to achieve thermodynamic similarity, the two-shaft PBMM must make use of the same turbochargers as that used in the three-shaft PBMM configuration.

7.3 Recommendations for future research

The following aspects are recommended for future research:

- Development of a high-speed permanent magnet generator to be implemented into the two-shaft PBMM.
- An investigation into integrating the high speed permanent magnet generator and a turbocharger to be implemented as the LP rotor in the two-shaft PBMM configuration.
- Since the two-shaft PBMM will actually generate electric power, it will be necessary to study the manner in which this power can be dissipated.

- Transient analysis of the two-shaft PBMM configuration in Flownex. The transient analysis will reveal the operating lines of the turbochargers during load following, load rejection and start-up.

REFERENCES

Baines, NC, 2005, *Fundamentals of Turbocharging*, Concepts NREC, Vermont, United States of America, 264p.

Ballinger, RG, Kadak, A, Todreas, N, 2003, *Balance of Plant System Analysis and Component Design of Turbo-Machinery for High Temperature Gas Reactor Systems*, Massachusetts Institute of Technology, Massachusetts, USA.

Bell, C, 1997, *Maximum Boost -- Designing, Testing and Installing Turbocharger Systems*, Bentley Publishers, Massachusetts, United States of America, 250p.

Boyce, MP, 2002, *Gas Turbine Engineering Handbook*, Second Edition, Gulf Professional Publishing, Houston, Texas, USA.

Botha, BW, 2002, *Application potential of the South African Pebble Bed Modular Reactor Power Plant*, Potchefstroom University for CHE.

Botha, BW, 2004, *Advanced Turbo-Machines*, Course Notes, MEG 887, School of Mechanical and Materials Engineering, North West University, South Africa.

Compact power systems, [Web:] http://www.tue.nl/internediensten/tueholdingskps.html used: 05/28/2005

Flownex 6.8, 2005, User Manual, M-Tech Industrial (Pty) Ltd, Potchefstroom, South Africa.

Garrett, *Turbo Tech 101 (Basic)*, [Web:] www.turbobygarrett.com/turbobygarrett/tech_center/turbo_tech101.html used: 2005/08/21

Greyvenstein, GP, Du Toit, B, Steyn, MM, 2002, *Turbocharger Design Report*, M-tech Industrial (Pty) Ltd, Potchefstroom, South Africa.

Greyvenstein, GP, Rousseau, PG, 2002, *Design of a physical model of the PBMR with the aid of Flownet*, Department of Mechanical Engineering, Potchefstroom University for Christian Higher Education, South Africa.

International Atomic Energy Agency (IAEA),"HTGR Knowledge Base". [web:] www.iaea.org/aws/htgr/topics/article_06.html [used: 25/05/2005].

Japikse, D, 1996, *Centrifugal Compressor Design and Performance*, Concepts EIT Inc.

MacInnes, H, 1984, *Turbochargers*, HPBooks, New York, USA, 159p.

Moolman, A, 2003, *Mathematical Loss Models for Centrifugal Compressors*, Masters Degree dissertation, Faculty of Engineering, PU for CHE.

Rousseau, PG, 2004, *Advanced Thermal-Fluid Systems*, Course Notes, MEG 833, School of Mechanical and Materials Engineering, North West University, South Africa.

Rousseau, PG, Greyvenstein, GP, 2002, *Conceptual Thermo-Hydraulic Design of the PBMR Micro Model*, M-Tech Industrial, Potchefstroom.

Rousseau, PG, Van Ravenswaay, JP, 2003, *Thermal-fluid Comparison of the Three- and Single Shaft Closed Loop Brayton Cycle Configurations for HTGR Power Conversion*, Faculty of Engineering, PU for CHE, South Africa.

Saravanamuttoo, HIH, Rogers, GFC, Cohen, H, 2001, *Gas Turbine Theory*, Pearson Education limited, Essex, England, Fifth Edition, 482p.

Sontag, RE, Borgnakke, C, Van Wylen, GJ, 1998, *Fundamentals of Thermodynamics*, John Wiley & Sons, United States of America, 783p.

S2M, *Magnetic Bearings & High speed motors,* [Web:] http://www.s2m.fr/index.html used: 28/05/2005.

Takase, K, 2004, *Design and development of 2MW, High Speed permanent magnet alternator*, Wakamutsurcho, Shinjuku, Tokyo, Japan.

TruckPro, *Typical Truck Turbocharger*, [Web:] www.truckpro.com/docs /resource_center/typical_truck_systems_charts/turbocharger_systems/turbo_typical_trk_turbo.html used: 2005/07/18

Van Ravenswaay, JP, Greyvenstein, GP, Van Niekerk, WMK, Labuschagne, JT, 2004, *Verification and Validation of the HTGR Systems CFD Code Flownex*, School of Mechanical Engineering, North West University, M-Tech Industrial (Pty) Ltd, Potchefstroom, South Africa.

Van Niekerk, WMK, Rousseau, PG, Greyvenstein, GP, 2003, *Operation and Simulation of a Three-Shaft, Closed-Loop, Brayton Cycle Model of the PBMR Power Plant*, Proceedings of ICAPP'03, Corboda, Spain, Paper 3264.

Watson, N, Janota, MS, 1982, *Turbocharging the Internal Combustion Engine*, Macmillan Education LTD, London, Great Britain, 608p.

Wilson, DG, Korakiatianitis, T, 1998, *The Design of High-Efficiency Turbomachinery and Gas Turbines*, Second Edition, Prentice Hall, New Jersey, USA, 593p.

Whitfield, A, Baines, NC, 1990, *Design of Radial Turbomachines*, Longman Group UK Limited, Essex, England, 397p.

APPENDIX A: THE TURBOCHARGER

A.1 Introduction

In Baines (2005:1) a turbocharger is defined as a turbine driven compressor. The word turbocharger is abbreviated from the word turbosupercharger. A supercharger is used in an internal combustion engine to increase the charge of the cylinder through compression of the inlet air. Superchargers are engine driven compressors. However, by utilizing the hot gases at the engine outlet the compressor can be driven by a turbine and taking power directly from the engine is avoided. Turbochargers have three major components: a compressor, a turbine shaft assembly, and bearing assembly to support the shaft.

Compressors for turbocharger applications are almost universally of the centrifugal type. Single-stage centrifugal compressors can be designed to operate at a pressure ratio up to 3.5:1 with reasonable efficiency and good reliability. This pressure ratio limit is well within the requirements of the majority of turbocharger engines. Although axial flow compressors operate more efficiently than the centrifugal type, they are more expensive, heavier, longer, and have a narrower operating range (Watson & Janota, 1982:20)

Turbines may be of the radial or axial flow type for turbocharger applications. However radial flow turbines are preferred for the following reasons (Watson & Janota, 1982:21):

- The single-stage radial turbine is undoubtedly simpler and cheaper to manufacture than the axial flow turbine, provided that the wheel can be cast.
- Axial flow turbines become less efficient as size is reduced. This is mainly due to short blades and narrow flow passages resulting in high boundary layer blockage.

Unfortunately it has proven difficult to achieve sound large castings with high temperature alloys, thus resulting in the use of axial flow turbines for large turbocharger applications.

The centrifugal compressor and radial turbine can be arranged in numerous ways to accommodate two necessary journal bearings and a thrust bearing to form the turbocharger, as shown in Figure A-1:

a) Outboard mounted bearings
b) Inboard mounted bearings
c) Combination of inboard and outboard mounted bearings
d) One ended outboard mounted bearings

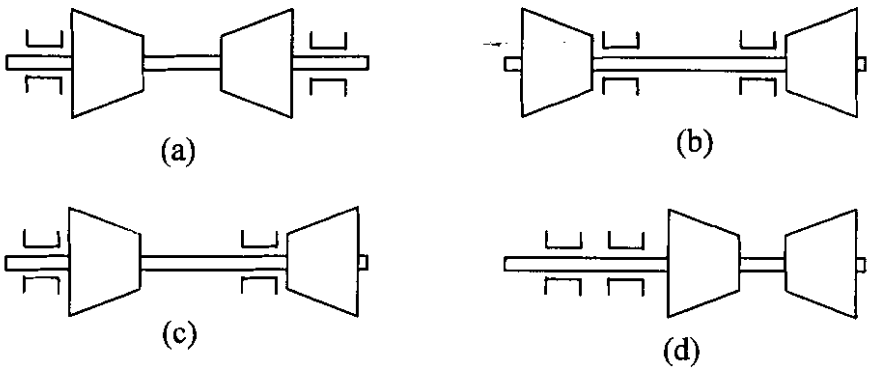

Figure A-1 Turbocharger bearing layouts (Baines, 2005:115)

However, Baines(2005:115) explains that the inboard mounted bearing arrangement is the most common arrangement for automotive applications. It keeps the housing a simple, rigid casting with relative easy separation of the lubricating oil from the gas path.

The inboard mounted bearing arrangement is ideally suited for turbocharger applications with radial turbines. In this arrangement, the flow of gas into and out of the compressor and turbine wheels can be direct. Compared to the other arrangements, the inboard mounted arrangement reduces the number of components, length and weight of the turbocharger, which results in a cheaper product (Watson & Janota, 1982:42)

Although it is rarely possible to position the first two critical speeds above the running range of the turbocharger, the rotor dynamics is acceptable if the bearings are sufficiently resilient to withstand these critical speeds during start-up and shut-down. The bearings in the inboard mounted arrangement are not accessible and are therefore designed for long life with minimum maintenance Baines (2005:115).

The inboard mounted bearing arranged turbocharger, in its simplest form, comprises of an assembly of three casings joint together to house a centrifugal compressor, a radial turbine and the bearing assembly. Figure A-2 shows a typical turbocharger with a centrifugal compressor and a radial flow turbine adopting the inboard mounted bearing arrangement.

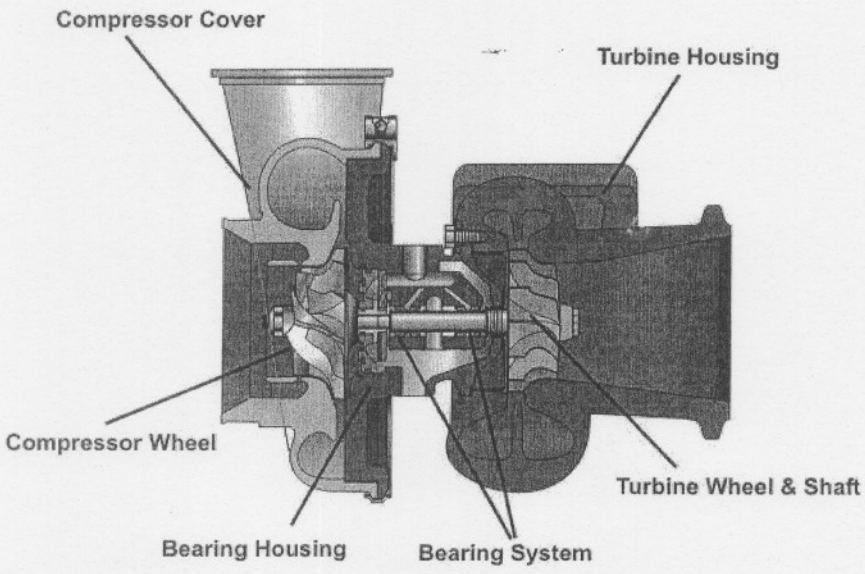

Figure A-2 Cross section view of a typical turbocharger (TruckPro)

A.2 The centrifugal compressor

The centrifugal compressor, Figure A-3, is essentially made up from four basic components or sections:

(1) Stationary inlet casing

(2) Rotating impeller

(3) Stationary diffuser

(4) Collector

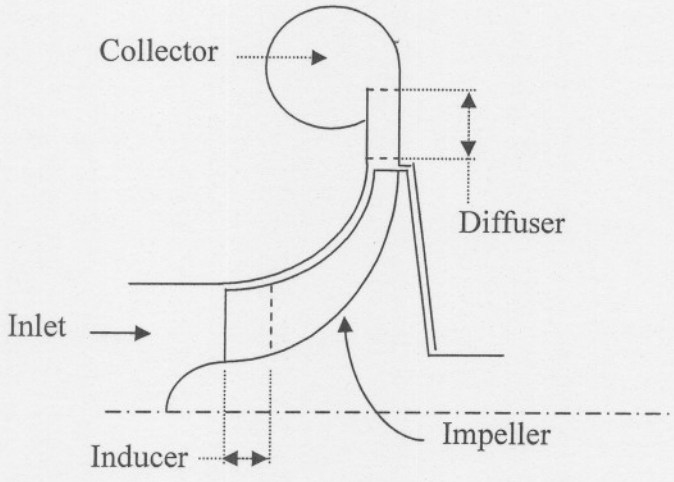

Figure A-3 General layout of the centrifugal compressor

Inlet casing

The function of the inlet casing is to deliver working fluid to the impeller eye with minimum loss and to provide a uniform velocity profile at the impeller entrance. The upstream duct arrangement strongly influences the nature of the flow at the impeller inlet. This could be a simple straight inlet duct, a curved inlet duct, a curved return passage of a multi-stage compressor, or the final stage of an axial flow compressor. These different configurations may lead to flow distortions at the impeller inlet. Whether it is radial or circumferential distortions the overall compressor performance deteriorates with the introduction of inlet flow distortions (Whitfield & Baines, 1990:14)

Impeller

The first function of the impeller is to ensure the efficient acceleration, increasing the kinetic energy, of the working fluid. This function is performed in a section known as the inducer (see Figure A-4). Normally the inducer is curved away from the direction of rotation.

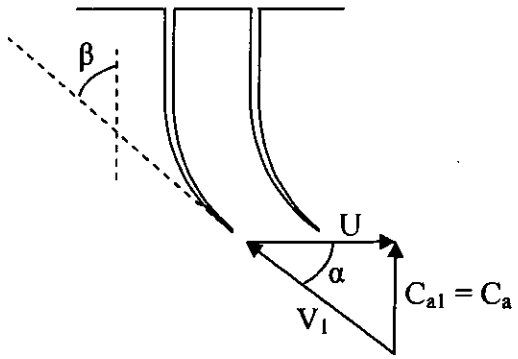

Figure A-4 Compressor inlet tri-angle

The angle of curvature at the inlet of the inducer blades is designed so that the working fluid enters at a relative angle, α, which is equal to the blade angle, β, ensuring minimum inlet losses. Once the kinetic energy of the working fluid have been increased by the inducer the rest of the blade passage must ensure the efficient slowing down of the working fluid to provide a low relative discharge velocity (Whitfield & Baines, 1990:14).

Diffusers

The diffuser is a stationary component situated directly around the impeller. The flow discharges from the compressor impeller with a high absolute velocity. The roll of the diffuser is to reduce the kinetic energy, thereby increasing the static pressure. Two types of diffusers are used with centrifugal compressors. They are the parallel-wall or the vaned diffuser.

Compressors with vane-type diffusers normally have high peak efficiency but a narrower operating range than compressors with vaneless diffusers. Since approximately half of the fluid energy leaving the impeller is kinetic, diffusers will directly influence the compressor efficiency (Whitfield & Baines, 1990:17)

Collector

The function of the collector or volute is simply to collect the diffuser exit flow and guide it as efficiently as possible to the exit pipe or manifold, without reducing the effectiveness of the diffuser (Watson & Janota, 1982:96)

A.2.1 Thermodynamics

The compression process may be plotted on an enthalpy-entropy diagram, Figure A-5. Station 00 represents the inlet conditions of the working fluid. Acceleration of the working fluid in the inlet casing causes a pressure drop from p_{00} to p_1, the change in enthalpy being equivalent to the increase in kinetic energy ($C_1^2/2$). The process is subjected to frictional losses resulting in the reduction of total pressure from p_{00} to p_{01}. Energy transfer to the working fluid takes place in the impeller and the process is indicated by the line 1-2. If all the kinetic energy of the working fluid leaving the impeller ($C_2^2/2$) is converted to pressure (isentropically), the delivery pressure would be p_{02} (point 02). Since the diffusion process (2-3) is not accomplished isentropically, and some kinetic energy remains at the diffuser exit ($C_3^2/2$), the static delivery pressure at point 3 is p_3 (Watson & Janota, 1982:76)

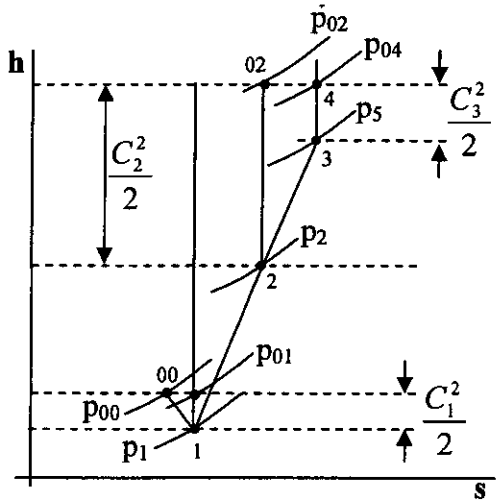

Figure A-5 Centrifugal compressor enthalpy-entropy diagram (Watson & Janota, 1982:75)

Losses

The enthalpy-entropy diagram, Figure A-5, has illustrated that compression is subjected to various losses. The energy losses in the centrifugal compressor can be broadly divided into two major groups. They are internal and parasitic losses. Internal losses are subdivided into incidence, blade loading, skin friction, clearance. mixing and vaneless diffuser losses. Parasitic losses include disc friction, recirculation and leakage losses (Moolman, 2003)

A.2.2 Compressor characteristics

Compressor characteristics are specified by curves of delivery pressure and temperature plotted against mass flow for various fixed values of rotational speed. However, these characteristics are dependent on other variables such as the conditions of pressure and temperature at the entry of the compressor and the physical properties of the working fluid. The full variation of these properties would involve an excessive number of experiments and a practical presentation of these results would prove to be impossible. In Saravanamuttoo *et al.* (2001:173) this complication is eliminated by using the technique of dimensional analysis. Through dimensional analysis the variables may be combined to form a more manageable number of dimensional groups. The dimensional analysis of a compressor is backed by the following important points:

- When considering the dimension of temperature it is useful to associate it with the gas constant R. this results in a combined variable RT that is equal to p/ρ and has the dimensions $\mathbf{ML^{-1}T^{-2}/ML^{-3} = L^2T^{-2}}$, which is the same as $(\text{velocity})^2$. Using the same gas during the testing and subsequent use of the compressor, R can finally be eliminated. However, if there is a change from one gas to another R must be retained in the final expression.
- The behaviour of the compressor is undoubtedly influenced by the density of the gas. However, if the pressure p and the RT product is also sited, its inclusion is not required since $\rho = p/RT$.
- The viscosity μ of the gas can be included since in theory it will also influence the behaviour of the compressor. The addition of this variable would result in the emergence of the Reynolds number. Due to the highly turbulent flow during normal operating conditions for compressors, experience indicates that the influence of this variable is negligibly small, and its effect may be excluded.

Keeping the above points in mind, the various quantities which will both influence the behaviour of the compressor and dependent on it can be considered. The solution takes on the form of an equation, (A- 1), in which a function of all the variables equates to zero.

$$f_1(D, N, \dot{m}, p_{01}, p_{02}, RT_{01}, RT_{02}) = 0 \quad \text{(A- 1)}$$

Where D is a characteristic geometrical parameter of the compressor, usually taken as the impeller diameter and N is the rotational speed. The subscripts 1 and 2 denotes to the inlet and exit stations respectively.

Using dimensional analysis the seven variables in Equation (A- 1) can be reduced to four non-dimensional groups. The resulting dimensionless parameters are:

$$f_2\left(\frac{p_{02}}{p_{01}}, \frac{T_{02}}{T_{01}}, \frac{\dot{m}\sqrt{RT_{01}}}{D^2 p_{01}}, \frac{ND}{\sqrt{RT_{01}}}\right) = 0 \quad \text{(A- 2)}$$

For a compressor the pressure ratio is defined as

$$PR_c = \frac{p_{02}}{p_{01}} \quad \text{(A- 3)}$$

Using isentropic flow relations, it is possible to replace the temperature ratio parameter with isentropic efficiency. For a compressor isentropic efficiency is defined as

$$\eta_c = \frac{\left(PR_c^{(\gamma-1)/\gamma} - 1\right)}{\left(\frac{T_{02}}{T_{01}} - 1\right)} \quad \text{(A- 4)}$$

Subsequently, for a compressor Equation (A- 2) reduces to

$$f_2(PR_c, \eta_c, NDM, NDS) = 0 \quad \text{(A- 5)}$$

Where the Non-Dimensional Mass flow rate (NDM) is defined as

$$NDM = \frac{\dot{m}\sqrt{RT_{01}}}{D^2 p_{01}} \quad \text{(A- 6)}$$

And the Non-dimensional Speed (NDS) is defined as

$$NDS = \frac{ND}{\sqrt{RT_{01}}} \quad \text{(A- 7)}$$

Using the four variables in Equation (A- 5) the performance for any compressor can be given as a set of two curves, namely pressure ratio as a function of NDM for various constant NDS curves, as well as isentropic efficiency, plotted in the same manner. These curves, although

plotted in two dimensions, are really representing a surface formed in three-dimensional space (Flownex, 2005).

Before describing a typical set of characteristics, it is useful to consider what will happen if a valve, placed in the delivery line of a compressor operating at constant speed, and is slowly opened. The resulting variation of pressure ratio with increased mass flow rate can be understood by a rather simplified but realistic analysis as shown in Figure A- 6 (Watson & Janota, 1982:128).

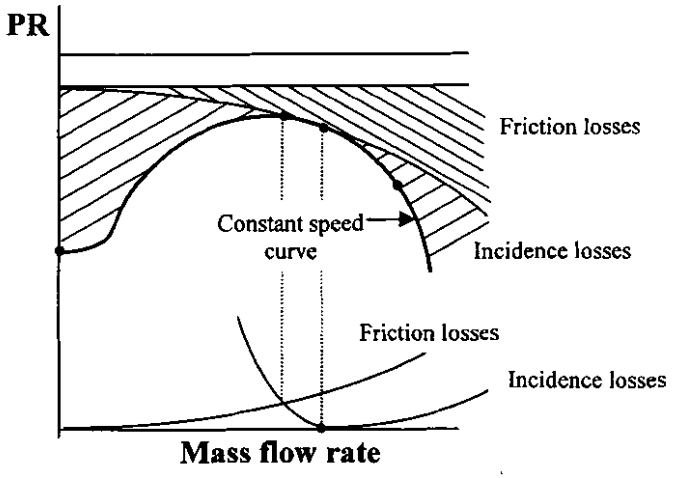

Figure A- 6 Theoretical compressor characteristic (Watson & Janota, 1982:128)

Since specific energy transfer is a function of tip speed and slip factor, it will remain constant as mass flow rate increases (Watson & Janota, 1982:80). Because of increasing velocities frictional losses in the impeller and diffuser passages must increase with mass flow rate. Incidence losses increases as the mass flow rate (and hence the flow angle) deviates from the design point. When the frictional and incidence losses are both subtracted from the energy input the typical constant speed curve is obtained (Watson & Janota, 1982:128).

Constant speed curves, like that in Figure A- 6, are generated at different speeds for a compressor. When these curves are superimposing on one graph a complete compressor map is obtained, Figure A-7.

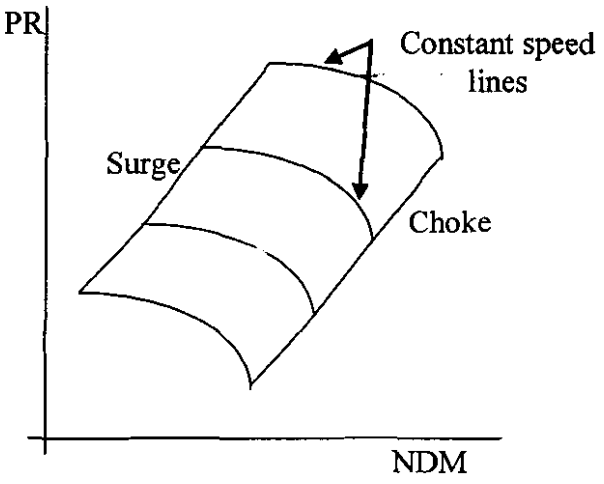

Figure A-7 Typical compressor pressure ratio characteristic

Similarly to the constant speed curves for pressure ratio, efficiency is plotted against NDM. Figure A- 8 shows the typical efficiency characteristic of a compressor at various constant speeds.

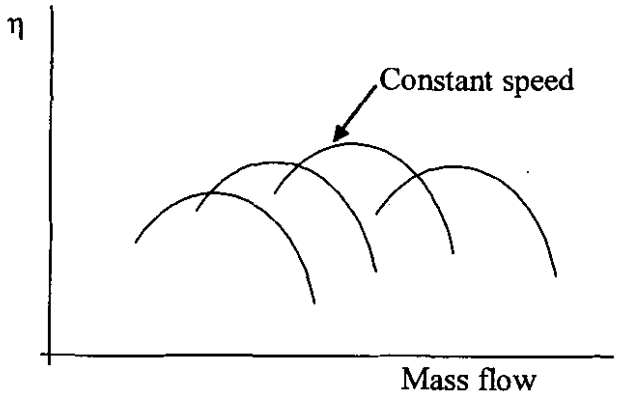

Figure A- 8 Typical compressor efficiency characteristic

A.2.3 Compressor instabilities

The compressor map in Figure A-7 shows three identifiable regions. The region to the left is known as the surge region while the region to the right is known as the choke region. Stable operation is represented by the region bounded by these two regions of instability.

The instabilities occurring in a centrifugal compressor can be identified as component stall, stage instability or stage stall and system instability described as surge. Information on compressor instabilities was found in Watson & Janota (1982:129) and is subsequently summarized.

Inducer stall

Inducer stall happens when at a certain constant speed the mass flow rate through the compressor is gradually reduced. A breakdown in the flow process occurs which leads to instability. As the mass flow is reduced, the axial component of the absolute velocity decreases, resulting in an increased incidence angle of the working fluid approaching the impeller. The incidence angle will continue to increase until the flow can no longer adhere to the suction side of the inducer blade. This leads to flow separation which creates a stall condition and subsequently encouraging reversal of flow.

Rotating stall

If the flow at inducer inlet is non-uniform, the breakdown of flow in one channel causes fluid in the next channel to be deflected in such a way that it receives fluid at an increased incidence angle. The one channel will then stall and restores normal flow in the previous channel. Stall passes from one channel to the next creating rotating stall. Rotating stall may lead to stage instability and aerodynamically induced vibrations resulting in an increased noise level.

Impeller stall

Impeller stall is the result of a wake formed during the separation of flow on the suction side of the radial portion of the impeller. The use of backsweep reduces the wake region and provides a more stable diffuser operation.

Vaneless diffuser stall

Reversal of flow occurring on the shroud side of the diffuser causes flow separation in vaneless diffusers. This flow separation is highly influenced be the fluid leaving the impeller. Flow in parallel walled diffusers tries to maintain a constant flow angle in order to conserve angular momentum. However, due to compressibility and viscosity effects the streamlines close to the wall have less kinetic energy and follow a path of much reduced spiral angle until they are eventually swept back towards the impeller. This backflow is known as a diffuser stall.

Stage stall

The compressor can still be in stable operation, although some components may be in a mode of stall. However, at a critical point, the reduced mass flow at constant speed of rotation

causes a critical number of components to stall, introducing a strong reversal of flow. This phenomenon is known as stage stall.

Surge

Surge is the instability that occurs when stage stall becomes self-exiting, periodic and grows to a large magnitude. During surge violent cyclic periods of backflow through the whole compressor occurs. Surge reduces the performance of the compressor and can cause damage to the compressor and its installation. Surge tends to occur where the constant speed line becomes horizontal.

Choking

The other limit to the flow range of a compressor is due to choking. Choking occurs when the flow exceed the velocity of sound at some cross-section. In centrifugal compressor it is normally the flow at the throat of the inducer that exceeds this limit.

A.3 The Radial turbine

The radial flow turbine is similar in appearance to the centrifugal compressor, but with flow directed in the inward direction. In general the radial flow turbine consists of a scroll or inlet casing, a set of inlet nozzles followed by a short vaneless gap and the turbine wheel itself. However, in small radial turbines for turbocharger applications the inlet nozzles is omitted to improve the flow range at some penalty of peak efficiency, but also reducing the cost (Watson & Janota, 1982:147). Figure A- 9 shows the major components or sections in the radial flow turbine.

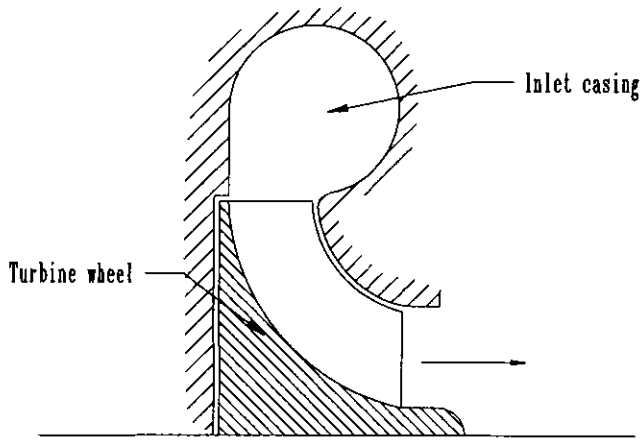

Figure A- 9 Meridional view of radial turbine

Inlet casing

In addition to distributing and accelerating the flow, the inlet casing or scroll, of a radial turbine without inlet nozzles, must provide flow guidance at the entry of the rotor. The geometry of the scroll determines the gas angle at volute exit or rotor tip (Watson & Janota, 1982:154).

Rotor

In the rotor the energy is transferred from the fluid to the shaft. The rotor is designed for maximum kinetic energy at rotor exit to ensure optimum energy transferral (Watson & Janota, 1982:160).

A.3.1 Thermodynamics

The expansion process through the radial turbine can be plotted on an enthalpy-entropy diagram, Figure A- 10.

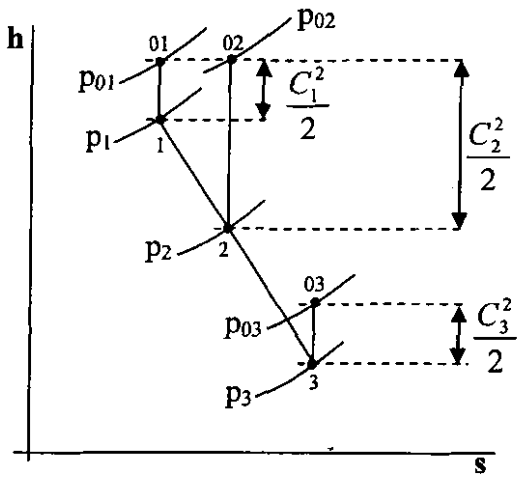

Figure A- 10 Radial turbine enthalpy-entropy diagram (Watson & Janota, 1982:148)

Station 01 refers to the stagnation conditions at the entry of the scroll, the working fluid will already have a velocity (C_1). The scroll accelerates the flow from station 1 to 2. Since the process is subjected to various losses, the total pressure has dropped from p_{01} to p_{02}. Energy transfer occurs in the rotor, between stations 2 and 3. Since exit velocity (C_3) remains significant the total pressure p_{03} will be slightly higher than the static pressure p_3 (Watson & Janota, 1982:148).

Losses

The enthalpy-entropy diagram, Figure A- 10, have shown that the expansion process in the radial turbine do not occur without losses. There are several sources of energy loss in the radial flow turbine. These may be divided into those that occur in the stationary flow passages and those that occur in the rotor. Those in the rotor may be sub-divided into incidence losses at the blade entry, fluid friction losses within the rotor passage, losses due to clearance between the rotor and the adjacent wall of the casing (Watson & Janota, 1982:167).

A.3.2 Turbine characteristics

Turbine characteristics can be represented in the same manner as a compressor by the four non-dimensional groups is Equation (5-2). For a turbine the pressure ratio is defined as:

$$PR_t = \frac{p_{01}}{p_{02}} \tag{A- 8}$$

Using isentropic flow relations, it is possible to replace the temperature ratio in Equation (5-2) with isentropic efficiency. For a turbine, isentropic efficiency is defined as:

$$\eta_t = \frac{\left(PR_t^{(\gamma-1)/\gamma} - 1\right)}{\left(\frac{T_{02}}{T_{01}} - 1\right)} \tag{A- 9}$$

Subsequently, for a turbine Equation (5-2) reduces to

$$f_2\left(PR_t, \eta_t, NDM, NDS\right) = 0 \tag{A- 10}$$

Where NDM and NDS is defined by Equation (5-6) and (5-7) respectively.

Using the four variables in Equation (5-10), the performance for any turbine can be given as a set of two curves, namely pressure ratio as a function of NDM for various NDS curves (Figure A- 11), as well as the isentropic efficiency (Figure A-12), plotted in the same manner (Flownex, 2005).

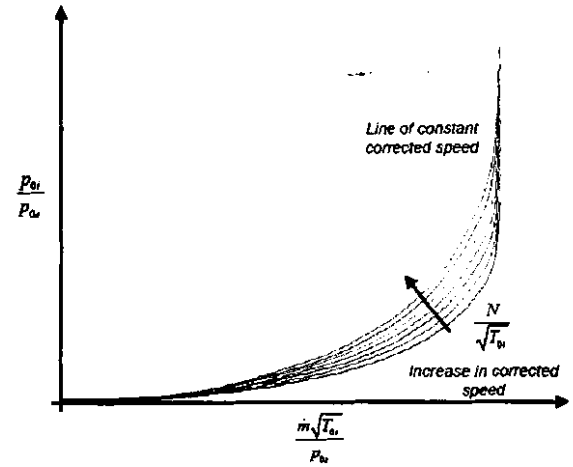

Figure A- 11 Typical turbine pressure ratio characteristic (Flownex, 2005)

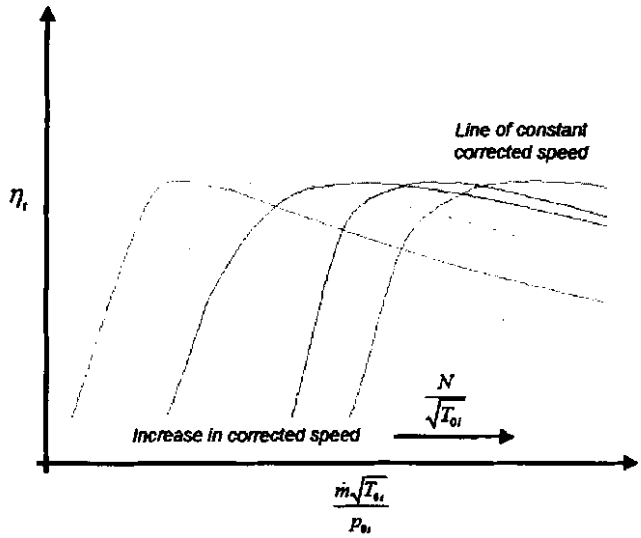

Figure A-12 Typical turbine efficiency characteristic (Flownex, 2005)

In practice, however, it is found that turbines do not exhibit significant variation in non-dimensional mass flow with non-dimensional speed. The turbine operating region is restricted by another component downstream of it, in most cases (Saravanamuttoo, 2001:378).

A.4 Turbocharger mechanical design

The mechanical design of a turbocharger is aimed at ensuring economical manufacturing and that it maintains its performance over a prescribed lifetime of operation without serious deterioration of failure.

A.4.1 Bearing types

Shaft bearings support the rotating bearing assembly and must do so without failure and with minimum frictional losses. The bearing assembly must also make provision for the imbalance axial force generated in the turbine and compressor by means of some sort of thrust bearing.

One of the disadvantages of the inboard mounted bearing arrangement is the inherently unstable running of the rotating assembly due to the short distance between the bearings and the heavy over hanging weight of the turbine wheel. It calls for well damped bearings and a carefully balanced rotating assembly (Watson, 1982:43).

A.4.1.1 Journal bearings

In small turbochargers fixed sleeve bearings, pressed into the housing, were used. As turbocharger technology developed this type of bearings was found to be unstable when operating under lightly loaded, high speed conditions. This unstable condition is the result of "oil whirl" which causes the shaft to orbit around its centre in the same direction of shaft rotation and at about half the shaft speed. Oil whirl often leads to severe wear on the journal and bearing if not controlled (MacInnes, 1984:24).

For small turbochargers, operating at high speeds, fixed bearings were replaced with various types of floating bearings that have an outer out film, between the bearing sleeve and the housing, in addition to that between the shaft and the sleeve. The increased resilience and damping led to floating bearings becoming the industry standard (Baines, 2005:116).

A fully floating bearing is allowed to rotate freely, with rotation as high as one third of the shaft speed. This posse the problem of oil starvation and bearing housing wear. Although the bearing might only have a thin wall thickness, the oil supply holes to the inner surface will act as a centrifugal pump. At high rotational speeds the pressure differential between the inner surface and outer surface may be enough to overcome the oil supply pressure. This will lead to oil starvation and subsequently rapid failure will occur (MacInnes 1984:25). The rotation of the bearing sleeve further influences the choice of bearing materials. Bearing housings that are cast in aluminium require a cast iron or steel sleeve to be pressed in place (Baines, 2005:116). A typical fully floating sleeve bearing is shown in Figure A-13.

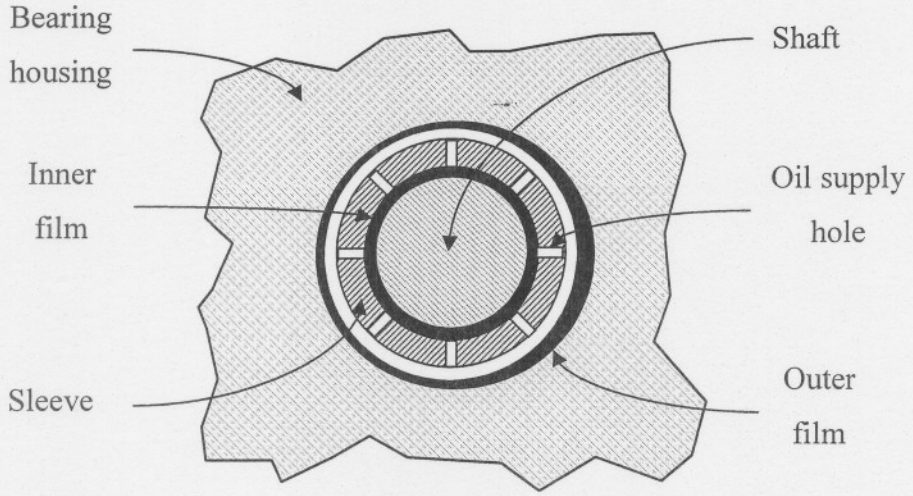

Figure A-13 Typical fully floating journal bearing

To understand the issues involved in the design of journal bearings for a turbocharger, it is useful looking at Petroff's Equation (A- 11) for power dissipation in a fixed bearing.

$$P_b = \frac{\pi}{4}\frac{\mu\omega^2 LD^3}{\varepsilon_r} \qquad \textbf{(A- 11)}$$

Where μ the oil viscosity, ω the rotational speed, L and D the length and diameter, and ε_r the oil film thickness.

It is clear from the equation that the bearing diameter and the rotational speed have the largest influence on power loss. However, the aim to keep turbochargers small, which decreases their diameters and increases their speeds override this consideration. Increasing the oil film thickness, ε_r, reduces the power loss, but a large film thickness increases the tip clearances of the compressor and turbine blades which decrease the aerodynamic efficiency (Baines, 2005:117).

In a fully floating bearing two oil films surfaces are present, each with a relative surface velocity that is approximately half of the shaft speed. The total viscous shear in the bearing is considered to be 30 – 50 % lower than in a fixed journal bearing (Baines, 2005:118).

A.4.1.2 Thrust bearings

Pressure forces acting on the compressor and turbine wheels create a net imbalance axial force acting on the rotating assembly. The back-to-back configuration is aimed at minimizing this axial force by allowing the compressor and turbine forces to cancel each other. The net force, however, even with exactly balanced forces at the design point, will not equal zero

during the transient operation of the turbocharger. Therefore provision must be made to accommodate for axial thrust forces on the rotating assembly (Baines, 2005:123).

Figure A-14 shows a typical turbocharger thrust bearing assembly. In this thrust bearing arrangement oil is pumped internally to films on both sides of the thrust bearings. The bearing itself can be of the plain disk type, but to increase film pressure ensuring higher thrust capacity for a given thrust bearing size, tapered land bearings are used. In tapered land thrust bearings the oil flow is directed onto the ramped surfaces. The design variable which determines the thrust capacity of the turbocharger is the number of pads on the circumference (Baines, 2005:124).

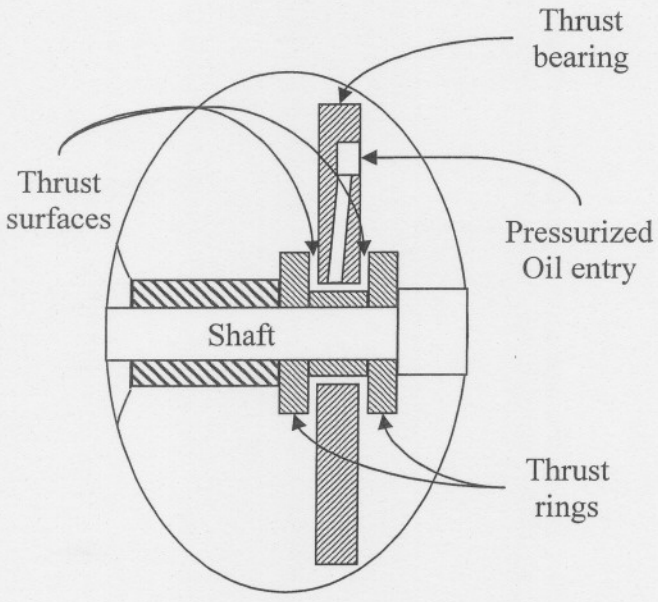

Figure A-14 Turbocharger thrust bearing

Frictional power loss in a plain double sided thrust bearing is given by a modified version of Petroff's Equation (A- 12):

$$P_f = \frac{\pi\mu\omega^2(r_2^4 - r_1^4)}{\varepsilon_x} \qquad \textbf{(A- 12)}$$

The inner and outer radii are given by r_1 and r_2 and the axial clearance by ε_x. From Equation (A- 12) it is evident that the least power will be dissipated in the smallest thrust bearing. In a small thrust bearing, however, the bearing will not be able to sufficiently disperse of the heat generated. If the oil heats up beyond a critical point, the drop in viscosity will result in metal-to-metal contact (Baines, 2005:124).

Axial thrust is calculated by equating the sum of all the axial forces acting on the compressor and turbine rotors, which are due to pressure and momentum forces acting on them. The momentum equation for a controlled volume is given by Equation (A- 13).

$$\oiint \rho \mathbf{C}(\mathbf{C}d\mathbf{A}) = \oint p.\mathbf{A} + \mathbf{F} \qquad \textbf{(A- 13)}$$

Applying Equation (A- 13) to the control volume shown in, Figure A- 15, the axial thrust can be calculated. The accuracy of the calculation, however, is strongly depended on the pressure and velocity distributions, determined by means of a flow field analysis (Japikse, 1996:2-80).

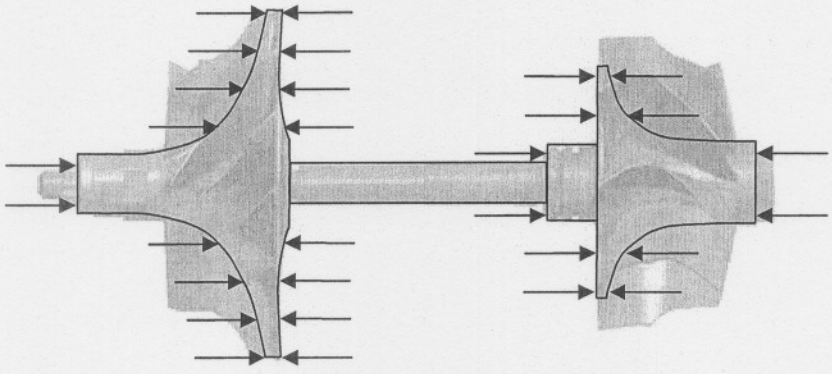

Figure A- 15 Pressure force components of axial load on the rotating assembly of a turbocharger (Garrett, 2005)

Pressure and velocity distributions are difficult to predict accurately and are sometimes reliant on empirical data which may not be applicable on the particular geometry. The back-to back configuration results in the calculation of a small difference between two large apposing forces, any errors in calculating these two components is magnified in the error of their difference. Axial thrust calculations are therefore inevitably approximate (Baines, 2005:125).

The radial turbine in a turbocharger has a heavily scalloped back face for reduced polar moment of inertia, while the compressor has a full back face for optimum aerodynamic efficiency. This reduces the axial force contribution of the turbine and means that the compressor is usually the largest contributor to the total axial force (Baines, 2005:125).

The thrust bearing capacity requirement is determined by disk pressures acting on the compressor and turbine, which are directly related to turbine and compressor design (Baines, 2005:125).

In a turbine reaction is defined as the ratio of pressure ratio across the turbine rotor to the total pressure ratio of the turbine (Baines, 2005:85). The choice of reaction will therefore control the static pressure at rotor inlet, which is the static pressure acting on the upstream face of the turbine rotor. However, to achieve optimum aerodynamic efficiency an intermediate reaction is usually chosen, leaving the designer with little freedom to manipulate the axial thrust through the choice of reaction (Baines, 2005:125).

In a centrifugal compressor the pressure acting on the impeller back face is determined by the relative amounts of diffusion that occur in the impeller and the diffuser. Increasing impeller diffusion increases the static pressure at impeller outlet. Impeller diffusion is increased by wider impeller exits and using backsweep. Since impellers using the backsweep design produce high efficiency, they are used through out the range of turbocharger applications. This together with a larger impeller diameter to achieve the required pressure ratio increases the axial thrust component of the compressor (Baines, 2005:125).

A.4.1.3 Rolling bearings

For automotive turbochargers the bearings described above is normally used, however, ball bearings over an attractive alternative. Ball bearings have small frictional power losses, can be heavily overloaded and tolerate oil starvation for short periods. Traditionally low-cost roller bearings did not meet the durability requirements at the very high speed speeds that are normal (Watson, 1982:43). But with the ever developing bearing technology, roller bearings are gradually being introduced in smaller and higher speed turbochargers (Baines, 2005:118). In addition to radial support to the rotating assembly, angular contact bearings can be used to carry axial thrust loads. Depending on the application angular contact bearings can be configured on a number of ways, Figure A- 16.

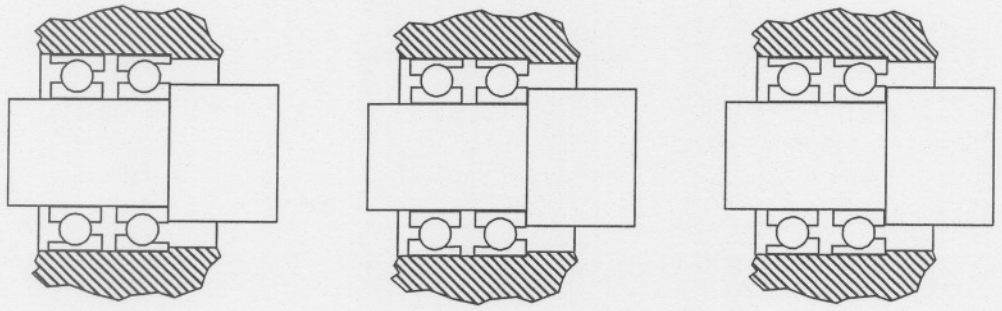

Figure A- 16 Angular contact bearing arrangements (Baines, 2005:119)

The front-to-front arrangement, although having the lowest radial stiffness, has a high degree of tolerance to misalignments. The back-to-back arrangement has the greatest radial moment stiffness. When the turbocharger is subjected to high, unidirectional thrust, the tandem configuration is the best choice (Baines, 2005:119).

A.4.2 Rotor Dynamics

The bearings in a turbocharger are dynamically loaded from three identifiable sources. These are rotating assembly unbalance, inertial forces from engine motion, and gyroscopic forces due vehicle motion. Aerodynamic side loading, gear loading, and gravity is the sources for static loads. The unbalance force is the largest in magnitude calling for careful balancing of the rotating assembly. The compressor and turbine wheels are individually balanced so that they can be assembled and reassembled without exceeding the eccentricity limits for the complete rotating assembly (Baines, 2005:121).

In Baines (2005:121) the first three critical speeds of the rotating assembly, shown inFigure A- 17, is described.

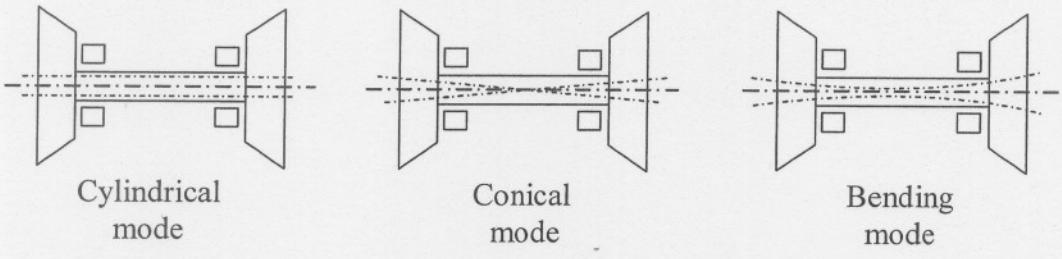

Figure A- 17 Rotating assembly critical modes (Baines, 2005:122)

The first critical mode, the cylindrical mode, is well damped by most bearing arrangements, but normally controlled to be situated below the running range of the turbocharger. The conical mode is poorly damped when using the inboard mounted bearing arrangement because of the close proximity of the bearings to the nodal point. Therefore this mode is also designed to occur below the operating range of the turbocharger. Having the first two critical modes located below the running range calls for quick acceleration during start-up and shut-down to avoid damage (Baines, 2005:121).

The third critical mode known as the bending mode is the natural shaft bending frequency which depends on the shaft stiffness and the rotating masses. The aim is to keep the rotating

masses to a minimum but since this is always a compromise with aerodynamic performance and life requirements, the designer is often only left with the freedom to control the choice of shaft length and diameter. The shaft is therefore designed to be as short as possible consistent with the space requirements for the bearing housing and bearing assembly. The shaft diameter is designed to keep the critical speed safely above the maximum operating speed of the turbocharger (Baines, 2005:121).

A.4.3 Lubrication

Bearings in a turbocharger require a sufficiently thick oil film for the complete separation of the shaft, the bearing sleeve and the bearing housing. With the separation established, the bearing material is only of consequence to ensure that it keeps its shape under the loads transmitted by the oil film. Turbochargers are designed to share the engine oil system meaning the bearings must work with the same oil composition, supply temperature, and degree of filtration. Turbochargers with roller bearings, however, require a separate oil supply system. Roller element bearings use light oil for minimum frictional loss and a high level of filtration for improved durability (Baines, 2005:126).

Lack of lubrication

Lack of turbocharger lubrication is normally the result of the delay between engine start and turbocharger lubricant arrival, but may also occur during normal operation. The bearings is designed to tolerate brief lubrication lapses, however, successive lubrication lapses will result in wear leading to rotordynamic instability, excessive shaft motion, and rapid failure. This failure mode is identified to wear on the bearing inner surface (Baines, 2005:126).

Lubricant contaminants

Even though turbochargers are designed to work with lubricant of the same filtration quality as the engine, they require complete filtration. Small quantities on foreign matter in the turbocharger can cause bearing failure, whereas the same amount of foreign matter in the engine bearing system would cause little or no damage. In the engine bearing system the contaminant material is driven into the soft bearing material while in the turbocharger the contaminant material cuts both the bearing and the bearing bore. Lubrication contaminant failure is identified by damage to the bearing outer surface because the heavy particles do not travel against the centrifugal pressure field to the inner surface (Baines, 2005:127).

Type of lubrication

Wide-range multiviscosity oils should be avoided as the material added to achieve this wide range increases blockage due to oil residue (known as Coking). The best lubricant will be one with a straight viscosity, with a ten point higher viscosity in the summer. Two type of lubricant can be chosen, synthetic-based or mineral-based lube. Because synthetic-based lubrication can be more rigidly controlled a very consistent, uniform molecular structure, with highly predictable properties can be accomplished (Bell, 1997:40).

Lubricant drainage

Lubricant passing through the turbocharger must drain quickly without restriction. The only force available to drain the lubricant is gravity. To assist the small gravitational force the lubricant drainage system has the following features (Bell, 1997:44):

- The lubricant exit angle must be vertically downward. If this is not possible the exit angle must not exceed a deviation of 30°.
- After the bearings no lubricant pressure exists. In order to achieve the required flow the drain hose must be larger than the inlet hose.
- The drain hose must be as smooth as possible.

A.4.4 Shaft seals

Seals in a turbocharger are required where the shaft exits the bearing housing to connect the compressor and turbine rotors. The seals must prevent lubricant leakage from the bearings to the turbine and compressor and prevent air leaking into the bearing housing (Baines, 2005:127).

Under normal operating conditions the gas pressure behind the turbine and compressor wheels is much larger that the lubricant pressure inside the bearing housing. Despite the higher temperatures, sealing at the turbine end is much easier because bearing housing pressure is always kept positive. The sealing is normally done by a piston ring in a grove at the turbine end of the shaft. The ring does not rotate and fits very snugly in the bearing housing (MacInnes, 1984:22).

The piston ring seal requires a positive pressure difference to be maintained across the seal at all times. At the compressor end, however, this is not always the case. At high-speed, low load operation of the engine the compressor is subjected to high flow, low boost conditions.

This causes the impeller exit pressure to drop below that of the bearing housing. In order to prevent lubricant leaking from the bearing housing, the piston ring seal at the compressor end has a small centrifugal pump to prevent lubricant from reaching the seal (MacInnes, 1984:23).

A.4.5 Bearing housing

The bearing housing between the compressor and the turbine is kind of a necessary evil to hold the whole turbocharger together. Although bearing housings can take on various shapes and sizes, they are essentially the same (MacInnes, 1982:21).

The bearing housing, normally manufactured from aluminium or cast iron, is precisely machined with perfect alignment. Apart from keeping everything in place the bearing housing must limit the heat transfer from the hot turbine gases to the lubricant and the compressor air. The over heating of the lubricant will result in bearing failure while the heating of the compressed air will reduce the compressor efficiency and increase the demand on a inter-cooler (Baines, 2005:129).

APPENDIX B: FIRST ORDER CYCLE ANALYSIS

B.1 Simulation Diagram

Assumptions and limitations:

Boundary values:

p_{min} = 250 [kPa]

$\dot{m}$ = 1 [kg/s]

TIT = 700 [°C]

T_w = 20 [°C]

Component characteristics:

f_{pipe} = 0.006

f_{RXHP} = 0.005

ε_{rx} = 0.88

ε_{hx} = 0.95

η_{comp} = 0.76

η_{turb} = 0.72

η_m = 0.98

$PR_{HPC} = PR_{LPC}$

OPR = 2.88 (Max. efficiency)

Cycle layout:

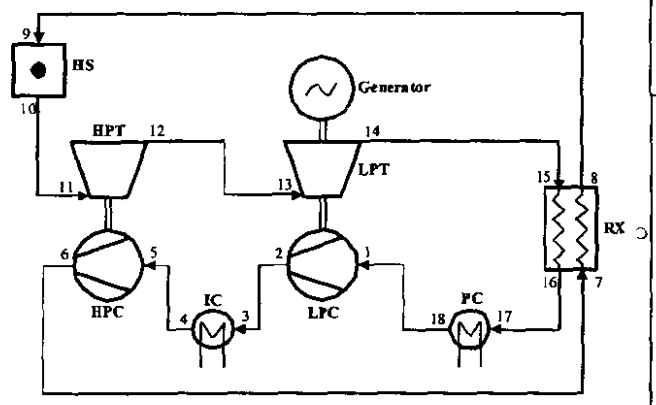

Performance parameters:

Q_{gen} = 46.75 [kW/kg.s^{-1}]

η_{sys} = 0.1916

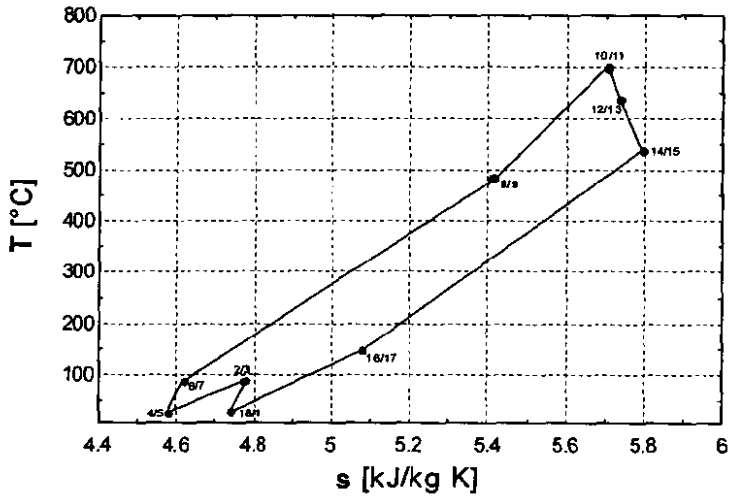

B.2 Simulation Code

```
"..."
"Functions"
FUNCTION Comp(m,cp,T,eta,PR,gamma)
Comp  =     (m*cp*(T+273))/eta*(PR^((gamma-1)/gamma)-1)
end

FUNCTION Turb(m,cp,T,eta,PR,gamma)
Turb  =     (m*cp*(T+273)*eta)*((1/PR)^((gamma-1)/gamma)-1)
end

FUNCTION c_p(T)
theta  =    T+273.15
c_p    =    -1.38e-19*theta^6 + 9.11e-16*theta^5 - 2.26e-12*theta^4 + 2.5e-9*theta^3 - 1.07e-
6*theta^2 + 1.93e-3*theta + 1.03
end

FUNCTION mma(T,P)
R      =    0.2968
c_p    =    CP(N2,T=T)
mma    =    c_p/(c_p - R)
end

FUNCTION ave(T_1,T_2)
ave    =    (T_1 + T_2)/2
end
"..."

"Main"
"_____"
"First order assumptions"
p_min          =    250
m_dot          =    1
TIT            =    700
f_pipe         =    0.6/100
f_hx           =    0.005
epsilon_rx     =    0.88
epsilon_hx     =    0.95
eta_comp       =    0.76
eta_turb       =    0.72
PR_HPC         =    PR_LPC
T_w            =    20
eta_m          =    0.98

"_____"

OPR   =    2.88    "Maximum efficiency"
{OPR  =    4.414}
OPR            =    PR_LPC*PR_HPC

">>>>>>>>>>>>>"
"Node 1"
p[1]   =    p_min
p[1]   =    p[18] - DELTA_p181
T[1]   =    T[18] + Q_181/(m_dot*CP(Nitrogen,T= ave(T[18],T[1]),P=ave(p[18],p[1])))
">>>>>>>>>>>>>"

"....."
"LPC 1-2"
eta_LPC        =    eta_comp
```


```
Q_LPC       =       Comp(m_dot,CP(Nitrogen,T=
ave(T[1],T[2]),P=ave(p[1],p[2])),T[1],eta_LPC,PR_LPC,mma(ave(T[1],T[2]),ave(p[1],p[2])))
"""""""""""""""""""""""""

">>>>>>>>>>>>>>"
"Node 2"
p[2]    =       p[1]*PR_LPC
T[2]    =       T[1] + Q_LPC/(m_dot*CP(Nitrogen,T= ave(T[1],T[2]),P=ave(p[1],p[2])))
">>>>>>>>>>>>>>"

"""""""""""""""""""""""""
"Pipe 2-3"
DELTA_p23   =       f_pipe*p[2]
Q_23        =       0
"""""""""""""""""""""""""

">>>>>>>>>>>>>>"
"Node 3"
p[3]    =       p[2] - DELTA_p23
T[3]    =       T[2] + Q_23/(m_dot*CP(Nitrogen,T= ave(T[2],T[3]),P=ave(p[2],p[3])))
">>>>>>>>>>>>>>"

"""""""""""""""""""""""""
"IC 3-4"
epsilon_IC  =       epsilon_hx
f_IC        =       f_hx
Q_IC        =       epsilon_IC*m_dot*CP(Nitrogen,T= ave(T[3],T[4]),P=ave(p[3],p[4]))*(T_w -
T[3])
DELTA_pIC   =       f_IC*p[3]
"""""""""""""""""""""""""

">>>>>>>>>>>>>>"
"Node 4"
p[4]    =       p[3] - DELTA_pIC
T[4]    =       T[3] + Q_IC/(m_dot*CP(Nitrogen,T= ave(T[3],T[4]),P=ave(p[3],p[4])))
">>>>>>>>>>>>>>"

"""""""""""""""""""""""""
"Pipe 4-5"
DELTA_p45   =       f_pipe*p[4]
Q_45        =       0
"""""""""""""""""""""""""

">>>>>>>>>>>>>>"
"Node 5"
p[5]    =       p[4] - DELTA_p45
T[5]    =       T[4] + Q_45/(m_dot*c_p(ave(T[4],T[5])))
">>>>>>>>>>>>>>"

"""""""""""""""""""""""""
"HPC 5-6"
eta_HPC     =       eta_comp
Q_HPC       =       Comp(m_dot,CP(Nitrogen,T=
ave(T[5],T[6]),P=ave(p[5],p[6])),T[5],eta_HPC,PR_HPC,mma(ave(T[5],T[6]),ave(p[5],p[6])))
"""""""""""""""""""""""""

">>>>>>>>>>>>>>"
"Node 6"
p[6]    =       p[5]*PR_HPC
T[6]    =       T[5] + Q_HPC/(m_dot*CP(Nitrogen,T= ave(T[5],T[6]),P=ave(p[5],p[6])))
```

```
">>>>>>><<<<<<"

"""""""""""""""""""""
"Pipe 6-7"
DELTA_pPV   =       f_pipe*p[6]
Q_67        =       0
"""""""""""""""""""""

">>>>>>><<<<<<"
"Node 7"
p[7]    =       p[6] - DELTA_pPV        "Net presure rise"
T[7]    =       T[6] + Q_67/(m_dot*CP(Nitrogen,T= ave(T[6],T[7]),P=ave(p[6],p[7])))
">>>>>>><<<<<<"

"""""""""""""""""""""
"RX hp side 7-8"
f_RXHP      =       0.005
C_min       =       min((m_dot*CP(Nitrogen,T=
ave(T[7],T[8]),P=ave(p[7],p[8]))),m_dot*CP(Nitrogen,T= ave(T[15],T[16]),P=ave(p[15],p[16])))
Q_RXHP      =       C_min*epsilon_RX*(T[15] - T[7])
DELTA_pRXHP=        f_RXHP*p[7]
"""""""""""""""""""""

">>>>>>><<<<<<"
"Node 8"
p[8]    =       p[7] - DELTA_pRXHP
T[8]    =       T[7] + Q_RXHP/(m_dot*CP(Nitrogen,T= ave(T[7],T[8]),P=ave(p[7],p[8])))
">>>>>>><<<<<<"

"""""""""""""""""""""
"Pipe 8-9"
DELTA_p89   =       f_pipe*p[8]
Q_89        =       0
"""""""""""""""""""""

">>>>>>><<<<<<"
"Node 9"
p[9]    =       p[8] - DELTA_p89
T[9]    =       T[8] + Q_89/(m_dot*CP(Nitrogen,T= ave(T[8],T[9]),P=ave(p[8],p[9])))
">>>>>>><<<<<<"

"""""""""""""""""""""
"HS 9-10"
f_HS        =       0.001
DELTA_pHS   =       f_HS*p[9]
Q_HS        =       m_dot*CP(Nitrogen,T= ave(T[9],T[10]),P=ave(p[9],p[10]))*(T[10] - T[9])
"""""""""""""""""""""

">>>>>>><<<<<<"
"Node 10"
p[10]   =       p[9] - DELTA_pHS
T[10]   =       TIT
">>>>>>><<<<<<"

"""""""""""""""""""""
"Pipe 10-11"
DELTA_p1011 =       f_pipe*p[10]
Q_1011      =       0
"""""""""""""""""""""
```

```
">>>>>>><<<<<<"
"Node 11"
p[11]   =       p[10] - DELTA_p1011
T[11]   =       T[10] + Q_1011/(m_dot*CP(Nitrogen,T= ave(T[10],T[11]),P=ave(p[10],p[11])))
">>>>>>><<<<<<"

"""""""""""""""""""""""""
"HPT 11-12"
eta_HPT         =       eta_turb
Q_HPT=          -Q_HPC/eta_m
Q_HPT=          Turb(m_dot,CP(Nitrogen,T= ave(T[11],T[12]),P=ave(p[11],p[12]))
,T[11],eta_HPT,PR_HPT,mma(ave(T[11],T[12]),ave(p[11],p[12])))
"""""""""""""""""""""""""

">>>>>>><<<<<<"
"Node 12"
p[12]   =       p[11]/PR_HPT
T[12]   =       T[11] + Q_HPT/(m_dot*CP(Nitrogen,T= ave(T[11],T[12]),P=ave(p[11],p[12])))
">>>>>>><<<<<<"

"""""""""""""""""""""""""
"Pipe 12-13"
DELTA_p1213 =       f_pipe*p[12]
Q_1213          =       0
"""""""""""""""""""""""""

">>>>>>><<<<<<"
"Node 13"
p[13]   =       p[12] - DELTA_p1213
T[13]   =       T[12] + Q_1213/(m_dot*CP(Nitrogen,T= ave(T[12],T[13]),P=ave(p[12],p[13])))
">>>>>>><<<<<<"

"""""""""""""""""""""""""
"LPT 13-14"
eta_LPT         =       eta_turb
Q_LPT           =       Turb(m_dot,CP(Nitrogen,T= ave(T[13],T[14]),P=ave(p[13],p[14]))
,T[13],eta_LPT,PR_LPT,mma(ave(T[13],T[14]),ave(p[13],p[14])))
"""""""""""""""""""""""""

">>>>>>><<<<<<"
"Node 14"
p[14]   =       p[13]/PR_LPT
T[14]   =       T[13] + Q_LPT/(m_dot*CP(Nitrogen,T= ave(T[13],T[14]),P=ave(p[13],p[14])))
">>>>>>><<<<<<"

"""""""""""""""""""""""""
"Pipe 14-15"
DELTA_p1415 =       f_pipe*p[14]
Q_1415          =       0
"""""""""""""""""""""""""

">>>>>>><<<<<<"
"Node 15"
p[15]   =       p[14] - DELTA_p1415
T[15]   =       T[14] + Q_1415/(m_dot*CP(Nitrogen,T= ave(T[14],T[15]),P=ave(p[14],p[15])))
">>>>>>><<<<<<"

"""""""""""""""""""""""""
"RX lp side 15-16"
f_RXLP                  =       f_hx
```

```
DELTA_p1516 =       f_RXLP*p[16]
Q_RXLP      =       -Q_RXHP
""""""""""""""""""""""""


">>>>>>><<<<<<"
"Node 16"
p[16]   =       p[15] - DELTA_p1516
T[16]   =       T[15] + Q_RXLP/(m_dot*CP(Nitrogen,T= ave(T[15],T[16]),P=ave(p[15],p[16])))
">>>>>>><<<<<<"

""""""""""""""""""""""""
"Pipe 16-17"
DELTA_p1617 =       f_pipe*p[16]
Q_1617      =       0
""""""""""""""""""""""""

">>>>>>><<<<<<"
"Node 17"
p[17]   =       p[16] - DELTA_p1617
T[17]   =       T[16] + Q_1617/(m_dot*CP(Nitrogen,T= ave(T[16],T[17]),P=ave(p[16],p[17])))
">>>>>>><<<<<<"

""""""""""""""""""""""""
"PC 17-18"
epsilon_PC      =       epsilon_hx
f_PC            =       f_hx
Q_PC            =       epsilon_PC*m_dot*CP(Nitrogen,T=
ave(T[17],T[18]),P=ave(p[17],p[18]))*(T_w - T[17])
DELTA_pPC       =       f_PC*p[17]
""""""""""""""""""""""""

">>>>>>><<<<<<"
"Node 18"
p[18]   =       p[17] - DELTA_pPC
T[18]   =       T[17] + Q_PC/(m_dot*CP(Nitrogen,T= ave(T[17],T[18]),P=ave(p[17],p[18])))
">>>>>>><<<<<<"

""""""""""""""""""""""""
"Pipe 18-1"
DELTA_p181  =       f_pipe*p[18]
Q_181 =     0
""""""""""""""""""""""""

"{}{}{}{}{}{}{}{}{}{}{}{}{}{}{}{}{}{}{}{}{}{}{}{}{}{}{}{}{}"
"Performance paramenters"
eta_sys         =       Q_gen/Q_HS
Q_LPT           =       -(Q_LPC/eta_m + Q_gen)
"{}{}{}{}{}{}{}{}{}{}{}{}{}{}{}{}{}{}{}{}{}{}{}{}{}{}{}{}{}"


s_0     =       5
Duplicate i=1,18
        s[i]    =       s_0     +       ENTROPY(Nitrogen,T=T[i],P=p[i])
        h[i]    =       ENTHALPY(Nitrogen,T=T[i],P=p[i])
end
```

B.3 Simulation Results

C_{min} = 1.07
Δ_{p1415} = 1.543 [kPa]
Δ_{p181} = 1.509 [kPa]
Δ_{p89} = 4.2 [kPa]
Δ_{pPC} = 1.264 [kPa]
ε_{hx} = 0.95
ε_{rx} = 0.88
η_{HPT} = 0.72
η_m = 0.98
f_{HS} = 0.001
f_{PC} = 0.005
f_{RXLP} = 0.005
PR_{HPC} = 1.697
PR_{LPT} = 1.898
Q_{1213} = 0 [kW/kg.s^{-1}]
Q_{181} = 0 [kW/kg.s^{-1}]
Q_{67} = 0 [kW/kg.s^{-1}]
Q_{HPC} = 66.51 [kW/kg.s^{-1}]
Q_{IC} = -69.87 [kW/kg.s^{-1}]
Q_{PC} = -124.1 [kW/kg s^{-1}]
s_0 = 5 [kJ/kg.K]

Δ_{p1011} = 4.171 [kPa]
Δ_{p1516} = 1.271 [kPa]
Δ_{p23} = 2.546 [kPa]
Δ_{pHS} = 0.6959 [kPa]
Δ_{pPV} = 4.247 [kPa]
ε_{IC} = 0.95
η_{comp} = 0.76
η_{LPC} = 0.76
η_{sys} = 0.1916
f_{hx} = 0.005
f_{pipe} = 0.006
$\dot{m}$ = 1 [kg/s]
PR_{HPT} = 1.407
p_{min} = 250 [kPa]
Q_{1415} = 0 [kW/kg.s^{-1}]
Q_{23} = 0 [kW/kg.s^{-1}]
Q_{89} = 0 [kW/kg.s^{-1}]
Q_{HPT} = -67.86 [kW/kg.s^{-1}]
Q_{LPC} = 66.94 [kW/kg.s^{-1}]
Q_{RXHP} = 426.8 [kW/kg.s^{-1}]
TIT = 700 [°C]

Δ_{p1213} = 2.946 [kPa]
Δ_{p1617} = 1.526 [kPa]
Δ_{p45} = 2.518 [kPa]
Δ_{pIC} = 2.109 [kPa]
Δ_{pRXHP} = 3.518 [kPa]
ε_{PC} = 0.95
η_{HPC} = 0.76
η_{LPT} = 0.72
η_{turb} = 0.72
f_{IC} = 0.005
f_{RXHP} = 0.005
OPR = 2.88
PR_{LPC} = 1.697
Q_{1011} = 0 [kW/kg.s^{-1}]
Q_{1617} = 0 [kW/kg.s^{-1}]
Q_{45} = 0 [kW/kg.s^{-1}]
Q_{gen} = 46.75 [kW/kg.s^{-1}]
Q_{HS} = 244 [kW/kg.s^{-1}]
Q_{LPT} = -115 [kW/kg.s^{-1}]
Q_{RXLP} = -426.8 [kW/kg.s^{-1}]
T_w = 20 [°C]

APPENDIX C: MATCHING

C.1 Matching Procedure

1.) Satisfy flow compatibility between the HPT and the LPT.

2.) Satisfy flow and work compatibility between the HPC and HPT.

3.) Satisfy flow and pressure ratio compatibility for the LPC.

C.2 Map approximation

In order to do the matching of the turbo machines, interpolations must be done between constant speed lines. To simplify this procedure the following simplifications are implemented:

- The map is resized so that the non-dimensional mass flow rates at which pressure ratio and efficiency is known, correspond.
- Every constant speed pressure ratio vs. non-dimensional mass flow rate line is simplified to three straight lines.
- The resized maps are then used to calculate DTpT constant speed lines. After observing these lines it was apparent that they can be represented by straight lines.

The above simplifications reduce a specific speed line to be represented by the following characteristic factors:

- m1 – Slope of pressure ratio line 1
- m2 – PR of pressure ratio line 1 at NDM = 0
- m3 – Slope of pressure ratio line 2
- c1 – PR of pressure ratio line 2 at NDM = 0
- c2 – Slope of pressure ratio line 3
- c3 – PR of pressure ratio line 3 at NDM = 0
- NDM_{surge} – NDM at which surge occur
- NDM_2 – NDM on pressure ratio line 2
- NDM_3 – NDM on pressure ratio line 3

- NDM_{choke} – NDM at which choke occur
- mDTT – Slope of DTT line
- cDTT – DTT of DTT line at NDM = 0

C.2.1 Original Map

50.532		71.516		87.522		95.077		100.721		107.543		113.585	
NDM	PR	NDM	PR	NDM	PR	NDM	PR	NDM	PR	NDM	PR	NDM	PR
1.825	1.480	3.107	2.040	6.547	2.720	7.319	3.140	7.851	3.450	8.377	3.840	9.009	4.200
2.341	1.470	3.694	2.050	7.263	2.730	8.104	3.130	8.490	3.450	9.102	3.800	9.592	4.060
2.865	1.460	4.773	2.050	8.049	2.640	8.849	3.040	9.232	3.370	9.646	3.610	9.995	3.760
3.635	1.440	5.762	2.010	8.787	2.500	9.522	2.840	9.723	3.090	10.050	3.320	10.342	3.460
4.445	1.390	6.987	1.890	9.478	2.260	9.946	2.470	10.016	2.680	10.321	2.940	10.455	3.030
5.359	1.310	8.147	1.720	9.759	1.980	10.101	2.060	10.154	2.290	10.384	2.500	10.552	2.630
6.302	1.200	8.929	1.400	9.853	1.620	10.129	1.730	10.160	1.940	10.402	2.110	10.573	2.280
NDM	ETA	NDM	ETA	NDM	ETA	NDM	ETA	NDM	ETA	NDM	ETA	NDM	ETA
2.659	0.720	4.135	0.720	2.585	0.740	7.585	0.740	8.206	0.720	9.251	0.700	9.989	0.650
3.049	0.740	4.544	0.740	7.043	0.760	9.417	0.740	9.571	0.720	9.844	0.680	10.437	0.600
3.429	0.760	5.020	0.760	7.328	0.770	9.643	0.720	9.751	0.700	10.147	0.650	10.484	0.550
4.237	0.760	5.294	0.770	8.001	0.770	9.773	0.700	9.861	0.680	10.344	0.600	10.579	0.500
4.597	0.740	6.793	0.770	8.520	0.760	9.857	0.680	9.977	0.650	10.380	0.550		
4.863	0.720	7.034	0.760	9.005	0.740	9.940	0.650	10.092	0.600	10.402	0.500		
5.078	0.700	7.410	0.740	9.238	0.720	10.028	0.600	10.151	0.550				
5.254	0.680	7.698	0.720	9.394	0.700	10.085	0.550	10.160	0.520				
5.473	0.650	7.927	0.700	9.509	0.680	10.128	0.500						
5.766	0.600	8.111	0.680	9.626	0.650								
6.010	0.550	8.326	0.650	9.739	0.600								
6.224	0.500	8.581	0.600	9.810	0.550								
		8.749	0.550	9.859	0.500								
		8.858	0.500										

FLOWNEX -- CE

C.2.2 EES code to resize Map

```
Function  MP (SP)
  If ( SP = 1 ) Then
     MP := 15
  If ( SP = 2 ) Then
     MP := 17
  If ( SP = 3 ) Then
     MP := 19
  If ( SP = 4 ) Then
     MP := 21
  If ( SP = 5 ) Then
     MP := 23
  If ( SP = 6 ) Then
     MP := 25
  If ( SP = 7 ) Then
     MP := 27
End  MP
```

```
<><><><><><><><><><><><><><><><><><><><><><><><><
SP = 7
eta$ = 'eta7'
PR$ = 'PR7'
NDMeta$ = 'NDMeta7'
NDMPR$ = 'NDMPR7'
C = MP ( SP )
```

NDM_1 = **Lookup** ('CE', 1 , C)

NDM_{range} = **Lookup** ('CE', **Lookup** ('CE', SP , 'NOR_{eta}'), C) – NDM_1

N = 9

η_i = **Interpolate** ('CE', NDMeta$, eta$, NDMeta$ = NDM_i) for i = 1 to N

PR_i = **Interpolate** ('CE', NDMPR$, PR$, NDMPR$ = NDM_i) for i = 1 to N

$$NDM_{i+1} = NDM_i + \frac{NDM_{range}}{9} \quad \text{for } i = 1 \text{ to } N$$

η_{10} = **Interpolate** ('CE', NDMeta$, eta$, NDMeta$ = NDM_{10})

PR_{10} = **Interpolate** ('CE', NDMPR$, PR$, NDMPR$ = NDM_{10})

C.2.3 Resized Map

50.532		71.516		87.522		95.077		100.721		107.543		113.585		
NDM	PR	NDM	PR	NDM	PR	NDM	PR	NDM	PR	NDM	PR	NDM	PR	
2.659	1.464	4.135	2.054	7.043	2.738	7.585	3.142	8.206	3.441	9.251	3.766	9.989	3.765	
3.055	1.456	4.660	2.052	7.356	2.724	7.868	3.139	8.423	3.448	9.379	3.727	10.050	3.768	
3.451	1.446	5.185	2.039	7.669	2.694	8.150	3.127	8.640	3.452	9.507	3.678	10.120	3.762	
3.847	1.429	5.709	2.013	7.982	2.651	8.433	3.104	8.857	3.443	9.635	3.616	10.190	3.728	
4.243	1.405	6.234	1.972	8.295	2.603	8.715	3.065	9.074	3.412	9.763	3.551	10.250	3.653	
4.640	1.375	6.759	1.918	8.607	2.543	8.998	3.021	9.292	3.355	9.890	3.465	10.320	3.526	
5.036	1.341	7.284	1.866	8.920	2.483	9.280	2.951	9.509	3.261	10.020	3.353	10.380	3.315	
5.432	1.303	7.808	1.796	9.233	2.399	9.563	2.835	9.726	3.088	10.15	3.381	10.45	3.059	
5.828	1.259	8.333	1.664	9.546	2.273	9.845	2.64	9.943	2.827	10.27	3.157	10.51	2.968	
6.224	1.21	8.858	1.439	9.859	1.591	10.13	1.744	10.16	1.94	10.4	2.11	10.58	2.154	
NDM	ETA	NDM	ETA	NDM	ETA	NDM	ETA	NDM	ETA	NDM	ETA	NDM	ETA	
2.659	0.720	4.135	0.720	7.043	0.760	7.585	0.740	8.206	0.720	9.251	0.700	9.989	0.650	
3.055	0.740	4.660	0.745	7.356	0.771	7.868	0.709	8.423	0.704	9.379	0.690	10.050	0.795	
3.451	0.761	5.185	0.766	7.669	0.773	8.150	0.702	8.640	0.702	9.507	0.686	10.120	0.862	
3.847	0.768	5.709	0.780	7.982	0.770	8.433	0.711	8.857	0.710	9.635	0.684	10.190	0.866	
4.243	0.760	6.234	0.782	8.295	0.766	8.715	0.727	9.074	0.721	9.763	0.682	10.250	0.824	
4.640	0.737	6.759	0.771	8.607	0.758	8.998	0.741	9.292	0.727	9.890	0.678	10.320	0.753	
5.036	0.704	7.284	0.747	8.920	0.745	9.280	0.745	9.509	0.724	10.020	0.668	10.380	0.669	
5.432	0.656	7.808	0.711	9.233	0.721	9.563	0.729	9.726	0.704	10.150	0.650	10.450	0.587	
5.828	0.588	8.333	0.649	9.546	0.672	9.845	0.683	9.943	0.660	10.270	0.653	10.510	0.525	
6.224	0.500	8.858	0.500	9.859	0.500	10.130	0.500	10.160	0.520	10.400	0.500	10.580	0.500	

Resize – CE

C.2.4 DTpT constant speed lines

NDM	DTpT	NDM	DTpT	NDM	DTpT	NDM	DTpT	NDM	DTpT	NDM	DTpT	NDM	DTpT
2.659	0.160	4.135	0.317	7.043	0.439	7.585	0.523	8.206	0.588	9.251	0.658	9.989	0.708
3.055	0.153	4.660	0.306	7.356	0.430	7.868	0.545	8.423	0.603	9.379	0.661	10.050	0.580
3.451	0.146	5.185	0.295	7.669	0.423	8.150	0.548	8.640	0.605	9.507	0.657	10.120	0.534
3.847	0.140	5.709	0.284	7.982	0.417	8.433	0.537	8.857	0.596	9.635	0.649	10.190	0.527
4.243	0.134	6.234	0.274	8.295	0.411	8.715	0.519	9.074	0.583	9.763	0.639	10.250	0.544
4.640	0.129	6.759	0.265	8.607	0.403	8.998	0.501	9.292	0.568	9.890	0.629	10.320	0.576
5.036	0.124	7.284	0.261	8.920	0.398	9.280	0.487	9.509	0.555	10.020	0.618	10.380	0.611
5.432	0.120	7.808	0.256	9.233	0.394	9.563	0.476	9.726	0.540	10.150	0.640	10.450	0.641
5.828	0.116	8.333	0.241	9.546	0.393	9.845	0.468	9.943	0.523	10.270	0.595	10.510	0.694
6.224	0.112	8.858	0.219	9.859	0.284	10.130	0.344	10.160	0.401	10.400	0.476	10.580	0.490

DT_034/T_03

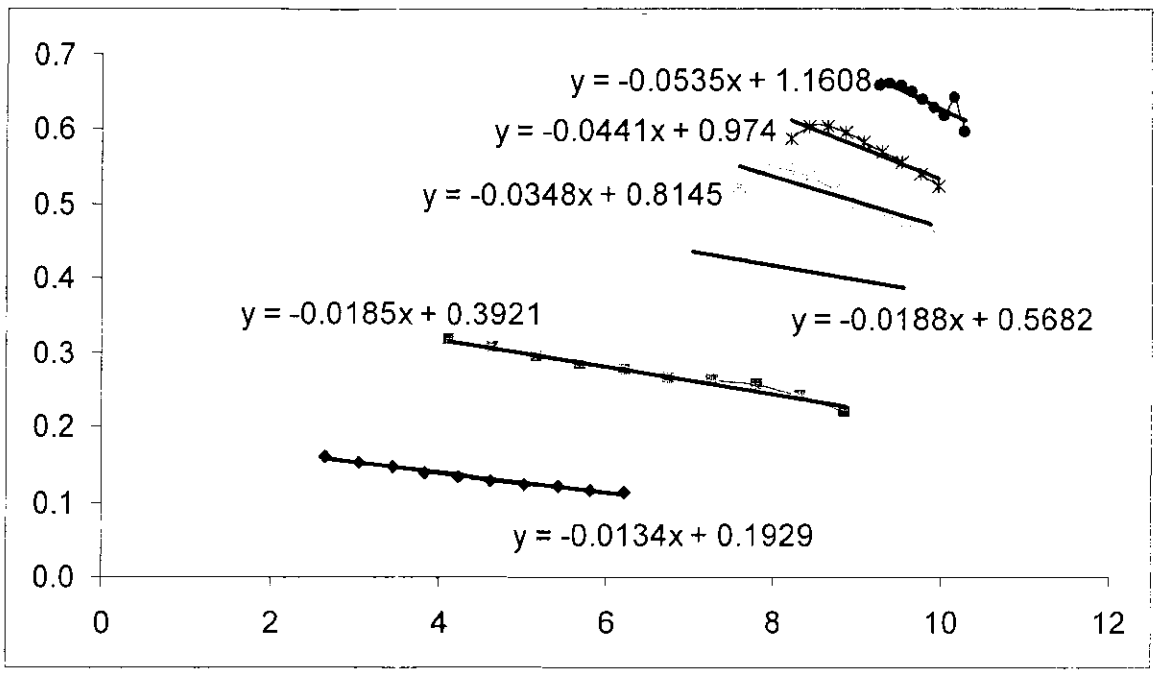

C.2.4 Characteristic factors

	1	2	3	4	5	6
m1	-0.0192	0.0060	-0.0533	-0.0654	-0.0579	-0.1813
m2	-0.0443	-0.0723	-0.2659	-0.5193	-0.8803	-0.9929
m3	-0.1023	-0.2523	-1.7032	-4.0400	-5.1350	-10.2711
c1	1.5151	2.0214	3.0688	3.6183	3.9045	5.3587
c2	1.5869	2.3949	4.7803	7.6350	11.4971	13.1879
c3	1.8447	3.6529	18.4022	42.6531	54.1135	108.9448
NDMsurge	1.8249	3.1071	6.5469	7.3186	7.8506	8.3773
NDM2	2.8647	4.7731	8.0486	8.8486	9.2325	9.6460
NDM3	4.4445	6.9873	9.4776	9.9463	10.0163	10.3207
NDMchoke	6.3018	8.9295	9.8534	10.1295	10.1605	10.4015
mDTT	-0.0134	-0.0185	-0.0188	-0.0348	-0.0441	-0.0535
cDTT	0.1929	0.3921	0.5682	0.8145	0.9740	1.1608
	50.53	**71.52**	**87.52**	**95.08**	**100.72**	**107.54**

C.3 Flow compatibility between LPT and HPT

$PR_{LPT,1} = 1$

$PR_{choking} = 2.23$

LPT$ = 'TEi'

HPTi$ = 'TEi'

HPTe$ = 'TEe'

LPT

$NDM_{LPT,i}$ = **Interpolate** ('TEi', 'PR', 'NDM', 'PR' = $PR_{LPT,i}$) for i = 1 to 11

$$PR_{LPT,i+1} = PR_{LPT,i} + \frac{PR_{choking} - PR_{LPT,1}}{10} \quad \text{for } i = 1 \text{ to } 11$$

HPT

$PR_{HPT,i}$ = **Interpolate** ('TEe', 'NDM', 'PR', 'NDM' = $NDM_{LPT,i}$) for i = 1 to 11

$NDM_{HPT,i}$ = **Interpolate** ('TEi', 'PR', 'NDM', 'PR' = $PR_{HPT,i}$) for i = 1 to 11

$OPR_i = PR_{HPT,i} \cdot PR_{LPT,i}$ for i = 1 to 11

$PR_{HPT,12} = PR_{HPT,11}$

$PR_{HPT,13} = PR_{HPT,12}$

$PR_{LPT,13} = PR_{LPT,12} + 0.5$

Maximum pressure ratio, determined by LPT choke

$PR_{max} = PR_{HPT,11} \cdot PR_{LPT,11}$

C.4 Compressor Matching

```
"<><><><><<><><><><><><><><><><><><><><><><><><><><><><><><><>"
"Procedure to select two speed lines needed for intropolation"
"<><><><><<><><><><><><><><><><><><><><><><><><><><><><><><><>"
PROCEDURE SPselect(NDM,PR:SPA,SPB,SP1,SP2)

PRsurge1    =    LOOKUP('CE',1,1)*LOOKUP('CE',7,1) + LOOKUP('CE',4,1)
PRsurge2    =    LOOKUP('CE',1,2)*LOOKUP('CE',7,2) + LOOKUP('CE',4,2)
PRsurge3    =    LOOKUP('CE',1,3)*LOOKUP('CE',7,3) + LOOKUP('CE',4,3)
PRsurge4    =    LOOKUP('CE',1,4)*LOOKUP('CE',7,4) + LOOKUP('CE',4,4)
PRsurge5    =    LOOKUP('CE',1,5)*LOOKUP('CE',7,5) + LOOKUP('CE',4,5)
PRsurge6    =    LOOKUP('CE',1,6)*LOOKUP('CE',7,6) + LOOKUP('CE',4,6)


    IF(PR < PRsurge1) then
        NDM_inter     =     NDM_inter(PR,1)
        IF(NDM > NDM_inter) then
            SPA   =   1
            SPB   =   2
            SP1   =   50.53
            SP2   =   71.52
        else
            SPA   =   1
            SPB   =   1
            SP1   =   50.53
            SP2   =   50.53
        endif
    endif

    IF(PR > PRsurge1) AND  (PR < PRsurge2) then
        NDM_inter     =     NDM_inter(PR,2)
        IF(NDM < NDM_inter ) then
            SPA   =   1
            SPB   =   2
            SP1   =   50.53
            SP2   =   71.52
        else
            SPA   =   2
            SPB   =   3
            SP1   =   71.52
            SP2   =   87.52
        endif
    endif

    IF(PR > PRsurge2) AND  (PR < PRsurge3) then
        NDM_inter     =     NDM_inter(PR,3)
        IF(NDM < NDM_inter ) then
            SPA   =   2
            SPB   =   3
            SP1   =   71.52
            SP2   =   87.52
        else
            SPA   =   3
            SPB   =   4
            SP1   =   87.52
            SP2   =   95.08
        endif
    endif

    IF(PR > PRsurge3) AND  (PR < PRsurge4) then
```

```
            NDM_inter       =       NDM_inter(PR,4)
            IF(NDM < NDM_inter ) then
                    SPA     =       3
                    SPB     =       4
                    SP1     =       87.52
                    SP2     =       95.08
            else
                    SPA     =       4
                    SPB     =       5
                    SP1     =       95.08
                    SP2     =       100.72
            endif
    endif

    IF(PR > PRsurge4) AND  (PR < PRsurge5) then
            NDM_inter       =       NDM_inter(PR,5)
            IF(NDM < NDM_inter ) then
                    SPA     =       4
                    SPB     =       5
                    SP1     =       95.08
                    SP2     =       100.72
            else
                    SPA     =       5
                    SPB     =       6
                    SP1     =       100.72
                    SP2     =       107.54
            endif
    endif

    IF(PR > PRsurge5) AND  (PR < PRsurge6) then
            NDM_inter       =       NDM_inter(PR,6)
            IF(NDM < NDM_inter ) then
                    SPA     =       5
                    SPB     =       6
                    SP1     =       100.72
                    SP2     =       107.54
            else
                    SPA     =       6
                    SPB     =       6
                    SP1     =       107.5
                    SP2     =       107.5
            endif
    endif

    IF(PR > PRsurge6) then
            SPA     =       6
            SPB     =       6
            SP1     =       107.5
            SP2     =       107.5
    endif
end


"<><><><><><><><><><><><><><><><><><><><><><><><><><><><><><><><><>"

"<><><><><><><><><><><><><><><><><><><><><><><><><><><><><><><><><>"
"Function assigning characteristic factors for particular speed line "
"<><><><><><><><><><><><><><><><><><><><><><><><><><><><><><><><><>"
PROCEDURE CHFasign(SPEED:m1,m2,m3,c1,c2,c3,NDM1,NDM3,mDTT,cDTT)
    m1              =       LOOKUP('CE',1,SPEED)
```

```
        m2              =       LOOKUP('CE',2,SPEED)
        m3              =       LOOKUP('CE',3,SPEED)
        c1              =       LOOKUP('CE',4,SPEED)
        c2              =       LOOKUP('CE',5,SPEED)
        c3              =       LOOKUP('CE',6,SPEED)
        NDM1            =       LOOKUP('CE',8,SPEED)
        NDM3            =       LOOKUP('CE',9,SPEED)
        mDTT            =       LOOKUP('CE',11,SPEED)
        cDTT            =       LOOKUP('CE',12,SPEED)
end
"<><><><><><><><><><><><><><><><><><><><><><><><><><><><><><><><>"

"<><><><><><><><><><><><><><><><><><><><><><><><><><><><><><><><>"
"Function determining PR from the characteristic-factors selected"
"<><><><><><><><><><><><><><><><><><><><><><><><><><><><><><><><>"
FUNCTION PR(NDM,m11,c11,NDM11,m12,c12,m13,c13,NDM13)
"SPEED1"
if (NDM < NDM11) Then
        PR      =       m11*NDM + c11
else
if(NDM > NDM13) Then
        PR      =       m13*NDM + c13
        else
        PR      =       m12*NDM + c12
endif
endif
end
"<><><><><><><><><><><><><><><><><><><><><><><><><><><><><><><><>"

"<><><><><><><><><><><><><><><><><><><><><><><><><><><><><><><><>"
"Function NDM_inter"
"<><><><><><><><><><><><><><><><><><><><><><><><><><><><><><><><>"
FUNCTION NDM_inter(PR_c,SP)
                CALL  CHFasign(SP:m1,m2,m3,c1,c2,c3,NDM1,NDM3,mDTT,cDTT)
                PR2             =       m2*LOOKUP('CE',8,SP)    + c2
                PR3             =       m3*LOOKUP('CE',9,SP)    + c3
                PRchoke         =       m3*LOOKUP('CE',10,SP)   + c3

                IF(PR_c > PR2) then
                        NDM_inter       =       (PR_c - c1)/m1
                endif
                IF(PR_c < PR2) AND (PR_c > PR3) then
                        NDM_inter       =       (PR_c - c2)/m2
                endif
                IF(PR_c < PR3) then
                        NDM_inter       =       (PR_c - c3)/m3
                endif
end
"<><><><><><><><><><><><><><><><><><><><><><><><><><><><><><><><>"
```

C.4.1 Flow and Work compatibility between the HPC and HPT

```
"......................................................................................................................"
"MAIN"
"       Values known or assumed "
"HPT operating point"
{NDM_HPT        =       5}
{PR_HPT         =       1.28}
```

```
gamma=      1.4
eta_t       =       0.7

DTpTt  =    eta_t*(1-(1/PR_HPT)^((gamma-1)/gamma))

"Work compatibility"
DTpTt  =    DTpTx*((T_03 + 273.15)/(T_06+273.15))*cp_c/(cp_h*eta_mH)
T_03   =    25
T_06   =    700

cp_h   =    CP(Nitrogen,T=700,P=850)
cp_c   =    CP(Nitrogen,T=25,P=250)
eta_mH      =       0.99

"Select speeds"
CALL SPselect(NDM,DTpTx:SPA,SPB,SP1,SP2)

"Assign characteristic factors"
"Characteristic factors for speed A"
m1A         =       LOOKUP('CE',1,SPA)
m2A         =       LOOKUP('CE',2,SPA)
m3A         =       LOOKUP('CE',3,SPA)
c1A         =       LOOKUP('CE',4,SPA)
c2A         =       LOOKUP('CE',5,SPA)
c3A         =       LOOKUP('CE',6,SPA)
NDM1A       =       LOOKUP('CE',8,SPA)
NDM3A       =       LOOKUP('CE',9,SPA)
mDTTA       =       LOOKUP('CE',11,SPA)
cDTTA       =       LOOKUP('CE',12,SPA)

"Characteristic factors for speed B"
m1B         =       LOOKUP('CE',1,SPB)
m2B         =       LOOKUP('CE',2,SPB)
m3B         =       LOOKUP('CE',3,SPB)
c1B         =       LOOKUP('CE',4,SPB)
c2B         =       LOOKUP('CE',5,SPB)
c3B         =       LOOKUP('CE',6,SPB)
NDM1B       =       LOOKUP('CE',8,SPB)
NDM3B       =       LOOKUP('CE',9,SPB)
mDTTB       =       LOOKUP('CE',11,SPB)
cDTTB       =       LOOKUP('CE',12,SPB)
"For any given non-dimensional mass flow rate the speed will be SPx in order to satisfy work
compatibility"
SPx    =    (SP2 - SP1)*(DTpTx - DTpT1)/(DTpT2 - DTpT1) + SP1
       DTpT1 =      NDM*mDTTA + cDTTA
       DTpT2 =      NDM*mDTTB + cDTTB

"Pressure ratio to satisfy work compatibility, for any NDM"
PR_work     =       (PR_B - PR_A)*(SPx - SP1)/(SP2 - SP1) + PR_A
       PR_A  =      PR(NDM,m1A,c1A,NDM1A,m2A,c2A,m3A,c3A,NDM3A)
       PR_B  =      PR(NDM,m1B,c1B,NDM1B,m2B,c2B,m3B,c3B,NDM3B)

"PR to satisfy flow compatibility, for any NDM"
PR_flow     =       NDM*1/NDM_HPT*PR_loss*sqrt((273.15 + 700)/(273.15 + 25))

PR_loss     =       1.1

"Work and flow compatibility must be satisfied"
PR_flow     =       PR_work
eta_c       =       1/DTpTx*(PR_work^((gamma-1)/gamma)-1)
```

C.4.2 Flow and pressure ratio compatibility for the LPC

```
"MAIN"
"Known and assumed values"
PR_LPT      =     2.14
PR_HPT      =     1.515
OPR         =     PR_HPT*PR_LPT
PR_HPC      =     1.827
NDM_HPC     =     8.189

T_01        =     28
T_03        =     29
gamma=      1.4
"To achieve required OPR"
PR_LPC      =     OPR/PR_HPC

"Flow compatibility between LPC and HPC"
PR_LPC      =     NDM_LPC*(1/NDM_HPC)*(1/PR_ICL)*sqrt(T_03 +273.15)/sqrt(T_01
+273.15)
PR_ICL      =     1.02

CALL  SPselect(NDM_LPC,PR_LPC:SPA,SPB,SP1,SP2)
CALL  CHFasign(SPA:m1A,m2A,m3A,c1A,c2A,c3A,NDM1A,NDM3A,mDTTA,cDTTA)
CALL  CHFasign(SPB:m1B,m2B,m3B,c1B,c2B,c3B,NDM1B,NDM3B,mDTTB,cDTTB)

SPx   =     (SP2 - SP1)*(PR_LPC - PR_A)/(PR_B - PR_A) + SP1
      PR_A  =     PR(NDM_LPC,m1A,c1A,NDM1A,m2A,c2A,m3A,c3A,NDM3A)
      PR_B  =     PR(NDM_LPC,m1B,c1B,NDM1B,m2B,c2B,m3B,c3B,NDM3B)

DTpTx       =     (SPx - SP1)/(SP2 - SP1)*(DTpTB - DTpTA) + DTpTA
      DTpTA       =     NDM_LPC*mDTTA + cDTTA
      DTpTB       =     NDM_LPC*mDTTB + cDTTB

eta_c =     1/DTpTx*(PR_LPC^((gamma-1)/gamma)-1)
```